INFORMATION TO USERS

This manuscript has been reproduced from the microfilm master. UMI films the text directly from the original or copy submitted. Thus, some thesis and dissertation copies are in typewriter face, while others may be from any type of computer printer.

The quality of this reproduction is dependent upon the quality of the copy submitted. Broken or indistinct print, colored or poor quality illustrations and photographs, print bleedthrough, substandard margins, and improper alignment can adversely affect reproduction.

In the unlikely event that the author did not send UMI a complete manuscript and there are missing pages, these will be noted. Also, if unauthorized copyright material had to be removed, a note will indicate the deletion.

Oversize materials (e.g., maps, drawings, charts) are reproduced by sectioning the original, beginning at the upper left-hand corner and continuing from left to right in equal sections with small overlaps.

Photographs included in the original manuscript have been reproduced xerographically in this copy. Higher quality 6" x 9" black and white photographic prints are available for any photographs or illustrations appearing in this copy for an additional charge. Contact UMI directly to order.

Bell & Howell Information and Learning
300 North Zeeb Road, Ann Arbor, MI 48106-1346 USA

UMI®
800-521-0600

The Recent Star Formation History of Galaxies in X-Ray Clusters

by

Michael Lajos Balogh
B.Sc., Math & Physics, McMaster University 1995

A Dissertation Submitted in Partial Fulfillment of the
Requirements for the Degree of

DOCTOR OF PHILOSOPHY

in the Department of Physics and Astronomy

We accept this thesis as conforming
to the required standard.

Dr. C. J. Pritchet, Supervisor (Physics & Astronomy)

Dr. F. D. A. Hartwick, Departmental Member (Physics & Astronomy)

Dr. A. Babul, Departmental Member (Physics & Astronomy)

Dr. S. L. Morris, Outside Member (DAO, NRC, HIA)

Dr. T. W. Dingle, Outside Member (Chemistry)

Dr. D. Schade, External Examiner (DAO, NRC, HIA)

Supervisor: Dr. C. J. Pritchet

Abstract

We have measured spectral indices for $\sim$ 2000 galaxies in the CNOC1 redshift survey of 15 X-ray luminous clusters at $0.2 < z < 0.55$. A detailed comparison is made between the star formation histories of galaxies in these clusters with an identically selected sample of galaxies in the lower density field population, to establish the effects these cluster environments have on galaxy evolution. We find that the mean star formation rate, as determined from the [OII]λ3727 emission line, is suppressed in all cluster galaxies, out to and even beyond the virial radius. The number of actively star forming galaxies, and the mean star formation rate among cluster galaxies, increases with increasing distance from the cluster centre. This correlation is not completely due to the morphology- radius relation, as cluster galaxies of a given physical size, fractional bulge luminosity and redshift have lower star formation rates than similar galaxies in the field environment.

We find no evidence that the cluster environment induces star formation in its constituent galaxies. Galaxies with positive W_o(OII), of any strength, are more common in the field than they are in the clusters. In particular, the A+em galaxies, which have spectra that may reflect dust obscured starburst activity, make up only 6.3$\pm$2.1% of the field population, and are twice as common there as they are in the cluster sample.

If star formation is terminated in a galaxy after a short starburst, the spectrum will show strong Balmer absorption lines without [OII] emission; we find that less than $\sim$5% of all galaxies have such a spectrum, and there is no evidence that they are preferentially found within the cluster sample. Spectrophotometric model results suggest that many of these galaxies may have had their star formation abruptly truncated without such a starburst. Alternatively, Hα observations of Abell 2390 cluster galaxies suggest that the

lack of [OII] emission in some such galaxies may be due to dust obscuration, and not necessarily indicative of the absence of star formation activity.

These results suggest that star formation is terminated in galaxies that are incorporated into these clusters. This termination need not be abrupt, and may take place over a period of several Gyr. Thus, the differential evolution of cluster galaxies may result because field galaxies are able to refuel their stellar disk with gas from an extended halo, thus perpetuating star formation, while such a halo would be disrupted within rich clusters, and star formation would gradually cease.

Examiners:

Dr. C. J. Pritchet, Supervisor (Physics & Astronomy)

Dr. F. D. A. Hartwick, Departmental Member (Physics & Astronomy)

Dr. A. Babul, Departmental Member (Physics & Astronomy)

Dr. S. L. Morris, Outside Member (DAO, NRC, HIA)

Dr. T. W. Dingle, Outside Member (Chemistry)

Dr. D. Schade, External Examiner (DAO, NRC, HIA)

Contents

List of Tables

List of Figures

Acknowledgements

This research has made use of data obtained from the Canada-France-Hawaii Telescope, which is operated by the NRC of Canada, the CNRS of France and the University of Hawaii. I gratefully acknowledge NSERC for both encouraging my interest in research through two summer undergraduate awards, and for supporting my graduate research through PGS A and PGS B awards, and through grants to C. J. Pritchet. I wish to thank all members of the CNOC team for successfully planning and undertaking this large survey, on which my work has been largely based. In particular, I am very grateful to my thesis advisor, Simon Morris, for his patience, guidance, faith and sensibility. I have had the great pleasure to benefit from the unbridled enthusiasm and clever insight of David Hartwick. Many thanks also are due to Chris Pritchet for initiating my interest in astronomy, for his unwavering support (both financial and scientific) and for his confidence in my work. Over the past four years, I have benefited from stimulating discussions/arguments with many people, including J. Navarro, A. Babul, A. Zabludoff, D. Zaritsky and I. Smail. I am especially grateful to James Merleau for reminding me what science should be about, and to Alan Dressler, for reminding me what it is actually about.

Dedicated to my mother, Sonia J. Balogh, who died July 14, 1995, and to my father, Louis Balogh, who lives bravely on.

Chapter 1

Introduction

1.1 Justification

One of the most active fields in astronomy today is the study of galaxy formation and evolution. Recent years have seen the discovery and study of galaxies at very high redshifts, $z > 1$ (e.g., Steidel et al. 1996a, 1996b; Giavalisco et al. 1996), at an epoch when they are observed soon after formation and probably only indirectly related to the galaxies we see around us today. Individual galaxies must undergo dramatic changes over their lifetime, if only when they create their first generation of stars out of the primordial hydrogen gas. When and where these stars form is currently unknown, but clearly varies from galaxy to galaxy, as the local universe is filled with galaxies with different structures, stellar populations and gas contents. The largest, most luminous galaxies are structurally composed of a disk and/or bulge component, and can be found with any and all intermediate bulge/disk ratios. The stellar populations in these galaxies range from very old (i.e., no new stars have formed for many billions of years) to very young

(i.e., stars are currently being created). There are strong relations between, though great ranges in, galaxy luminosity, size and surface brightness (e.g. Kormendy 1985). Dwarf galaxies of almost arbitrarily low luminosity also exist, and have a wide variety of morphologies and surface brightnesses; these objects are of particular importance in the universe, as they may be the building blocks out of which larger galaxies are built (White and Rees 1978). It is clearly of interest to determine how such a wide variety of galaxy types can exist at this time, given the homogeneous nature of the gas out of which they must have formed at early times.

Most galaxies are found in loose groups; the Milky Way itself is one of two large galaxies that make up the Local Group, a bound association which includes ~ 30 low luminosity dwarfs (e.g., van den Bergh 1994), within about 1 Mpc^3 of space. Large clusters of galaxies, which contain several hundred galaxies of Milky Way size within the same volume, are relatively rare, but visually striking regions of the universe. One of the strongest correlations with galaxy type (almost independent of how "type" is defined) is found with the environment in which it is located; i.e., whether it is in a loose group, a rich cluster, or isolated. If we can understand how local, galaxy specific properties such as morphology and star formation can depend on the space density of neighbouring galaxies, we will learn something fundamental about which physical processes are responsible for the evolution of galaxies.

It is the purpose of this dissertation to investigate some aspects of these correlations. In this introduction, we will discuss the previous work that has led to the current understanding of how and why galaxy evolution depends on environment. A brief description of galaxy clusters is presented in §1.2. We

discuss evidence for the dependence of galaxy morphology on environment in §1.3, and consider further correlations with star formation rates in §1.4. The evolution of these correlations with time provides useful constraints on the mechanisms responsible for the observed diversity of galaxies; observational evidence for such evolution is presented in §1.5. Important clues on the history of galaxy populations may be present in a rare class of galaxy which may have only recently ceased strong star formation activity; this galaxy type is discussed in §1.6. The objectives of this dissertation, and the data on which it is based, are introduced in §1.7. Finally, the structure of the remainder of this document is outlined in §1.8.

1.2 Galaxy Clusters

A small fraction ($\sim 5\%$) of the total number of galaxies in the universe are found in rich clusters of galaxies; the high surface density of bright galaxies in these clusters allows them to stand out markedly in surveys, and to be observable out to large distances. Because of this ability to study clusters over large redshift ranges, they have long been considered useful tools for the study of the cosmological parameters and large scale structure of the universe (e.g., Hubble 1936; Zwicky 1938; Henry and Arnaud 1991; Lauer and Postman 1994; Eke et al. 1996; Carlberg et al. 1996; Hudson et al. 1999).

Abell (1958) constructed the first large catalogue of clusters, by identifying concentrations of galaxies on the Palomar Sky Survey plates. He classified these clusters according to their "richness", a classification which is still in

wide use today. Richness class is assigned by counting the number of galaxies which are not more than 2 magnitudes fainter than the third brightest cluster member, within an arbitrarily chosen radius of 1 h^{-1} Mpc. This integer classification ranges from 0 (30–49 galaxies) to 5 (more than 300 galaxies). Velocity dispersions of the richest clusters are typically $\sim$ 1000 km/s, which imply mass–to–light ratios of several hundred (e.g., Carlberg et al. 1996); in fact, this type of analysis provided the first observational evidence for large amounts of unseen matter in the universe (Zwicky 1933).

Galaxy clusters are filled with hot ($\sim 10^8$ K) gas which emits strong X–ray radiation. This allows for easy and uniform selection of clusters, independent of projection effects, which is important for the study of the evolution of cluster abundances (e.g., Abramopoulos and Ku 1983; Gioia et al. 1990; Kaiser 1991; Ebeling et al. 1997; Nichol et al. 1997; Eke et al. 1998). Furthermore, measurements of the gas temperature and luminosity profiles provide a nearly direct probe of the total cluster potential, as well as its shape, and confirm the very high mass–to–light ratios (e.g., Cavaliere and Fusco-Femiano 1976; Bahcall and Sarazin 1977; Fujita and Takahara 1999; Lewis et al. 1999). These mass determinations are somewhat complicated by the fact that an early injection of energy into the gas provides it with a minimum entropy such that the temperature is no longer a direct reflection of the gravitational potential (e.g., Ponman et al. 1999; Balogh et al. 1999a).

Galaxy clusters provide an excellent laboratory for studying the distribution of galaxy properties, in particular the morphology–dependent luminosity function (e.g., Trentham 1997; Smith et al. 1997; Phillipps et al. 1998), as the relative properties of galaxies within a cluster can be determined without

a knowledge of their individual distances, since the distance to a cluster is generally much larger than the distance between its constituent galaxies.

1.3 The Dependence of Galaxy Morphology on Environment

Even before it was recognised that many of the diffuse nebulae observed in the skies are external to the Milky Way, it was known that their morphologies vary with environment. Curtis (1918) observed 304 small, diffuse and featureless nebulae in the Coma cluster which looked quite different from the spiral-shaped nebulae observed elsewhere. However, he incorrectly attributed these observations to an inability to resolve spiral structure in such small objects; it was later recognised that rich clusters of galaxies are in fact dominated by early type galaxies (particularly S0 and dwarf spheroidals), while spiral galaxies dominate the low-density field, (e.g., Hubble and Humason 1931; Spitzer and Baade 1951; Morgan 1961; Abell 1965).

Spitzer and Baade (1951) appear to be the first authors to suggest that the collision of two spiral galaxies will result in a galaxy which looks, morphologically, like an S0. At the time, it was thought that the velocity dispersions of clusters were low enough to allow efficient galaxy merging and, hence, the destruction of spirals in this manner could explain the relative overabundance of S0 galaxies in clusters. However, revision of the extragalactic distance scale resulted in the discarding of this theory, as typical cluster galaxy velocities are actually on the order of ~ 1000 km/s, much too high for effective merging to occur. However, the numerical simulation work of Moore et al. (1996,

1998) showed that complete merging may not be necessary to effect morphological change. Cluster galaxies will undergo many high velocity encounters with other galaxies in their lifetime, and Moore et al. found that these encounters alone, though not resulting in a merger product, may transform a spiral galaxy into the dwarf spheroidal type commonly found in clusters.

The constituent galaxy population depends strongly on the cluster type, as first effectively shown in the study of Oemler (1974). In this survey of fifteen rich galaxy clusters, he showed that the most centrally concentrated clusters (which contain a central cD galaxy) are rich in ellipticals and strongly deficient in spirals within the core (also noted by Abell, 1965). On the other hand, less concentrated, irregular clusters have a large fraction of spiral galaxies, though it is still not as large as the fraction found in the low density field. Oemler interpreted this as a reflection of the different dynamic states of the clusters, as first detailed in Gunn and Gott (1972): the irregularly shaped, loosely concentrated clusters have not yet collapsed, while the cD clusters have. In this case, Oemler speculated that spiral galaxies are transformed into E/S0 types *during* the cluster collapse. The most likely mechanism for affecting this change seemed to be the expulsion of the cold gas found in the disks of spiral galaxies, by the ram–pressure exerted by the hot, diffuse intracluster medium (ICM, Gott and Gunn 1972; Fujita and Nagashima 1999), even though the existence of this medium would not be confirmed for two more years (Scheepmaker et al. 1976; Mitchell et al. 1976). From a sample of six concentrated, X–ray luminous clusters, in which ram–pressure forces might be the most effective, Melnick and Sargent (1977) found that the proportion of S0 galaxies relative to spiral galaxies increases toward the cluster

centre (where the gas density is highest), and correlates with cluster velocity dispersion in the sense that clusters with the largest velocity dispersion (the most massive) have the largest S0/Spiral ratio. If ram-pressure is able to efficiently remove the gas from spiral galaxies, the lack of stellar fuel may allow the galaxy to evolve into an S0 morphology, with a smooth, faint disk in which there is no ongoing star formation. The anaemic spirals observed in the Virgo cluster (van den Bergh 1960, 1991) may be the result of such stripping; also, recent Hα images of spiral galaxies in the Virgo cluster show strong signs that gas is being stripped from the disk (Veilleux et al. 1999; Kenney and Koopmann 1999). For ram-pressure stripping to be effective, however, galaxies must encounter the hot gas in a nearly face-on orientation and at a high relative velocity. Alternatively, Nulsen (1982) showed that other types of galaxy-gas interactions (such as viscous stripping, thermal conduction and turbulence effects) may be even more effective at removing disk gas at lower velocities, independently of orientation.

A third explanation for the observed morphological segregation was proposed by Larson, Tinsley and Caldwell (1980). The star formation rates (SFRs) in normal, field spiral galaxies like the Milky Way are sufficiently high that the galaxies will deplete their entire gas supply in about 1-2 Gyr (e.g., Gallagher et al. 1989). There must therefore be some method for "refuelling" the disk, if we are not to consider ourselves to be in a special epoch where star formation is dying out. Larson et al. proposed that the disk gas is replenished by infall from gas in a large, diffuse envelope surrounding the galaxy. Recently, Blitz et al. (1999) argue that the numerous high velocity clouds of HI are Local Group objects, and the primeval building blocks

of galaxies. Their simulations suggest that clouds like these will have been accreted by the Milky Way over its lifetime, at a rate of about 1 $M_{\odot}\mathrm{yr}^{-1}$, enough to keep star formation active in the disk over the Galaxy's lifetime. The numerical simulations of Larson et al. (1980) showed that it is very easy to strip away this loosely bound gas during cluster collapse; thus, cluster spirals can be expected to exhaust their gas supply shortly after cluster formation, after which the disk will fade, and transform the galaxy morphology into that of an S0 galaxy.

If spiral galaxies are indeed destroyed during cluster collapse, then the global cluster morphology (if it is indicative of dynamical state) should be the best determinant of the morphological composition of its galaxy population. However, Dressler (1980) showed that the fraction of galaxies of a given morphological type (E, S0 or Spiral) correlates very well with the *local* galaxy density (defined as the background–corrected surface density within an area containing the 10 nearest neighbours of each galaxy). He found in particular that, over a large range in density, the fraction of spiral galaxies decreases with increasing density, and that this is almost exactly matched by a corresponding increase in the fraction of S0 galaxies. Elliptical galaxies, on the other hand, only become important in the regions of highest density. Perhaps the most important result of this work is the discovery that the correlation is universal, in the sense that it holds for irregular clusters as well as concentrated clusters; it was subsequently also shown to hold in the less massive group environment, which can actually cover a similar range in local densities (Bhavsar 1981; Postman and Geller 1984). However, Dressler also found that the absolute bulge sizes and the bulge–to–disk ratios of S0 galaxies

are systematically larger than the corresponding properties of spiral galaxies, at all local densities. Furthermore, ram–pressure forces should not play a role in the diffuse, irregular clusters or groups, since the ICM is less dense and galaxy velocities tend to be lower; therefore Dressler concluded that ram pressure stripping is probably not the only cause of the morphology–density relation. He suggested instead that disk formation, which is thought to occur slowly over long timescales, might be strongly inhibited in dense environments, so that spiral galaxies rarely, if ever, actually form in these regions of the universe. In this case, the morphological composition of a cluster is due to conditions at the time of galaxy formation, rather than to evolutionary effects which take place later.

More recent, *Hubble Space Telescope* (HST) based observations of clusters at $z \approx 0.5$ have shown that these objects are strongly deficient in the S0 galaxies that dominate local clusters; from this, it was concluded that at least half of the S0 galaxies in local clusters are probably the remnants of stripped spiral galaxies (Dressler et al. 1997). Furthermore, this study revealed a strong difference in the morphology–density relation as a function of cluster type; unlike their low redshift counterparts, irregular clusters at $z = 0.5$ do not show a strong correlation of galaxy type with local density. This suggests that the mechanisms responsible for producing the morphological segregation may operate with different effectiveness in different types of clusters (c.f. Kauffmann 1995).

A number of objections have been raised against Dressler's suggestion that the morphology–density relation is universal (Giovanelli and Haynes 1985; Salvador-Soleé et al. 1989; Sanromà and Salvador-Soleé 1990). In par-

ticular, Whitmore and Gilmore (1991) and Whitmore et al. (1993) showed, using Dressler's data sample, that a better correlation could be found between morphology and *radius*, where the radius is taken to be the distance from either the X-ray centre or the brightest cluster galaxy (BCG), instead of the centroid of the galaxy distribution. In particular, within the central 0.2 Mpc, the surface density of spirals drops precipitously; this led Whitmore et al. to suggest that the central regions of clusters have a particularly strong effect on galaxy morphology. This issue has been re–addressed in Dressler et al. (1997), who explicitly show that the correlation between morphology and radius is weak for irregular clusters; however, these authors still take the centroid of the galaxy distribution as their choice of centre and, thus, do not appropriately consider the main source of discrepancy as suggested by Whitmore et al. (1993).

Whitmore et al. proposed a galaxy evolution model in which the first galaxies to form are the ellipticals, and that their formation occurs *before* the epoch of cluster collapse. This is consistent with recent analysis of the colour–magnitude relation of ellipticals in clusters, which show that these galaxies formed at least 5 Gyr ago, and have only evolved passively since (e.g., Ellis et al. 1997; Bower et al. 1998; Barger et al. 1998). S0 and spiral galaxies, on the other hand, form *after* cluster collapse (and the more massive S0s form before the spirals). If, during cluster collapse, all proto-galactic gas clouds are destroyed, then spirals would be rare within clusters, and the gas out of which they would have formed would contribute to the ICM. Like in Dressler's (1980) model, spiral galaxies are not transformed into S0 galaxies, so the discrepancy between their bulge sizes is no longer a problem. However,

there are other problems with this model, of which one of the most important is that the ICM is known to be metal–rich (e.g. Mitchell et al. 1976; David et al. 1991; Arnaud et al. 1992; Mushotzky et al. 1996; Markevitch et al. 1998), whereas Whitmore et al. propose that most of this gas comes from the destruction of proto–galactic clouds, in which no star formation has yet occured.

1.4 Star Formation

Since the hottest, most massive stars have very short lifetimes ($\lesssim$ 20 Myr), their presence in a galaxy indicates that formation of new stars must be occuring at the epoch of observation; from their abundance, then, the star formation rate of massive stars can be determined. These stars emit much of their light in the ultraviolet spectrum, at wavelengths shorter than that of Lyα; this light is readily absorbed and reemitted by the surrounding gas out of which they must have formed; this process will produce an unmistakable signature of Balmer emission lines in the galaxy spectrum. The flux in these lines can then be related to a total star formation rate (e.g., Osterbrock 1989). The most serious complication is that the emission line flux arises from only the most massive stars and, thus, some form of the initial mass function (IMF) must be assumed before the total star formation rate can be determined; Kennicutt (1983) and Gallagher et al. (1989) have shown that the form of the IMF can be constrained to something similar to a Salpeter (1955) function, from the broad band galaxy colours, which are sensitive to the longer term star formation history of the galaxy.

Kennicutt (1992a) showed that the Hα emission line is the best spectroscopic indicator of star formation; however, this line is redshifted out of the visual band at moderate redshifts, $z \gtrsim 0.5$. In this same work, Kennicutt showed that the [OII]λ3727 emission line is the blue feature which best correlates with Hα, and is thus useful for measuring SFRs in redshift surveys (e.g., Lin et al. 1996; Lilly et al. 1998; Hogg et al. 1998).

From the Hα emission lines in local galaxy spectra, Kennicutt (1992a) and Kennicutt et al. (1994) have determined star formation rates for a large sample of local galaxies. They found a strong correlation of SFR with galaxy morphology, in the sense that spiral galaxies show large amounts of star formation, mostly within the disk and spiral arms, whereas elliptical galaxies show little or no star formation. In particular, Kennicutt et al. (1994) showed that SFR is predominantly a property of galactic disks, and is insensitive to disk/bulge morphology.

Early observations by Osterbrock (1960) and Gisler (1978), for example, showed that emission line galaxies are less common in clusters than in the field, which demonstrates that morphology, star formation and global environment are all somehow interrelated. This provokes several questions; in particular, which has the dominant influence on a galaxy's SFR — morphology or environment? Pressing this further, do changes in environment influence star formation rates, morphology, or both? Do changes in star formation rate influence morphology? Dressler et al. (1985b) showed that the deficit of emission line galaxies in clusters could not be entirely accounted for by the difference in morphological composition relative to the field; this was confirmed by Koopmann and Kenney (1998), who showed that spiral galaxies

in the Virgo cluster have reduced star formation relative to similar galaxies in the field. However, from Hα images taken of eight nearby Abell clusters, Moss and Whittle (1993) concluded that, although this is true for late–type spirals (Sc and Sc–Irr), Sa and Sab spirals can actually show *enhanced* star formation in clusters. Finally, it has been established that galaxies in clusters contain less HI gas (as determined from 21 cm radio observations) than their field counterparts (e.g. Bahcall 1977; Giovanelli and Haynes 1985; White and Sarazin 1991). Thus, it seems clear that morphology is not the sole determinant of a galaxy's gas content and star formation properties. However, it is unlikely that the evolution of morphological and star formation properties are completely unrelated; for example, terminating star formation in a spiral galaxy may lead to subsequent morphological evolution (as determined by the light distribution) due to the surface brightness fading which will inevitably follow (e.g., Bothun and Gregg 1990; Abraham et al. 1996).

1.5 The Butcher–Oemler Effect

The first strong evidence for the evolution of cluster properties with time was found by Butcher and Oemler (1978a). They compared two–colour photometry of two rich, high concentration clusters at z=0.39 (Cl 0024+1654) and z=0.46 (Cl 3C295) with similar observations of local clusters (Butcher and Oemler 1978b), and found that the fraction of blue galaxies in the higher redshift clusters was significantly larger than the fraction in local clusters. Since larger redshifts are associated with longer lookback times, this implies strong evolution in the star formation properties (which affect galaxy

colour) over about 6 Gyr. Butcher and Oemler pointed out that it was not clear whether this evolution was restricted to rich clusters, or a reflection of galaxy evolution in the universe as a whole; this question is still largely unresolved.

The most serious problem with photometric studies like that of Butcher and Oemler is one of background subtraction, which must be done statistically from observations of nearby fields. Since non–cluster members will tend to look bluer than the red sequence formed by elliptical cluster members, due to the redshift effect, incorrect field subtraction could lead to anomalously high blue galaxy fractions. In fact, Mathieu and Spinrad (1981) and Dressler and Gunn (1982) showed that the cluster 3C295 was contaminated by a foreground cluster which, when accounted for, reduced the fraction of blue cluster galaxies to local levels. However, the high blue galaxy fraction was confirmed (though reduced in significance) in Cl 0024 (Dressler and Gunn, 1982). The issue was finally decided in a more careful study of 33 clusters, where a strong increase in the fraction of blue galaxies with redshift (out to $z = 0.5$) was observed (Butcher and Oemler 1984). The scatter in this relation is large, and there are examples of high redshift clusters with very low blue galaxy fractions, most notably cluster Cl 0016+16 at $z = 0.54$ (see also Koo 1981). The strongest evidence of evolution is the appearance of concentrated clusters at $z \approx 0.2$ in which 20% of the galaxies are blue; such a large fraction is not seen in any local, concentrated cluster. Rakos and Schombert (1995) showed that the increase in blue galaxy fraction extends out to $z \sim 1$ and is, perhaps, even steeper than determined from the original Butcher and Oemler study. In particular, their data show no clusters beyond

$z > 0.4$ with blue fractions less than 30%. However, their clusters are selected from the sample of Gunn et. al (1986), and *not* in any way selected based on central concentration. In the original Butcher and Oemler (1978b) study, it was clearly shown that up to 50% of the galaxies in many local clusters may be blue; it is only the most centrally concentrated, cD clusters that have low fractions of blue galaxies. Furthermore, it is likely that the type of cluster selected in the Gunn et al. (1986) survey varies strongly with redshift (i.e., it is more difficult to find loose, poor clusters at higher redshifts); thus, it is not clear that the same types of clusters are being compared at all redshifts.

Motivated by the appearance of these blue galaxies at moderate redshifts, Dressler and Gunn (1983) suggested that, instead of stripping the gas from the disk, interaction with the ICM might "shock or squeeze" the interstellar medium into forming many stars in a short period of time. Thus, in this interpretation, galaxies observed at high redshift are undergoing short starbursts which will shortly cease, and following which the galaxies will evolve without further star formation to the present epoch. As the disks fade and stars age, the clusters quickly grow to be dominated by red galaxies, as observed locally. A theoretical model in support of this was constructed by Gavazzi and Jaffe (1987); Byrd and Valtonen (1990) and Fujita (1998) later showed that interactions with the cluster tidal field could be even more effective at triggering nuclear and disk star formation activity. An intense burst of star formation might be able to consume all of the cold disk gas; thus, the net effect, following termination of the starburst, may be quite analagous to that of gas stripping.

More recently, images taken with the HST (Dressler et al. 1994; Couch

et al. 1994, 1998) have shown that, though there appears to be a higher incidence of disturbed and (apparently) interacting/merging galaxies than seen locally, most of the blue galaxies in moderate redshift clusters are late spirals or irregular galaxies with normal star formation rates, that are rare or absent in local, concentrated clusters (see also Rakos et al. 1997). This suggests that these blue galaxies (which have negligible spheroid components) will *not* evolve into the large–bulge S0 galaxies which dominate clusters at low redshift. It has been suggested that they are bursting dwarfs (Koo et al. 1997) or low–surface brightness (LSB) galaxies (Rakos and Schombert 1995, Rakos et al. 1997) that fade to become either dwarf spheroidals or LSB galaxies below local detection limits, respectively.

It is clearly of importance to determine whether or not the Butcher–Oemler effect is characteristic of rich clusters, or is independent of environment. In particular, redshift surveys of the field (e.g. Broadhurst et al. 1988; Lilly et al. 1995; Cowie et al. 1996, 1999) suggest that the fraction of blue, star forming galaxies, as well as the mean star formation rate, increases strongly with redshift, an effect that might be analagous to the Butcher–Oemler effect observed in clusters. On the other hand, Allington–Smith et al. (1993) found that the poorest galaxy groups found around radio galaxies are not significantly bluer at $z = 0.4$ than they are locally. More recently, Smail et al. (1998) presented a deep CCD survey of 10 high X–ray luminous clusters at $0.22 < z < 0.28$, and did not find a large population of star forming galaxies in the cores of these clusters. Both of these observations suggest that, at least, the strength of the Butcher–Oemler effect may be dependent on the type of cluster being considered (c.f. Kauffmann 1995).

Before the above, often discrepant, results can be correctly interpreted, the connection between high and low redshift clusters must be determined. In particular, selection effects can be responsible for generating samples in which the highest redshift clusters arise from larger density fluctuations than the lower redshift clusters. Clusters of different mass have different merger histories (e.g. Kauffmann 1995) and, thus, if the mass function is not equally sampled at all redshifts, the interpretation of correlations with redshift as evolutionary effects may be incorrect. Recently, Andreon and Ettori (1999) have shown that the higher redshift Butcher–Oemler clusters are more X–ray luminous than the low redshift clusters. Since fair samples show either no evolution, or even *negative* evolution in the X–ray luminosity function (e.g. Henry et al. 1992; Collins et al. 1997; Vikhlinin et al. 1998; Rosati et al. 1998), this confirms that the two sets of clusters may not be evolutionarily linked in a direct way.

1.6 Evidence for Young Stellar Populations

Since (and prior to) the confirmation of the Butcher–Oemler effect in 1984, concentration has focussed on the *nature* of the blue galaxies. The groundwork for this was laid by Dressler and Gunn (1983) who showed that, of the six confirmed blue member galaxies of 3C295, three possibly contain active galactic nuclei (AGNs; one Seyfert 1 and two Seyfert 2s), which are rare in local clusters (though Koo et al. (1997) show that Dressler's criteria for selecting AGNs are generally unsuccessful). The remaining three blue cluster members have no emission lines, but very strong Balmer absorption lines

(rest frame equivalent widths of $W_\circ$=7-8 Å), typical of A-stars and, hence, indicative of a young stellar population. Normal spiral galaxies have emission lines and weaker Balmer absorption ($W_\circ$=2-5 Å), due to the presence of O- and B- stars which overwhelm the A-star light: OB-stars have weaker intrinsic Balmer absorption, and their ionising fluxes will generate HII regions which exhibit Balmer emission that will "fill in" the stellar absorption in the composite galaxy spectrum. This led to the idea that a new population of galaxy, rare or absent locally, is appearing at $z \approx 0.3$; an introduction to these galaxies is the purpose of this section.

1.6.1 Definitions

Dressler and Gunn (1983) found that the combined spectrum of the three unusual, blue galaxies in 3C295 could be matched by a combination of a K-giant spectrum, typical of elliptical galaxies, and an A-star spectrum; they therefore named these galaxies "E+A" (later changed to "K+A"). Subsequently, there has been considerable inconsistency in the application of this terminology. In Chapter 4 we will use models and spectral properties of local galaxies to identify and classify galaxies based on their spectra; for the purpose of this introduction, we qualitatively define all galaxies with "unusually" strong Balmer lines (as represented by the rest frame equivalent width of the $H\delta$ line, $W_\circ(H\delta)$, to be consistent with the available data presented in Chapter 4) as Hδ-strong (HDS). The threshold at which we define "unusual" is colour-dependent, as blue, normal spiral galaxies have larger $W_\circ(H\delta)$ than red, normal elliptical galaxies. Any galaxy with nebular emission lines is expected to have moderate Hδ absorption, since continuum light and nebu-

lar emission contributions from massive stars dominate the spectrum; thus, galaxies of any colour with emission lines and strong $W_\circ(H\delta)$ lines are also considered unusual. The important types are:

- **K+A Galaxy:** This is an HDS galaxy of any colour, but with no detectable nebular emission lines. This implies the presence of recent star formation, which gives rise to a dominant A–star population, but without any current star formation, which would result in OB stars and, hence, strong emission lines.

- **Post–Starburst (PSB):** These are the bluest K+A galaxies, with the strongest $W_\circ(H\delta)$, as originally identified by Dressler and Gunn (1983). Although the absence of OB–stars requires only that star formation has recently terminated, models show that the blue galaxies with $W_\circ(H\delta) \gtrsim$ 7Å must have undergone a strong, short–lived starburst just prior to the termination of star formation.

- **Post–Star Formation (PSF):** First identified by Couch and Sharples (1987), these are red K+A galaxies. Although these galaxies require star formation to have terminated recently, the activity need not have occurred via a strong, short–lived starburst (e.g. Newberry et al. 1990; Abraham et al. 1996; Morris et al. 1998). The PSF galaxies with the strongest $W_\circ(H\delta) \gtrsim$ 5Å, present in the data of Couch and Sharples (see §1.6.2), have not been successfully matched by any reasonable model of star formation history.

- **A+em Galaxies:** This classification applies to the HDS galaxies with emission lines. Although these galaxies have shown up in most previous studies, they are not easily explained. Strong [OII] emission lines alone imply that the Hδ absorption strength should be greatly reduced by emission–filling (e.g. Barbaro and Poggianti 1997). Secondly, a population of OB–stars must be present to give rise to the emission lines, and the high intrinsic luminosity and low intrinsic $W_\circ(H\delta)$ strength of these stars should further reduce the global $W_\circ(H\delta)$ value. Poggianti et al. (1999) have recently suggested that the most massive stars may be strongly obscured by the dense dust clouds in which they are embedded, which reduces both their emission line and continuum flux. The A stars, on the other hand, live long enough to migrate out of these dusty environments, and their light can dominate the galaxy spectrum. In this scenario, A+em galaxies are currently undergoing massive star formation, but the light from the most massive stars is strongly suppressed.

Since the original Dressler and Gunn (1983) discovery, HDS galaxies have been found both locally (Caldwell et al. 1993; Zabludoff et al. 1996) and at moderate redshifts (e.g., Sharples et al. 1985; Lavery and Henry 1986; Couch and Sharples 1987; MacLaren et al. 1988; Broadhurst et al. 1988; Fabricant et al. 1991; Fisher et al. 1998; Dressler et al. 1999), in both cluster and field environments. However, the only *large*, statistically representative survey used to address this problem was the LCRS, at $z \sim 0.1$, analysed by Zabludoff et al. (1996). Furthermore, galaxies have been classified in

an inconsistent manner, due to a wide variety of data type and quality. Thus, it is still unclear what the true abundance of these galaxies is, and in what environments they are most likely to be found. As these galaxies may be in caught in a short-lived transition state between galaxy types, it is important to determine where they are preferentially found, and what possible mechanisms may give rise to their appearance.

1.6.2 Starbursts or Truncated Star Formation?

Couch and Sharples (1987) obtained spectra for 152 galaxies in the fields of three rich clusters at $z \sim 0.31$. These data show that galaxies with "abnormally" high Balmer absorption lines have a large range of colour, including the bluest and the reddest galaxies. Using the spectrophotometric models of Bruzual (1981), they constructed models of galaxy evolution for different star formation histories. In particular, they showed that the largest values of $W_\circ(H\delta)$ were obtained in model galaxies shortly after a brief ($\sim$ 1 Gyr) episode of star formation, in which a significant fraction ($\gtrsim$ 30%) of the galaxy's mass is converted into stars. After the end of the starburst, these galaxies remain fairly blue (similar to normal spirals) for a few hundred Myr, and gradually redden while $W_\circ(H\delta)$ decreases with time.

Couch and Sharples claim that all of their HDS galaxies are matched by the model in which a short, strong burst of star formation has just ended. However, none of their models match the reddest galaxies with $W_\circ(H\delta) > 3$Å. Secondly, they rule out models in which star formation is truncated without a starburst, as these do not reach $W_\circ(H\delta) > 7$Å. However, their 1σ uncertainties on $W_\circ(H\delta)$ are about 1.5–2 Å, and some of the strongest absorption

line measurements may simply be a reflection of these uncertainties. Even if the errors are ignored, it is only a small number of galaxies that require an initial burst of star formation to explain their line indices.

The Couch and Sharples data were modelled in more detail by Barger et al. (1996), who attempted to reconcile the number of galaxies in each of five regions within the $W_\circ(H\delta)$–colour plane with a single star formation history. They used the GISSEL (Bruzual and Charlot 1993) models to construct mock galaxy populations for different histories, and compared their spectral index and colour distributions with the data. Barger et al. concluded that the data were consistent with a model in which about 30% of the cluster galaxies have undergone a strong starburst (lasting about 0.1 Gyr) in the past 2 Gyr. They admit that this model is not unique but do not explicitly show that a model of truncated star formation cannot also match the observations. Finally, Poggianti and Barbaro (1996) also claim that only their starburst models can match the Couch and Sharples data, though this is perplexing, as their models all have $W_\circ(H\delta) < 5$Å and do not match most of the data with the strongest Hδ lines. It is likely that the model $W_\circ(H\delta)$ measurements are made with an index definition that differs from that used to analyse the data and, thus, it is not clear that their conclusions are as strong as they suggest.

A strong challenge to the starburst scenario described above was presented by a detailed analysis of the radial gradients in the Abell cluster A2390 (Abraham et al. 1996), as part of the first Canadian Network for Observational Cosmology (CNOC1) redshift survey. They showed that the radial gradients in galaxy colour, morphology (central concentration) and the fraction of HDS galaxies were all consistent with an age gradient, in the

sense that the last episode of star formation occurred more recently for the galaxies farthest from the centre of the cluster. No evidence for excess [OII] emission among cluster galaxies was observed, relative to the field, and they found that the distribution of HDS galaxies could be modelled with a simple *truncation* of star formation; that is, the blue galaxies are an infalling field galaxy population in which star formation is abruptly quenched. This would cause the disks to fade by about 1 magnitude after 1 Gyr, increasing the bulge–to–disk ratio by more than a factor of two. In this case, galaxies need not undergo a starburst; however, if starburst activity is episodic, or obscured by substantial dust reddening (which Abraham et al. rule out based on the fact that only 2–3 of the cluster members are detected in the radio band), galaxies undergoing such a phase would be rare and difficult to detect.

1.7 Goals

The nature of galaxy evolution in clusters is still very much uncertain. Two facts, however, seem reasonably secure. First, there does appear to be a strong increase in the mean star formation rate with redshift, in both cluster and field galaxy populations. Secondly, if clusters are largely built up of infalling field galaxies, as seems likely, than the large difference in galaxy morphologies and stellar populations between these two environments at the present time requires a strong mechanism to drive differential evolution. To what extent can we relate these two effects to each other? The answer to this question will tell a great deal about what physical mechanisms dominate galaxy evolution.

An important investigation which will lead to these answers is a comparison of the stellar populations in cluster *and* field galaxies in a large, statistically complete sample at moderate redshifts, $z \sim 0.3$, where the Butcher–Oemler effect is evident. The purpose of this dissertation is to address three fundamental questions from such a study: (1) How do current galaxy star formation rates depend on environment and morphology at these redshifts? (2) Is the Butcher–Oemler effect related to a cluster–specific evolutionary mechanism, or does it reflect universal phenomena? (3) To what extent can differential galaxy evolution be explained by the quenching of star formation, without a starburst?

The data that will be considered in Chapters 2–4 is drawn from the spectra taken in the CNOC1 survey. The goal of this redshift survey was to measure the mass density of the universe by determining the mass–to–light ratio of rich clusters (Carlberg et al. 1994). This required the acquisition of over 2000 spectra for galaxies in 16 rich clusters, over a redshift range 0.2 to 0.55 (Yee et al. 1996). From this analysis, a measurement of $\Omega_o = 0.2 \pm 0.1$ was obtained (Carlberg et al. 1996, 1997a), and the mass and light profiles of the clusters were determined (Carlberg et al. 1997b, 1997c). This analysis requires that the differential evolution between cluster and field galaxies be constrained, to correct the measured mass–to–light (M/L) ratio of the cluster to that of the field, for the determination of Ω_o (Carlberg et al. 1997b).

In addition to the redshifts required for the dynamical analysis which was the primary goal of the CNOC1 survey, each galaxy spectrum contains information about the stellar populations which contribute to its luminosity. Importantly, spectra were obtained for not only cluster members, but

field galaxies in the foreground and background of these clusters, which are projected on top of them. These field galaxies are sampled in a manner identical to the cluster galaxies; thus the survey consists of a large sample of directly comparable cluster and field galaxies, in the redshift range at which the Butcher–Oemler effect is observed. Any differential effects between the stellar populations of cluster and field galaxies at these redshifts can then be observed.

To answer the questions outlined above, we will use the CNOC1 spectra to compare the relative, *current* star formation rates among cluster galaxies with those of field galaxies, as a function of morphology and distance from the cluster centre. We also describe a more comprehensive search for massively starbursting galaxies in A2390, to determine how many such galaxies may have been missed by the CNOC1 survey. Finally, spectrophotometric models are used to determine the star formation *histories* (i.e., over the past 1 Gyr) of CNOC1 cluster and field galaxies, to try to distinguish between the starburst (e.g. Barger et al. 1996) and truncation (e.g. Abraham et al. 1996) mechanisms of ending star formation activity.

1.8 Outline

The following three chapters in this dissertation are almost exact reproductions of work that has either been published by (Chapters 2 and 3) or submitted to (Chapter 4) a refereed astronomical journal. These chapters are based on the CNOC1 data, which was obtained and reduced by that collaboration; for this reason, R. G. Carlberg, H. K. C. Yee and E. Ellingson

are listed as co-authors on these three papers. In addition, D. Schade provided the morphology measurements used in Chapter 3. Chapters 2 and 3 were published in the *Astrophysical Journal Letters* and, due to page length restrictions, some important detail was omitted. The relevant details are included in Chapter 4, which is a more comprehensive analysis of the same data.

First, we consider the relative distribution of star formation rates between galaxies in the cluster and field environment, based on measurements of the [OII] equivalent width (Chapter 2, Balogh et al. 1997). In Chapter 3 (Balogh et al. 1998), we consider how the dependence of SFR on morphology is affected by the global environment. A more detailed analysis of the spectral properties of CNOC1 galaxies is presented in Chapter 4 (Balogh et al. 1999b). In particular we attempt to identify populations of K+A or post-starburst spectra, to accurately determine their abundance and environmental preference.

The analysis of Chapters 2-4 is largely dependent on the use of [OII]λ3727 as a star formation indicator, and it is known that this index is sensitive to the presence of dust. To estimate how much star formation may be obscured in the CNOC1 galaxies, we present measurements of the Hα emission line in Abell 2390 in Chapter 5.

Finally, a summary of our conclusions are presented in Chapter 6.

Chapter 2

The Relative Star Formation Rates of Cluster and Field Galaxies

2.1 Introduction

It is well established that galaxy populations vary with the density of neighbouring galaxies (e.g., Dressler 1980; Whitmore et al. 1993); however, the physical mechanisms responsible for the variation are not known. It has also been observed that cluster galaxies have, on average, older stellar populations than field galaxies (e.g., Bower et al. 1990; Rose et al. 1994). Thus, if clusters evolve by accreting field galaxies, star formation in the infalling galaxies must be truncated prematurely, relative to isolated field galaxies. If clusters are to be used to determine the mass density of the universe (e.g., Carlberg et al. 1996), the effect of this differential evolution between cluster and field galaxies on the average galaxy stellar mass must be understood.

Star formation may be truncated following an increase in star forming

activity which rapidly consumes and/or expels the available gas in a galaxy. Several physical processes have been proposed which may have such an effect, including shocks induced by ram pressure from the intracluster medium (ICM, Bothun and Dressler 1986; Gavazzi and Jaffe 1987), effects of the cluster tidal field (Byrd and Valtonen 1990), and galaxy–galaxy interactions (Barnes and Hernquist 1991; Moore et al. 1996). The increase in the fraction of blue, star forming cluster galaxies with redshift (BO effect, Butcher and Oemler 1984), has been well established, and several authors (e.g., Couch and Sharples 1987; Moss and Whittle 1993; Caldwell et al. 1996; Barger et al. 1996) have shown that there are cluster galaxies, even at low redshift, in which significant star formation has occurred in the last 2 Gyr. It is not yet clear, however, whether or not this activity is in excess relative to the field.

Alternatively, star formation may be halted in infalling galaxies without an initial increase, as suggested by the results of the analysis of colours, spectral features and morphologies of galaxies in the Abell 2390 cluster (Abraham et al. 1996). This may be achieved by interaction with the hot ICM by ram pressure stripping (Gott and Gunn 1972) or transport processes such as viscous stripping and thermal evaporation (Nulsen 1982). In this case, cluster galaxies can be treated as representative of the field at the epoch of infall, and the BO effect is interpreted as an increase in the infall rate of field galaxies, which themselves show evidence of more star forming activity at higher redshift.

The luminosities of Balmer emission lines in galaxy spectra are directly related to the ionising fluxes of hot stars embedded in HII regions, and thus

can be used to determine the star formation rate (SFR) in the observed region of the galaxy (Kennicutt 1992a). Although Hα is the best observable indicator of SFR, it is redshifted out of convenient observing bands at even moderate redshifts. The [OII]λ3727 emission line is then the feature of choice, as its strength is found to be correlated with Hα in local samples (Kennicutt 1992a; Guzman et al. 1997, but see Hammer et al. 1997). It has been clearly shown (e.g., Dressler et al. 1985a; Hill and Oegerle 1993; Abraham et al. 1996; Biviano et al. 1997) that the fraction of galaxies with strong emission lines is much smaller in clusters than in the field. Since emission lines are much more commonly found in late spirals than in early type galaxies (e.g., Kennicutt 1992a; Biviano et al. 1997), this effect may be consistent with the morphology–radius relation, if the fraction of spiral galaxies is lower in clusters by the amount necessary to account for the decrease in observed emission. However, if star formation is truncated in field galaxies falling into the cluster, the number of galaxies with [OII] line emission will be lower than expected from the morphological composition at a given cluster–centric radius, as the [OII] feature disappears shortly after star formation ceases, whereas morphological change due to disk fading occurs on timescales of about 1 Gyr (Abraham et al. 1996).

In this work, the dependence of [OII] line strength on distance from the cluster centre is presented and compared with the field sample. In Section 2.2 the data sample is described, selection effects are considered, and cluster membership and cluster–centric radius are defined. In Section 2.3 the emission line properties of cluster galaxies are compared with the field sample. The results are interpreted in Section 2.4 by computing star formation rates

and comparing the fraction of emission line galaxies with the colour–radius relation. The conclusions are summarised in Section 2.5. Throughout this *Letter*, a cosmology of $q_o = 0.1$ is assumed for distance dependent calculations, which are given in terms of $h = H_o/100$.

2.2 Sample Selection and Measurements

The galaxy sample was selected from the Canadian Network for Observational Cosmology (CNOC, Yee et al. 1996) spectroscopic sample of fifteen[1] rich, X–ray luminous clusters at moderate redshift ($0.2 < z < 0.55$). This sample consists of about 2500 cluster and field galaxies with determined redshifts, for which selection effects are well understood (Yee et al. 1996).

For each spectrum the rest frame [OII]λ3727 equivalent width, W_o(OII), was automatically computed by summing the flux above the continuum in pixels between $3713 < \lambda < 3741$ Å. The continuum level was estimated by fitting a straight line to the flux between $3653 < \lambda < 3713$ Å and $3741 < \lambda < 3801$ Å using weighted linear regression, with weights from the Poisson noise vector generated by optimally extracting the spectra with IRAF[2]. The error in W_o(OII) is computed from equation A8 in Bohlin et al. (1983). An average W_o(OII), weighted by this error, is adopted for multiply observed galaxies in the sample. The mean and median error in W_o(OII) is 5 Å and 3 Å, respectively, for the full sample. The accuracy of the measurements and errors was verified by comparing measurements made on artificial spectra

[1]Omitting cluster E0906+11, for which a velocity dispersion could not be computed (Carlberg et al. 1996).

[2]IRAF is distributed by the National Optical Astronomy Observatories which is operated by AURA Inc. under contract with NSF.

which consist of a power law continuum component ($f_\nu \propto \nu^{0.5}$) added to the spectrum of M31 (making the bulge spectrum mimic a late type spiral in the continuum), and a Gaussian emission line at $\lambda = 3727$ Å with a velocity width of 5Å (400 km/s) FWHM. The standard deviation of $W_\circ$(OII) measurements for each set of 250-1000 spectra at the same signal-to-noise ratio (SNR) and $W_\circ$(OII) was found to compare well with the average error estimate. In addition, the difference between two independent measurements of the same (real) galaxy, when available, was compared with σ, the quadrature sum of the two error estimates. This analysis indicates that the $W_\circ$(OII) errors do not represent a normal distribution, as only about 50% of the differences between two measurements are less than 1σ, and only 92% are less than 3σ. The quoted error estimates are still meaningful, however, so long as they are interpreted in this sense. A copy of the FORTRAN code used to measure $W_\circ$(OII) and its error (as well as several other indices) can be obtained from the first author.

The CNOC selection procedure is described in Yee et al. 1996, and is designed to sample the cluster galaxies to $M_r \lesssim -18.5 + 5\log h$ with at least an 80% success rate. A magnitude weight W_m, which is the ratio of the total number of galaxies to the number of galaxies with redshifts in a magnitude bin centred around the galaxy, is calculated for each galaxy in the sample to correct for incompleteness. To ensure that the sample is not biased toward emission line objects, galaxies with $W_m > 5$ are excluded. The remaining, magnitude weighted sample is complete to about $M_r^k = -18.5 + 5\log h$; galaxies less luminous than this limit are excluded from the sample.

Cluster velocity dispersion profiles of the form $\sigma^2(r) = B/(r + b)$, where

r is the projected radius from the cluster centre, are calculated by Carlberg, Yee and Ellingson (1997b), based on a volume density function of the form $\nu(r) = A/r^{-1}(r + a)^{-3}$ and an anisotropy parameter $\beta = 0.5$. Galaxies with a velocity difference relative to the cluster mean of less than $3\sigma(r)$ are considered to be cluster members. The field sample is selected from galaxies with a velocity difference greater than $6\sigma(r)$, and which lie within a filter dependent redshift range which minimises selection effects (Yee et al. 1996). The population with intermediate velocities is classified as "near–field", and may contain infalling field galaxies. These galaxies are not included in the present analysis to ensure as clear a differentiation between field and cluster galaxies as possible. The W_o(OII) properties of this population are not, however, statistically different from those of the field.

The cluster–centric distance R for cluster members is defined as the projected distance from the brightest cluster galaxy (BCG). For field galaxies, R is the redshift difference from the cluster average assuming Hubble flow. Since the sample consists of clusters of different richness, R is normalised by R_{200}, the radius at which the cluster mass density is 200 times the critical density[3]. For these clusters, R_{200} is typically 1–1.5 h^{-1} Mpc (Carlberg et al. 1996). There is an apparent absence of field galaxies in the sample at $3 < R/R_{200} < 20$, due to the fact that field galaxies at that redshift, projected in front of and behind the cluster, have a velocity offset from the BCG less than $3\sigma(r)$ and are hence included in the cluster sample. Limited spatial coverage on the sky restricts the observed projected distance of galaxies in the sample

[3]The overdensity of virialisation is approximately $\delta\rho/\rho = 178\Omega^{-0.6}$, which corresponds to a radius of about $1.5R_{200}$ for $\Omega = 0.2$.

to less than about $3R_{200}$. For statistical analysis, each galaxy is weighted by $W_m * W_{ring}$, where W_{ring} is a geometrical correction to account for the fact that the clusters are not uniformly sampled as a function of radius.

The restricted sample considered in this analysis consists of 727 cluster galaxies and 346 field galaxies, whereas W_o(OII) measurements are available for a total of 1169 cluster and 783 field galaxies. The BCGs are considered atypical cluster members, and are excluded from all analysis. Also, no attempt was made to identify active galactic nuclei (AGN), as the Hβ and [OIII]λ5007 lines, which are common diagnostics, are usually redshifted out of the observed spectral range.

2.3 Results

Figure 2.1 shows the distribution of W_o(OII) as a function of R/R_{200}, where R is defined in Section 2.2. The dashed line separates the (inner) cluster galaxies from the field galaxies. As expected, emission line galaxies are clearly less common in clusters than in the field. The weighted mean W_o(OII) (and 1σ uncertainty) in the field is 11.2 ± 0.3 Å, compared with 3.5 ± 0.4 Å in the outer cluster regions ($0.3 < R/R_{200} < 2$) and 0.3 ± 0.4 Å in the central regions ($R/R_{200} < 0.3$). The mean error of an individual measurement, indicated by the sample error bar in the Figure, is 3.5 Å. (Forty of the 1073 galaxies in the selected sample have (formal) uncertainties in W_o(OII) greater than 10 Å and 117 have uncertainties less than 1 Å). There is no evidence of a population of cluster galaxies with excess emission relative to the field at any distance from the cluster centre, out to $R \approx 2R_{200}$.

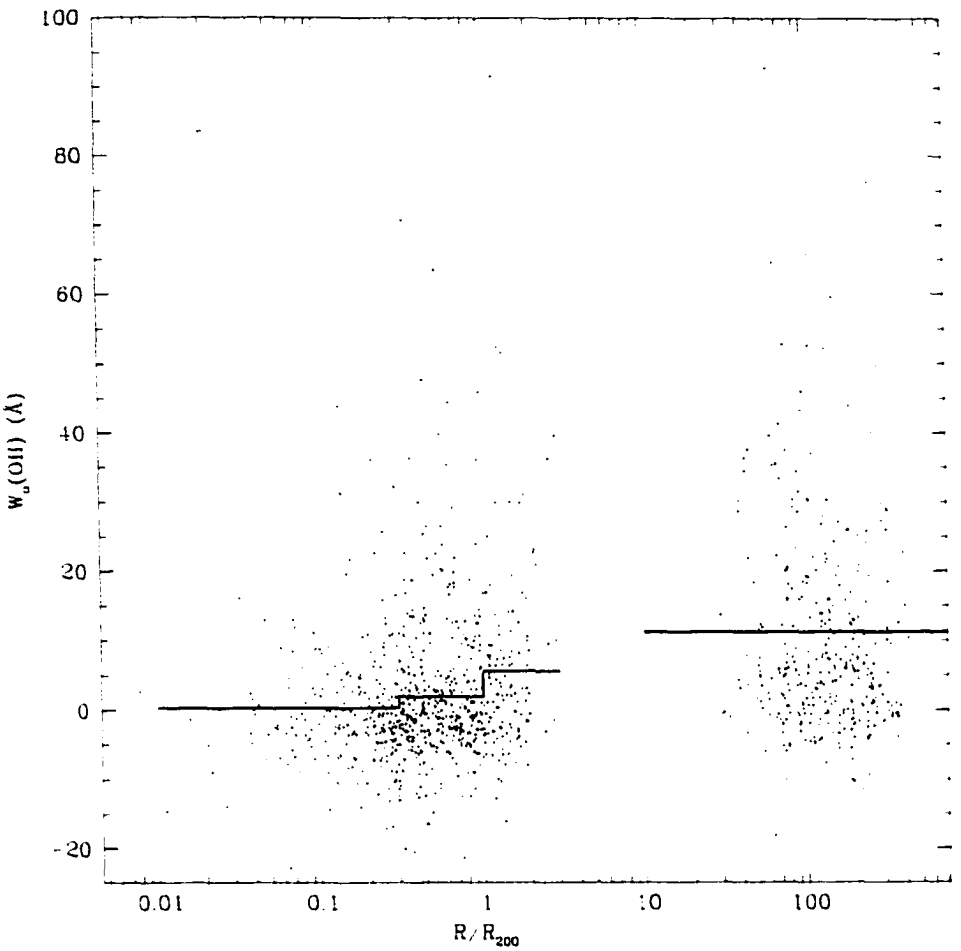

Figure 2.1: W_o(OII) as a function of cluster-centric distance R, for the selected subsample. The points to the left of the *dashed line* are cluster galaxies, for which R is the projected distance from the cluster centre. There is one cluster galaxy, with W_o(OII)=150 Å, which is off the scale. The more distant points are field galaxies, for which R is the Hubble flow distance determined from the redshift difference between the galaxy and the cluster mean. The *solid line* is the weighted mean in the field and three cluster radial bins. The sample error bar displayed is representative of the mean 1σ uncertainty in W_o(OII), 3.5 Å.

The difference between the cumulative W_o(OII) distributions of the cluster and field is shown in the top panel of Figure 2.2. The cluster galaxies at $R \geq 0.3R_{200}$ are represented by the solid line, the inner cluster galaxies ($R < 0.3R_{200}$) by the long dashed line and the field galaxies by the dotted line. The cluster sample shows a clear deficiency in emission line galaxies relative to the field in both the inner and outer cluster regions at all line strengths. There is no evidence of a population of cluster galaxies with stronger W_o(OII) than is observed in field galaxies. Since the cluster sample is partially contaminated by field galaxies projected on the cluster, the measurements of the mean W_o(OII) and SFR in the cluster are overestimates.

2.4 Discussion

Star formation rates (SFRs) have been calculated from Kennicutt's (1992a) relation with his adopted extinction correction of E(Hα) = 1 mag:

$$SFR(M_{\odot}yr^{-1}) = 6.75 \times 10^{-12} \frac{L_B}{L_B(\odot)} W_o(OII), \qquad (2.1)$$

where $L_B/L_B(\odot) = 10^{0.4(5.48-M_B)}$ depends on the absolute B band luminosity of the galaxy, which must be obtained from the available Gunn g and r photometry: $M_B = M_r + (g-r)_o - (g-B)_o$. Rest frame $(g-r)_o$ colours are computed from the colour-redshift relations in Patton et al. (1997; their figure 7), which are fits to the colour k-corrections of Yee et al. 1996, and the corresponding rest frame $(g-B)_o$ colour is found by linearly interpolating the published values in Fukugita, Shimasaku and Ichikawa (1995; their Table 3f). The cumulative SFR distributions for the cluster and field populations are shown in the bottom panel of Figure 2.2. For the inner cluster members,

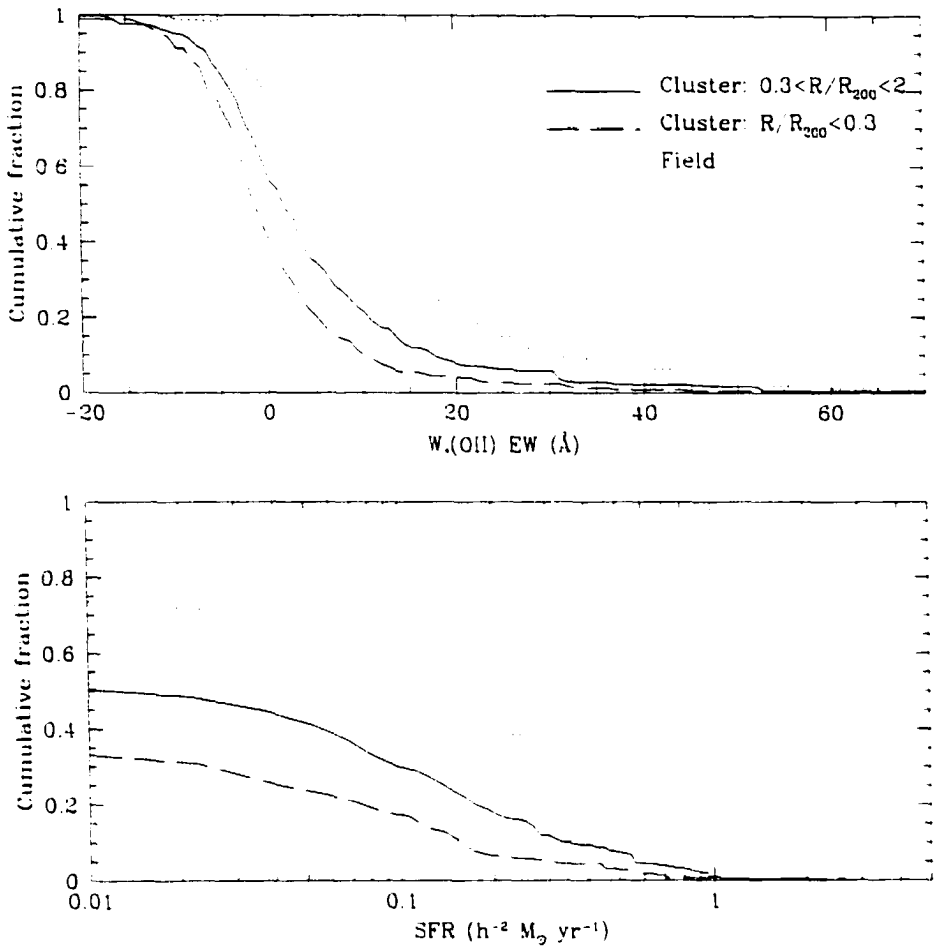

Figure 2.2: *Top panel:* The cumulative distribution of W_o(OII) in the inner cluster ($R/R_{200} < 0.3$, *long dashed line*), outer cluster ($0.3 < R/R_{200} < 2$, solid line) and field *(dotted line)* populations. *Bottom panel:* The cumulative distribution of star formation rates for the same three populations, calculated from the W_o(OII) and Kennicutt's (1992a) relation as described in the text. Note that galaxies with negative W_o(OII), produced by random errors about zero, correspond to negative SFRs; thus, the cumulative functions do not reach unity on this plot.

less than 35% have a SFR>0.01 $h^{-2}M_{\odot}\mathrm{yr}^{-1}$, whereas the median SFR in the field is about 0.2 $h^{-2}M_{\odot}\mathrm{yr}^{-1}$. The SFR calculated in this manner is most useful as an indication of the relative difference between the cluster and field; Guzman et al. (1997) suggest that the coefficient in equation 2.1 may be about three times lower than is used here.

It has been clearly shown (e.g., Couch and Sharples 1987; Moss and Whittle 1993; Caldwell et al. 1996; Barger et al. 1996) that a significant fraction of cluster galaxies have undergone episodes of star formation in the last 2 Gyr. In particular, Barger et al. (1996) suggest that 30% have undergone a 0.1 Gyr burst in the last 2 Gyr, which implies that 1.5% of cluster galaxies should be in such a state at any one time. There are cluster galaxies in the present sample with non-zero $W_{\circ}$(OII); however, they are less common than in the field population. For example, 4.3% of field galaxies have $W_{\circ}$(OII)> 40 Å, compared with only 1.4% of cluster galaxies. Thus, it seems unlikely that significant additional star formation activity in cluster galaxies is caused by the infall process or internal tides in the cluster. The weighted mean $W_{\circ}$(OII) of the cluster galaxies with $W_{\circ}$(OII)> 40 Å is 59 Å, which corresponds to an increase in stellar mass of only 4% over 0.1 Gyr from equation 2.1, assuming a stellar mass-to-light ratio of unity. No galaxy anywhere in the sample is observed to have $W_{\circ}$(OII)> 150 Å, or $SFR > 4M_{\odot}yr^{-1}$; if there are galaxies with $SFR \approx 30M_{\odot}yr^{-1}$ as suggested by Couch and Sharples (1987) and Barger et al. (1996), they may be located outside the sample, at $R > 2R_{200}$.

It is instructive to compare the $W_{\circ}$(OII)–radius relation with the well known morphology–radius relation, to determine whether or not they are

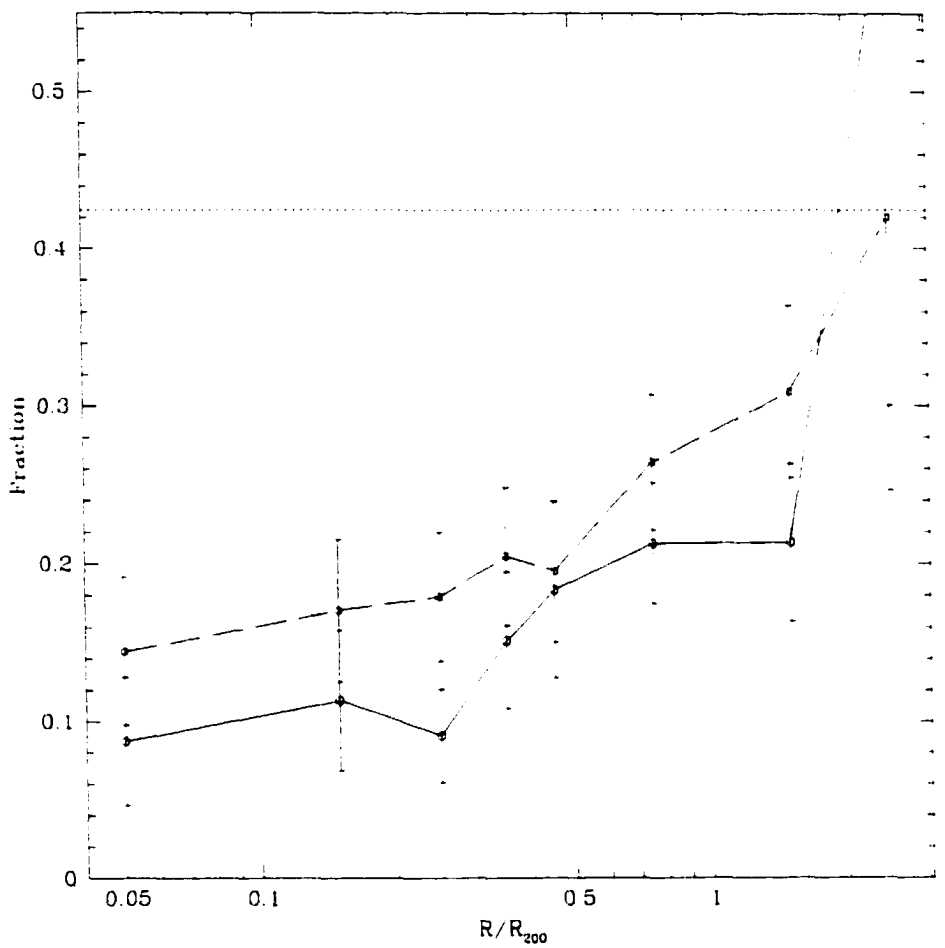

Figure 2.3: The fraction of cluster galaxies with W_0(OII)> 10 Å as a function of normalised distance from the cluster centre *(solid line)*, compared with the fraction that would be expected from the colour–radius relation *(long–dashed line)*. The horizontal, *short–dashed* line is the fraction in the field galaxy sample. See Section 2.4 for details.

consistent with one another. Unfortunately, morphological classifications are not yet available for the full CNOC sample. For now, the colour–radius relation is considered, as galaxy morphology is expected to be correlated with colour. The rest frame $(g-r)_0$ colours, computed as described above, are used to divide the sample into four classes, which correspond roughly to E, Sbc, Scd and Im morphological types, as in Patton et al. (1997). The fraction of field galaxies with W_0(OII)> 10 Å is 0.12±0.04, 0.29±0.06, 0.72±0.13 and 0.78±0.17 for the E, Sbc, Scd and Im classes, respectively. From the colour–radius relation of the cluster sample, the fraction of cluster galaxies with W_0(OII)> 10 Å in a given radial bin is predicted; this is shown as the dashed line in Figure 2.3. The observed fraction is shown as the solid line; it is significantly lower than expected from the colour–radius relation alone, for $R < 2R_{200}$. The fraction of galaxies with W_0(OII)> 15 Å, however, is consistent with the colour–radius relation; this may suggest that star formation is not truncated equally for all galaxy types, as already suggested by the results of Moss and Whittle (1993).

2.5 Conclusions

The mean W_0(OII) of cluster galaxies more luminous than $M_r^k < -18.5 + 5\log h$ in the CNOC spectroscopic sample of rich clusters at $0.2 < z < 0.55$ is 3.8 ± 0.3 Å, significantly less than the field galaxy mean of 11.2 ± 0.3 Å. The average SFR among cluster galaxies is less than the average in the field out to $2R_{200}$, which implies that whatever mechanism is responsible for truncating star formation in cluster galaxies is taking place at a large

distance from the cluster centre. Cluster galaxies of a given colour are less likely to show signs of significant star formation than their counterparts in the field at any distance from the cluster centre. Of cluster members, 1.4% have W_o(OII)> 40 Å, with a weighted mean of 59 Å, corresponding to an increase in stellar mass of less than 4% if the activity is due to a 0.1 Gyr burst. Many more (4.3%) field galaxies have W_o(OII)> 40 Å, suggesting that star formation in cluster galaxies is likely not induced by the infall process or internal tides. This supports the conclusions of Abraham et al. (1996) that star formation is truncated in infalling field galaxies without an initial increase. The BO effect in these clusters may then be due to the increased rate of infall of bluer field galaxies at higher redshift.

Chapter 3

The Morphological Dependence of Star Formation Rates

3.1 Introduction

In the hierarchical cold dark matter model of structure formation, galaxy clusters form by the collapse of rare, highly overdense regions of the universe and continually accrete mass from the surrounding regions as they evolve. The cluster population may consist of galaxies that formed long ago within the high density region, as well as those that formed in the less dense field environment and were subsequently accreted. In either case, there is ample reason to suspect that galaxies within clusters will be quite different from those in the field. A galaxy that forms in a high density region of the universe may be subjected to harassment and distortion from nearby protogalaxies (Dressler 1980; Whitmore et al. 1993; Ghigna et al. 1998), while one that forms in a low density environment and is subsequently accreted may be subjected to tidal forces due to the large gravitational potential, or interactions with other galaxies and the intra–cluster medium (Bothun and

Dressler 1986; Gavazzi and Jaffe 1987; Byrd and Valtonen 1990; Barnes and Hernquist 1991; Mushotzky et al. 1996; Ghigna et al. 1998; Moore et al. 1998).

It is not surprising, then, that cluster galaxies are observed to differ from field galaxies in their morphologies, colors and star formation rates (e.g., Dressler 1980; Whitmore et al. 1993; Abraham et al. 1996; Dressler et al. 1997; Balogh et al. 1997; Hashimoto et al. 1998; Fisher et al. 1998; Koopmann and Kenney 1998; Morris et al. 1998). Although it has been shown that the mean star formation rate (SFR) in cluster galaxies is always less than in field galaxies (Balogh et al. 1997), it is important to determine if this remains true when the different morphological composition of the two populations is accounted for, since SFR is known to be strongly correlated with morphological type (e.g., Kennicutt 1992a). This will distinguish between two simple scenarios: 1) the cluster environment favors galaxies of a certain morphological type, in terms of their size and relative bulge and disk components, but the SFR of these galaxies is statistically equivalent to that of similar galaxies in the field; or, 2) the SFR of a galaxy depends on its environment as well as its morphology. The results of this work will provide strong support for the second hypothesis.

The plan of this paper is as follows. In § 3.2 the data sample is defined, selection effects are considered, and the measurement techniques are described. In § 3.3 the emission line properties and morphologies of cluster galaxies are compared with the field sample. Implications are discussed in § 3.4, and the conclusions are summarized in § 3.5. A cosmology of $q_o = 0.1$ is assumed for distance dependent calculations, which are given in terms of

$h = H_\circ/100$ throughout.

3.2 Sample Selection and Measurements

The CNOC 1 cluster sample[1] consists of fifteen[2] X-ray luminous clusters, observed with MOS at CFHT, in the redshift range $0.18 < z < 0.55$. Redshifts were obtained for about 2500 galaxies, and observations extend as far out as 1–2 R_{200} in projected distance for most clusters, where R_{200} is the radius at which the mean interior mass density is equal to 200 times the critical density, and within which it is expected that the galaxies are in virial equilibrium (Gott and Gunn 1972; Crone et al. 1994). The observational strategy and details of the survey are detailed in Yee, Ellingson & Carlberg (1996). Cluster members are considered to be those galaxies with velocity differences from the brightest cluster galaxy (BCG[3]) less than $3\sigma(r)$, where $\sigma(r)$ is the cluster velocity dispersion as a function of projected radius r, as determined from the mass models of Carlberg, Yee & Ellingson (1997b). Field galaxies are selected to be those with velocities greater than $6\sigma(r)$. The cluster-centric distance parameter R is the projected distance from the cluster BCG, and will be normalized to R_{200}, since there is a small range in the mass and linear size of the clusters in this sample.

The equivalent width of the [OII]λ3727 emission line, $W_\circ$(OII), was au-

[1]The measured parameters discussed here, as well as others and the raw data itself, will soon be available from the CADC data archive.

[2]Omitting cluster E0906+11, for which a velocity dispersion could not be computed (Carlberg et al. 1996).

[3]Except for cluster MS 0451.5+0250, for which no redshift is available for the BCG. The velocities are measured relative to the mean for this cluster.

tomatically computed by summing the observed flux above the continuum in pixels between $3713 < \lambda < 3741$ Å. The continuum level was estimated by fitting a straight line to the flux between $3653 < \lambda < 3713$ Å and $3741 < \lambda < 3801$ Å using weighted linear regression, with weights from the Poisson noise vector generated by optimally extracting the spectra with IRAF[4]. The error in W_o(OII) is computed from equation A8 in Bohlin et al. (1983) and an average W_o(OII), weighted by this error, is adopted for multiply observed galaxies in the sample. The mean and median error in W_o(OII) is 5 Å and 3 Å, respectively, for the full sample. These error estimates were found to be reasonably representative of the reproducibility of multiple W_o(OII) measurements, as described in Balogh et al. (1997).

Morphological parameters for the Gunn r band MOS images were measured by fitting two dimensional models of exponential disk and $R^{1/4}$ law profiles to the symmetrized components of the light distribution, as described in Schade et al. (1996a; 1996b). The images are symmetrized to minimize the effects of nearby companions and asymmetric structure, and a χ^2 minimization procedure is applied to the models, convolved with the image point spread function, to obtain best fit values of the galaxy size, surface brightness and fractional bulge luminosity (bulge–to–total, or B/T ratio). Simulations show that the B/T measurements are reliable within about 20% for images of this quality (Schade et al. 1996b).

The data are weighted by two factors: a magnitude weight W_m which compensates for the fact that it is more difficult to obtain redshifts for faint

[4]IRAF is distributed by the National Optical Astronomy Observatories which is operated by AURA Inc. under contract with NSF.

galaxies, and W_{ring}, which corrects for non-uniform sampling as a function of distance from the cluster center (Yee et al. 1996). The latter weight is only important when global cluster properties are considered such that the properties of galaxies at large radii are averaged together with those at small radii. Good fits to the light profiles were obtained for 1143 (712 cluster, 373 field, 58 near-field) of the 1515 galaxies with $W_m \leq 5$ and errors in W_o(OII) of less than 10 Å, and these comprise the selected subsample[5]. The emission line properties and relative abundance of the galaxy population with poorly fit luminosity profiles are not significantly correlated with radial distance or cluster membership, and thus the exclusion of these galaxies from the sample is unlikely to bias the results. The selected sample includes galaxies with absolute Gunn r magnitudes less than about $-17.5 + 5\log h$, and is complete to $M_r = -18.5 + 5\log h$. The absolute magnitude distribution of the cluster sample is not significantly different from that of field. Furthermore, the absolute magnitude distribution is similar for the low and high redshift galaxies, a result of the longer exposure times in the high redshift cluster images (Yee et al. 1996). Although a proper treatment of the redshift evolution is not the present focus, it is noted that there is no significant difference in the results of this investigation between the low and high redshift clusters in the sample.

The sample is divided into three classes (hereafter referred to as B/T classes) based on the measured B/T value. The bulge dominated class (B)

[5]The BCGs are also omitted from the sample, as they are clearly non-typical cluster members. Only eight of the fourteen BCGs with redshifts are well fit by the simple two component model light profile, due to significant crowding and superposition of galaxies near the center of the cluster, and eight show strong emission lines, indicating very strong SFRs of between 1.8 and 21 $h^{-2}M_{\odot}\mathrm{yr}^{-1}$.

consists of those galaxies with $B/T > 0.7$, the disk dominated class (D) those with $B/T < 0.4$, and intermediate galaxies are classified "Int". These classes should not be confused with or forced to conform to more familiar Hubble types, which depend partly on star formation properties and the presence of spiral structure. The B/T ratio and the sizes of the disk and bulge components are more stable properties that reflect the true "morphology" of the galaxy and are less dependent on its star formation properties. However, the measured B/T may somewhat underestimate the "intrinsic" (i.e. representative of the mass distribution) value in star forming galaxies, as star formation takes place preferentially in the disk.

3.3 Results

The B/T–radius relation for the cluster sample is shown in the top panel of Figure 3.1. The fraction of field galaxies in each B/T class is shown at $R/R_{200} = 10$, strictly for display purposes. The radial bin sizes are equal in logarithmic intervals, except for the innermost bin, which represents all galaxies at $R < 0.16R_{200}$. The fraction of disk dominated galaxies, $f_D(r)$, decreases fairly steadily toward the center of the cluster, as expected, from about 70% in the field to 30% in the cluster center. The radial gradients of the B and Int populations ($f_B(r)$, $f_{Int}(r)$) are nearly identical, and their proportions increase by about 15% between the outer and central cluster regions.

The bottom panel of Figure 3.1 shows the mean $W_\circ$(OII) for galaxies in each B/T class as a function of radius. The field value, again shown at

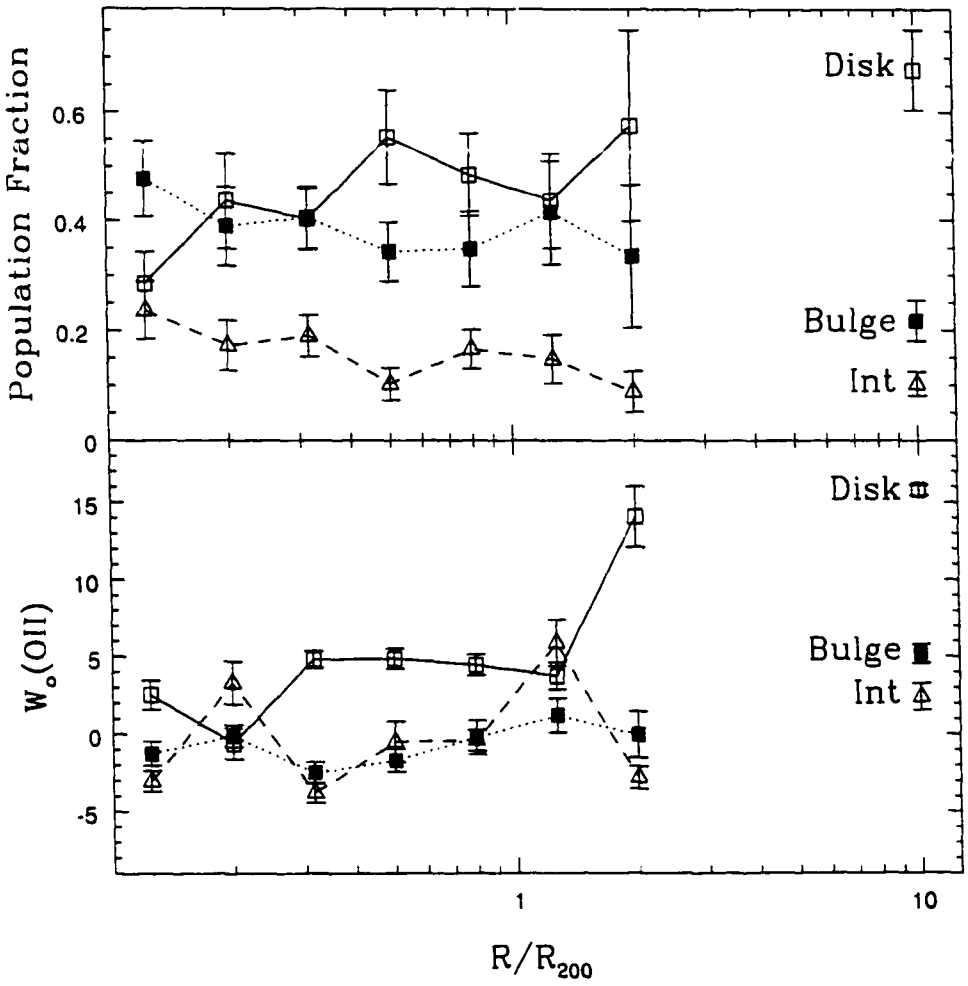

Figure 3.1: The top panel shows the fraction of galaxies in each B/T class as a function of cluster-centric radius. Open squares, connected by the solid line, represent the D class ($B/T < 0.4$). The solid squares (dotted line) represent the B class ($B/T > 0.7$), and the triangles (dashed line) the Int class. The field values are plotted at $R/R_{200} = 10$ for display purposes only. Shown in the bottom panel is the weighted observed $\overline{W_o}$(OII) for each class of galaxy as a function of radius, with the field values again plotted at $R/R_{200} = 10$.

$R/R_{200} = 10$, for galaxies of class B, Int, and D is $\overline{W_\circ}(\mathrm{OII})_B = 5.1 \pm 0.6$ Å, $\overline{W_\circ}(\mathrm{OII})_{Int} = 2.1 \pm 0.9$ Å, and $\overline{W_\circ}(\mathrm{OII})_D = 15.8 \pm 0.3$ Å respectively. The non-zero $\overline{W_\circ}(\mathrm{OII})$ for the B class is significant at the 3σ level, and many B galaxies have quite strong emission lines (10% have $W_\circ(\mathrm{OII}) > 14.0$ Å). Thus, signs of significant star formation are found in galaxies with little or no disk component, though this may partly reflect the uncertainty in B/T. Within the cluster the $\overline{W_\circ}(\mathrm{OII})$ for B and Int class galaxies is consistent with zero, and there is little variation with radius. The $\overline{W_\circ}(\mathrm{OII})$ of D galaxies is only consistent with the field at $2R_{200}$; at smaller radii it is always less than the field value by at least 10 Å. The value of $\overline{W_\circ}(\mathrm{OII})$ depends not only on the B/T parameter, but also on the environment, in the sense that it is lower for galaxies in clusters than for galaxies with the same B/T ratio in the field.

The actual SFR of a galaxy is directly related to the luminosity of the [OII] emission line (Gallagher et al. 1989; Kennicutt 1992a; Barbaro and Poggianti 1997), although the constant of proportionality is somewhat uncertain. The relation proposed by Barbaro & Poggianti (1997) will be used here, but since the present concern is the relative SFR of cluster and field galaxies, the constant of proportionality is unimportant. The luminosity of the [OII] line is calculated from the equivalent width and the galaxy's rest frame B magnitude following Kennicutt's (1992a) relation, with the suggested extinction at $H\alpha$ of 1 magnitude. The mean SFR for field galaxies in each B/T class is $\overline{SFR}_B = 0.14 \pm 0.02$, $\overline{SFR}_{Int} = 0.10 \pm 0.02$ and $\overline{SFR}_D = 0.52 \pm 0.02$, in units of $h^{-2} M_\odot \mathrm{yr}^{-1}$. If cluster galaxies of a given B/T type had identical $\overline{SFR}s$ to corresponding field galaxies, then the mean cluster SFR at radius r could be determined from the relation

$\overline{SFR}(r) = f_B(r) \times \overline{SFR}_B + f_{Int}(r) \times \overline{SFR}_{Int} + f_D(r) \times \overline{SFR}_D$. This "predicted" relation is shown as the solid line in Figure 3.2. The error bars displayed include both the error in the $\overline{SFR}$ values of each B/T class, and the uncertainty in the population fractions in each radial bin. The observed $\overline{SFR}$ is shown as the dotted line; it varies by $0.2h^{-2}M_{\odot}\mathrm{yr}^{-1}$ over the observed radial range, but for $R < R_{200}$ it is always less than the field value (corrected for the B/T–radius relation) by more than 3σ. At $2R_{200}$ the cluster galaxies still have lower star formation by more than a factor of two, although the difference is only significant at the 1.9 σ level. This suggests that large changes in SFR may occur well outside the virial radius.

3.4 Discussion

It was shown in Balogh et al. (Balogh et al. 1997) that, on average, cluster galaxies have less star formation than field galaxies, and that there is no evidence for ongoing star formation in excess of the field at any radius. Figures 3.1 and 3.2 show that this result cannot be accounted for by assuming a universal dependence of SFR on B/T. The B/T measure, however, is not sufficient to characterize a galaxy's physical structure, as there is a large range of physical bulge and disk sizes for a given B/T. To account for a dependence of W_o(OII) on galaxy size, cluster galaxies are compared with an analogous field sample in the following manner. For every class D cluster galaxy, a corresponding field galaxy is found which has a similar redshift, B/T, and disk scale length. Only those galaxies for which a match exists are considered. Thus, a cluster and matched field sample are chosen such

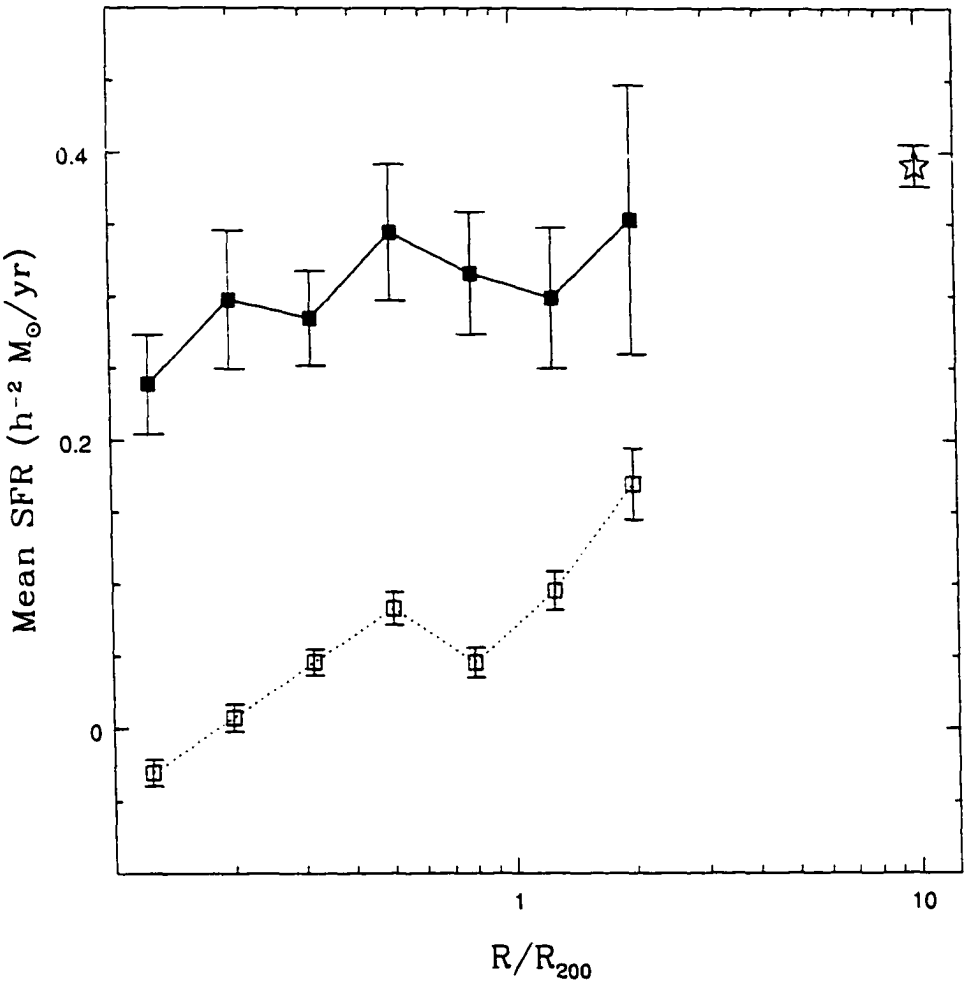

Figure 3.2: The weighted observed $\overline{SFR}$ (dotted line, open symbols) as a function of radius. The field value is represented as the large star at $R/R_{200} = 10$. The solid points (connected by the solid line) represent the $\overline{SFR}$ that would be observed at each radius if the $\overline{SFR}$ of galaxies in the B, Int and D classes was equal to its corresponding value in the field, $\overline{SFR}_B = 0.14 \pm 0.02$, $\overline{SFR}_{Int} = 0.10 \pm 0.02$ and $\overline{SFR}_D = 0.52 \pm 0.02$, in units of $h^{-2} M_\odot \mathrm{yr}^{-1}$. (see § 2.3 for details).

that the only significant difference in the selection of the two samples is the global environment of the galaxies. The $W_\circ$(OII) distributions of the cluster and matching field disk sample are shown in the top panel of Figure 3.3. A similar procedure is followed for the B class galaxies, where the field galaxies are chosen to match the cluster sample in redshift, B/T and physical bulge size; these distributions are shown in the bottom panel. For both B and D objects, the hypothesis that the cluster and field distributions of $W_\circ$(OII) are drawn from the same population is rejected with more than 99% significance by a standard Kolmogorov–Smirnov test. For the B galaxies, the difference is due to an excess of field galaxies with weak emission lines ($W_\circ$(OII)$<$ 10 Å) relative to the cluster; few galaxies are seen in either the cluster or field with stronger lines. The D galaxies, on the other hand, show a significant excess of emission lines of all strengths in the field, relative to the cluster. In the mean, galaxies in clusters have lower SFRs than galaxies in the field, independent of their B/T ratio or physical size.

Figure 3.2 indicates that the mean star formation rate in cluster galaxies is still lower than that in the field around 2 R_{200}, which is approximately the virial radius in an $\Omega = 0.2$ universe. If cluster galaxies have undergone strong bursts of star formation in the past 1–2 Gyr, as suggested by several authors (e.g., Couch and Sharples 1987; Moss and Whittle 1993; Barger et al. 1996; Caplan et al. 1996; Koo et al. 1997; Couch et al. 1998), then the elusive population of starbursting galaxies may be present beyond this radius. Ram pressure or tidal stripping may still be viable mechanisms for reducing the star formation in these galaxies without a burst if they have already passed through the cluster center at least once, a scenario for which there is some

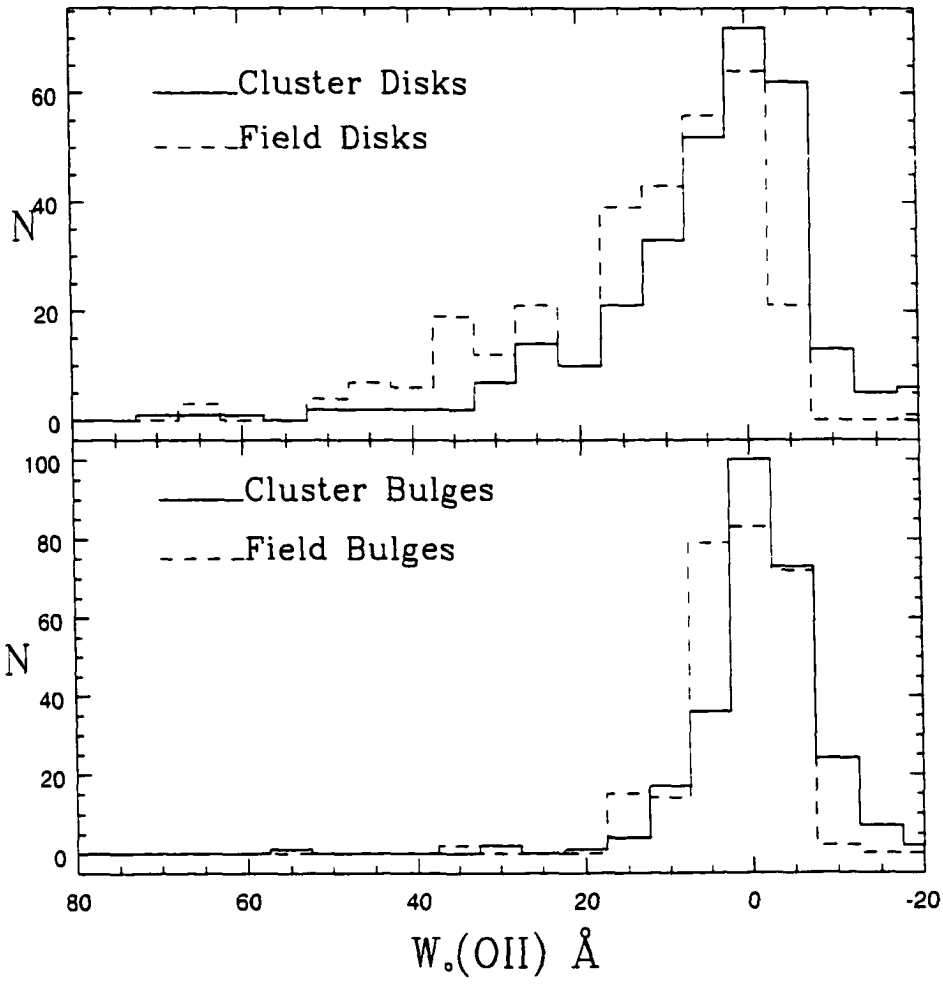

Figure 3.3: The top panel shows the W_o(OII) distributions for D galaxies in the cluster (solid line) and a morphologically matched field sample (dashed line, see § 2.4 for details). Similar distributions are shown for B galaxies in the bottom panel. For both B and D galaxies, the difference in W_o(OII) distributions between morphologically analagous cluster and field galaxies is significant with more than 99% confidence as determined by a standard K–S test.

support (Ghigna et al. 1998; Ramírez and de Souza 1998).

Alternatively, the star formation properties of galaxies may have been altered before they became bound to the cluster. In particular, Hashimoto et al. (1998) and Couch et al. (1998) suggest that galaxy–galaxy interactions and mergers are responsible for inducing starbursts in lower density environments. Such interactions would be favored in galaxy groups, which have relatively low velocity dispersions. In the hierarchical model of structure formation, groups will merge to form clusters, and it may be that the reduced star formation observed among some cluster galaxies today is the result of their previous existence in a group environment. In this case, the population of strongly star forming galaxies may be found in such groups, and not within clusters at all.

3.5 Summary

The result of Balogh et al. (1997), that current star formation among cluster galaxies is suppressed relative to an identically selected field sample, is not simply a reflection of a different morphological composition of the two populations. Although the fraction of galaxies with a significant disk component decreases from about 70% in the field to 30% in the cluster center, the $\overline{SFR}$ of cluster galaxies is much less than can be explained by this correlation alone, significant at more than the 3σ level. Cluster galaxies have less star formation than field galaxies of similar physical size, fractional bulge luminosity and redshift. Even at the virial radius, around 2 R_{200}, the amount of star formation in cluster galaxies is less than that in the field, which suggests

either that the global environment is affecting galaxy star formation at or beyond this radius (or within a group environment), or that a significant number of cluster galaxies near the virial radius have already passed through or near the cluster interior.

Chapter 4

Evidence for Recent Star Formation

4.1 Introduction

The formation and evolution histories of the galaxies that populate rare, rich clusters are currently unknown; however, it seems unlikely that a single history can accurately describe the whole population (e.g., Hashimoto et al. 1998). The giant elliptical galaxies which dominate the central regions of rich clusters seem to have been in place for well over 5 Gyr, and have only evolved passively since (e.g., Ellis et al. 1997; Bower et al. 1998; Barger et al. 1998). The remainder of the population is dominated in numbers by dwarf spheroidal galaxies and in mass by early type galaxies (E, S0, early spirals). There is strong theoretical (e.g., Gott and Gunn 1972; Antonuccio-Delogu and Colafrancesco 1994; van Haarlem and van de Weygaert 1993; Torman 1998) and observational (e.g., Zabludoff and Franx 1993; Henriksen and Jones 1996) evidence that much of the cluster galaxy population has been built up by the accretion of galaxies from the surrounding, low density, field

environment, which implies that the rich cluster environment has affected a morphological change in these galaxies. A clear correlation between galaxy morphology with local density (Dressler 1980; Dressler et al. 1997) and cluster–centric radius (Whitmore et al. 1993) has been observed. The well-known lack of emission line galaxies in clusters (Osterbrock 1960; Gisler 1978; Dressler et al. 1985b) has also been shown to correlate with cluster–centric radius (Balogh et al. 1997) and to be not entirely accounted for by the morphology–radius relation (Moss and Whittle 1993; Balogh et al. 1998). Recently, Abraham et al. (1996) and Morris et al. (1998) showed that these various effects could be interpreted as an "age" gradient, in the sense that galaxies farther from the cluster centre formed part of their stellar component more recently than the central galaxies.

Another key piece of evidence that cluster galaxies are evolving strongly is the observation that the fraction of blue, spiral galaxies in clusters increases with redshift (e.g., Butcher and Oemler 1978a, 1984, Dressler and Gunn 1983; Dressler et al. 1994; Couch et al. 1994; Rakos and Schombert 1995; Yee et al. 1995; Couch et al. 1998, but see Smail et al. 1998). This is usually referred to as the Butcher–Oemler (B–O) effect. To avoid possible misunderstanding, we will always refer to the B–O effect as this exclusively, a separate effect from the above problem of differential evolution between the cluster and field, though the two phenomena may be related. It has been shown that the star formation rate in the field also increases with redshift (Broadhurst et al. 1988; Lilly et al. 1995; Rowan-Robinson et al. 1997; Tresse and Maddox 1998; Lin et al. 1999); thus, the B–O effect as we consider it here may not be an exclusively cluster–specific effect and cannot naïvely be used

as an explanation of the different populations which inhabit cluster and field environments. Furthermore, it is not clear that the B–O effect can be directly interpreted as an evolutionary effect; Kauffmann (1995) has shown that rich clusters at $z \approx 0.4$ are not the direct progenitors of low redshift, comparably rich clusters. More recently, Andreon and Ettori (1999) have shown that the higher redshift Butcher–Oemler clusters have higher X–ray luminosities than their low redshift counterparts. Since fair samples of clusters generally show either no evolution, or even *negative* evolution in the X–ray luminosity function (e.g., Henry et al. 1992; Collins et al. 1997; Vikhlinin et al. 1998; Rosati et al. 1998), this confirms that the high redshift Butcher–Oemler clusters may not be the evolutionary predecessors of the low redshift clusters.

Various mechanisms may be responsible for the transformation of a star–forming field galaxy to a passively evolving cluster member. An infalling galaxy which passes through or near the centre of the cluster may have much of its gas content stripped by the hot intra–cluster medium (ICM), following which star formation will cease (Nulsen 1982; Bothun and Dressler 1986; Balsara et al. 1994). If only gas in an extended, diffuse halo is stripped, star formation may be allowed to continue by consuming the remaining disk gas but, without infall to replenish this supply, star formation will die out on timescales of a few Gyr (Larson et al. 1980). Interaction with the ICM near the virial radius, where the ICM density is not high enough to completely strip the galaxy of its gas, may induce intense bursts of star formation (Dressler and Gunn 1983; Evrard 1991; Gavazzi and Jaffe 1987) which use up the remaining gas supply. Such bursts may also be induced by interactions with nearby galaxies (Moore et al. 1996,1998, Fujita 1998) or, near the

cluster centre, by interactions with the tidal field of the cluster (Byrd and Valtonen 1990; Valluri 1993; Henriksen and Byrd 1996; Fujita 1998).

Understanding the mechanisms responsible for this change in star formation history is necessary to appropriately correct the CNOC1 universal mass density estimate (Carlberg et al. 1996) for the difference in mass-to-light (M/L) ratio in clusters, compared with the field. The correction applied in Carlberg, Yee and Ellingson (1997b) could be compromised if a large number of cluster galaxies underwent strong starbursts which do *not* occur in the field population.

Dressler and Gunn (1983) identified a galaxy population which they later termed E+A galaxies, that have strong Balmer lines but no detectable emission lines. These galaxies (which we will hereafter term K+A to be consistent with current nomenclature) appear to have recently terminated star formation, within the $\sim$1 Gyr prior to observation. As such, they play an important part in understanding the evolutionary history of galaxy populations. Evidence for these (and related) galaxies have been found both locally (Caldwell et al. 1993; Zabludoff et al. 1996) and at moderate redshift (e.g., Sharples et al. 1985; Lavery and Henry 1986; Couch and Sharples 1987; MacLaren et al. 1988; Broadhurst et al. 1988; Fabricant et al. 1991; Abraham et al. 1996; Fisher et al. 1998; Morris et al. 1998; Dressler et al. 1999), in both cluster and field environments. Many authors have interpreted the presence of these galaxies as evidence that a large percentage of cluster galaxies recently underwent strong starbursts (e.g., Dressler and Gunn 1983; Couch and Sharples 1987; Barger et al. 1996; Poggianti and Barbaro 1996; Couch et al. 1998; Poggianti et al. 1999). However, it is still debatable whether

or not starburst and post-starburst galaxies observed in clusters are unique to these environments. Furthermore, other authors have claimed that most K+A galaxies can largely be explained as the result of truncated star formation, without a large, initial burst (Newberry et al. 1990; Abraham et al. 1996; Morris et al. 1998). It is necessary both to distinguish between these two scenarios, and to compare their relative importance in the cluster and field environments, to determine which physical processes are plausible explanations for the differential evolution of cluster and field galaxies, and to determine how these processes will affect the M/L ratio in these environments.

The CNOC1 survey (Yee et al. 1996) provides an excellent sample of galaxy spectra for which a reliable estimate of the star formation history for clusters at $z \approx 0.3$ can be determined. This is a result of (1) a large sample size (over 2000 spectra); (2) well understood, and properly correctable, selection effects; (3) an identically selected field galaxy sample over the same redshift range; (4) objective measurements of spectral indices with well understood and empirically calibrated uncertainties; and (5) consistent comparison between data and spectrophotometric models. From these data, we will attempt to specifically address the following questions. First, what fraction of galaxies in the CNOC1 sample, regardless of environment, had significant star formation truncated in the last billion years or so? If this is truly larger than the low redshift fraction, it suggests a link with the B–O effect. Secondly, how does the abundance of these galaxies in the field compare with the abundance in clusters? An overabundance in clusters would suggest that the mechanism responsible for generating these galaxies may be what leads

to the differential evolution of cluster and field galaxies. Finally, *how* is the star formation in these galaxies truncated? We will use spectrophotometric models to try to distinguish between a) truncation following a short burst; or, b) abrupt truncation without a burst.

The paper is organised as follows. In §4.2 we define our data sample and spectral index measurements. In particular, we discuss the details of our sample selection, statistical corrections, magnitude limits, and index uncertainties. Interpretation of our line indices is made based on a comparison with PEGASE (Fioc and Rocca-Volmerange 1997) spectrophotometric models, described in §4.2.4. Our galaxy classification scheme is presented in §4.3, and is based on the line indices of local galaxies and results of the PEGASE models (detailed in the Appendix). We present our results in various forms in §4.4, and take care to explore systematic effects which result from the large uncertainties on our line indices. In §4.5 we compare our results with the work of Zabludoff et al. (1996), Barger et al. (1996), Dressler et al. (1999) and others, and show that there is some consistency of results, though considerable variety in interpretation. We discuss some of the implications of these results in §4.6, and summarise our findings in §4.7.

4.2 Observations and Measurements

4.2.1 A Review of the Full CNOC1 Sample

The CNOC1 cluster sample consists of CFHT MOS images (Gunn g and r) and spectra of galaxies in the fields of fifteen[1] X-ray luminous clusters in the redshift range $0.18 < z < 0.55$, selected from the EMSS survey[2] (Gioia and Luppino 1994). The observational strategy and full details of the survey can be found in Yee et al. 1996. In particular, Yee et al. carefully consider and detail the selection effects of this sample, and describe how these are corrected for. For convenience, we repeat here some of the details in that paper relevant to the present analysis.

The spectra are obtained with the O300 grism in place, which results in a dispersion of 3.45Å per pixel and covers the rest-frame wavelength range from (approximately) [OII]λ3727 to the G-band ($\lambda \approx 4300$Å) in most galaxies. Slits are 1.″5 wide, which results in a spectral resolution of about 16.5Å FWHM. Images and spectra of galaxies in each cluster are obtained from either one, three or five MOS fields mosaiced east-west or north-south, which provide non-uniform coverage as far out as 1-2 R_{200} in projected distance for most clusters, where R_{200} is the radius ($\approx$ 1.2 h^{-1} Mpc) at which the mean interior mass density is equal to 200 times the critical density, and within which it is expected that the galaxies are in virial equilibrium (Gott and Gunn 1972; Crone et al. 1994). For $\Omega_o = 0.2$, the cluster virial radius

[1]Omitting cluster E0906+11, for which a velocity dispersion could not be computed due to an apparent double component structure(Carlberg et al. 1996).

[2]Except Abell 2390, which is not in the EMSS sample, but of comparable richness and X-ray luminosity to the other CNOC1 clusters (Abraham et al. 1996).

is equal to approximately $1.2R_{200}$. The final catalogue contains redshifts for about 2500 galaxies, including field galaxies located in front of and behind each cluster.

In order to average over effects of non-sphericity, we will combine all fifteen clusters to produce a single sample, hereafter referred to as *the cluster*. Cluster membership is determined based on the observed radial velocity difference from the brightest cluster galaxy (BCG[3]). We use the mass model of Carlberg et al. (1997c) to determine the (projected) radial dependence of the cluster velocity dispersion, $\sigma(r)$, from the average, measured dispersion, σ_1. In Figure 4.1 we plot the galaxy velocities, normalised to σ_1, against their projected radius from the BCG, normalised to R_{200}. The 3σ and 6σ contours of the mass model are shown as the solid and dashed lines, respectively. Galaxies with normalised velocities less than $3\sigma(r)$ are considered cluster members (squares), while those with normalised velocities greater than $6\sigma(r)$ comprise our field sample (circles). The population with intermediate velocities is represented by the solid triangles, and are considered "near-field". The extent of the vertical axis in this figure is limited for clarity; hence only a small fraction of the total field population is displayed. The cluster population appears well separated from the field in this figure, and exhibits a rising velocity dispersion toward the cluster centre. We will only include galaxies within $2R_{200}$ in our cluster sample, as larger radii are much more sparsely sampled.

By extracting the spectra with standard IRAF[4] routines, an error vec-

[3]Except for cluster MS 0451.5+0250, for which no redshift is available for the BCG. The velocities and positions are measured relative to the mean for this cluster.

[4]IRAF is distributed by the National Optical Astronomy Observatories which is oper-

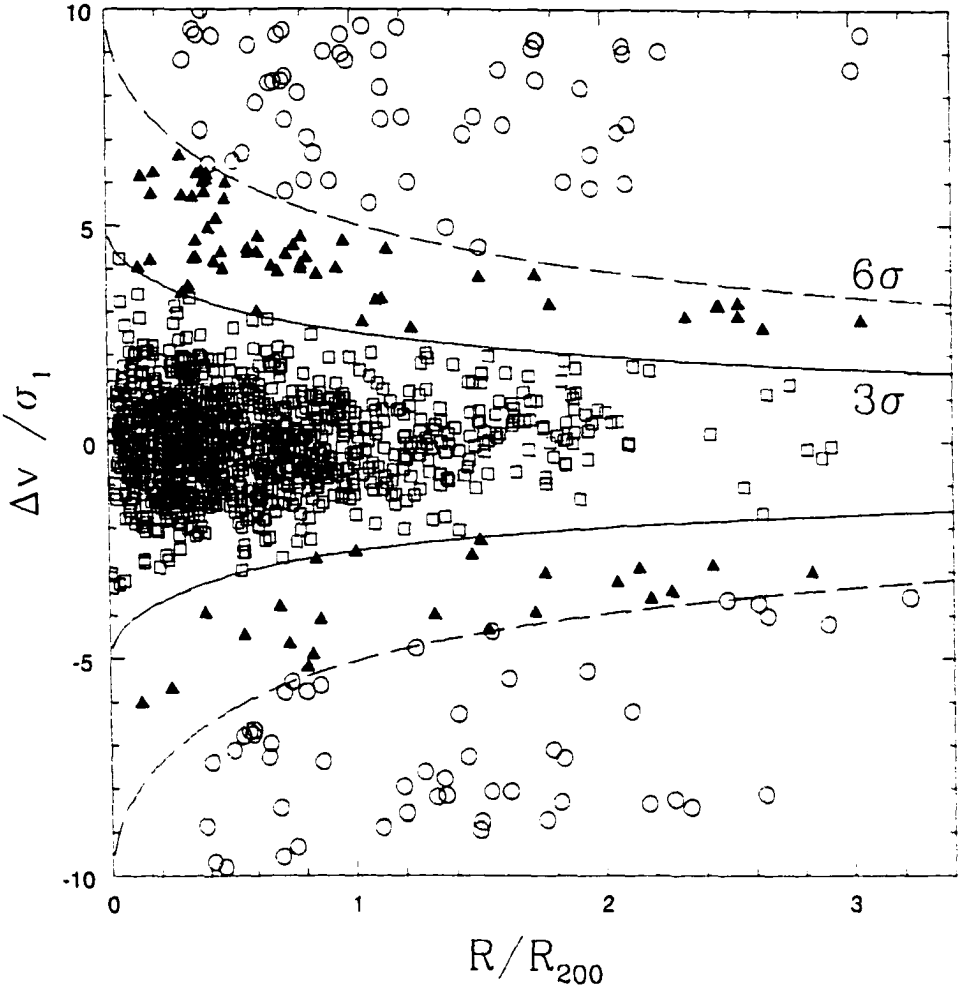

Figure 4.1: This figure shows how we define our cluster and field samples. The data plotted are radial velocity differences from the BCG, normalised to the cluster velocity dispersion, σ_1, against projected radii from the BCG, in units of R_{200}. The *solid* and *dashed lines* are the $3\sigma(r)$ and $6\sigma(r)$ contours, respectively, of the cluster mass model of Carlberg et al. (1997c). We define cluster members (*squares*) as those which lie within $3\sigma(r)$, and field galaxies (*circles*) as those with velocities greater than $6\sigma(r)$. The intermediate population (*solid triangles*) are termed "near-field". The extent of the vertical axis is limited to clearly show the cluster population; only a small fraction of the field sample is shown in this figure.

tor is created which includes Poisson errors, read noise and sky subtraction uncertainties. This allows a good determination of both the signal–to–noise (S/N) ratio of the data, and also reliable errors on any measured quantities (see §4.2.2). The S/N ratio is defined as the mean value of the flux per pixel divided by the error per pixel, in the wavelength range $4050 < \lambda/\text{Å} < 4250$. The resulting S/N distributions for the cluster and field samples are shown in Figure 4.2. The mode of the distribution is at S/N$\approx$7 per pixel (or 15 per resolution element), and 94% of spectra have S/N$\gtrsim$ 3.

The entire CNOC1 data sample, including the raw data and all measured quantities included in this paper, will soon be available from the Canadian Astronomy Data Centre (http://cadcwww.hia.nrc.ca/). All cosmologically dependent calculations in this paper are made assuming $q_0 = 0.1$, $\Lambda = 0$. The Hubble constant is parameterised as usual by $h = H_0/100$ km s^{-1} Mpc^{-1}.

4.2.2 Spectral Index Definitions

We will consider three spectral indices, tabulated in Table 4.1, which are automatically measured by an IRAF *IMFORT* routine available from the first author on request. The break strength at 4000Å (D4000) is defined as the ratio of the flux in the red continuum to that in the blue continuum. We have chosen a much narrower definition of this break than the standard definition (Hamilton 1985). There are two principal reasons for this. First, the uncertainty in the standard index value, assuming Poisson noise, was found to be a poor representation of the difference between multiple measurements of the same galaxy (this analysis is discussed further in §4.2.2.1). Reducing

ated by AURA Inc. under contract with NSF.

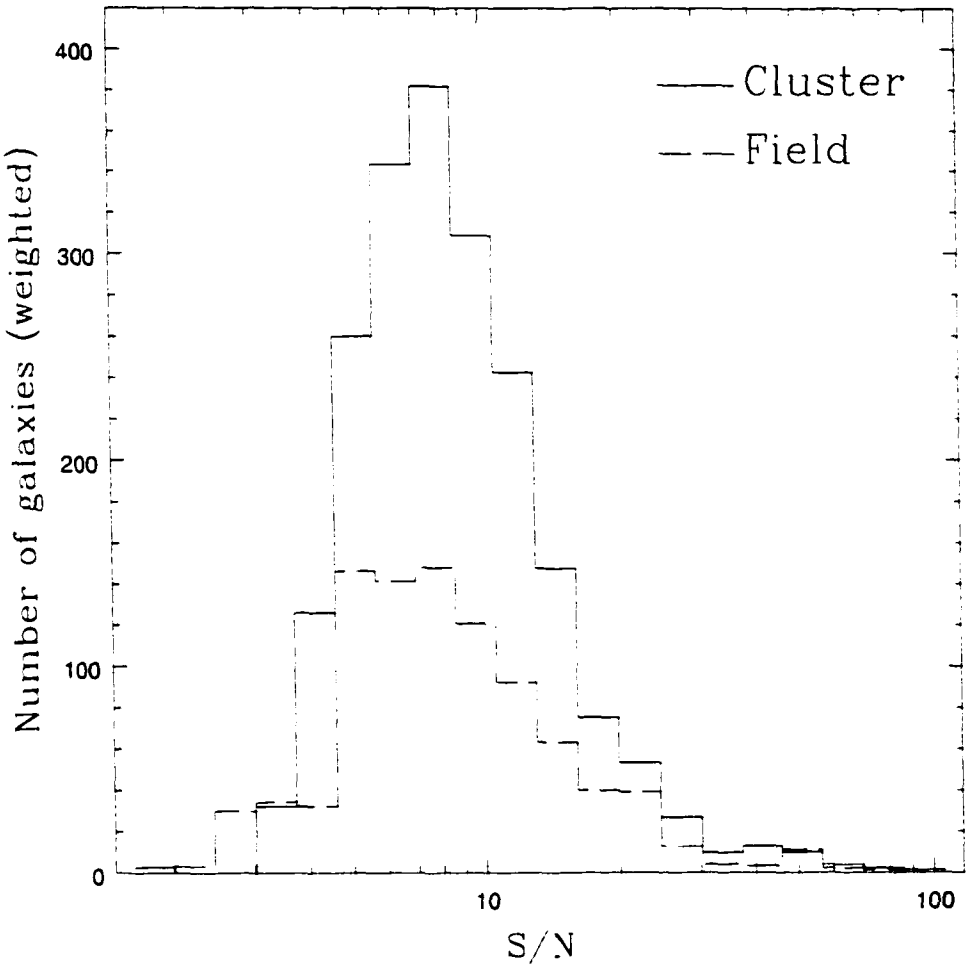

Figure 4.2: The distribution of signal-to-noise per pixel is shown for the cluster *(solid line)* and field *(dashed line)* samples. The number of galaxies in each bin is weighted as described in §4.2.3.1 and, thus, represents the number of galaxies in the photometric sample, though the distribution is computed from the spectroscopic sample.

Table 4.1: Line Index Definitions

Index	Blue continuum (Å)	Line (Å)	Red continuum (Å)
D4000	3850–3950	—	4000–4100
[OII]λ3727	3653–3713	3713–3741	3741–3801
$H\delta$	4030–4082	4082–4122	4122–4170

the width of the continuum definitions significantly improved this correspondence. Secondly, the new index is much less sensitive to reddening effects, which may be important (see §4.4.4).

There are considerable advantages in using D4000 instead of the available *g-r* colour. Most importantly, computing a rest frame colour from the observed photometry requires calculating K–corrections from the very models we will be using to determine star formation histories and, thus, introduces a circular argument. Furthermore, the galaxy spectra are obtained from slits which only sample the central regions of the galaxy, while the photometry represents the integrated light from the whole galaxy. Thus, the photometric colours and observed spectral features may not arise from the same environments. (However, at $z = 0.3$, the slit width of 1.″5 corresponds to a linear size of $4.4h^{-1}$ kpc, which is a sizable region). In addition, especially for our unusually narrow definition of D4000, this index is very reddening insensitive. The principal disadvantage is that the measurement uncertainties in the D4000 measurements are generally larger than those of the *g-r* colours.

The rest frame equivalent widths of the $H\delta$ Balmer absorption line, $W_\circ(H\delta)$, and the [OII]λ3727 emission line, $W_\circ$(OII), were automatically com-

puted by summing the observed flux (accounting for partial pixels) above ($W_\circ$(OII)) or below ($W_\circ(H\delta)$) the continuum level, which itself is estimated by fitting a straight line to the flux in the continuum regions. The continuum data are weighted by the inverse square of the noise (from the IRAF noise vector), and the fit is then constructed by weighted linear regression. The blue and red continuum regions are defined in Table 4.1; the line flux is summed over the region defined "Line" in the same table. *Note that the $W_\circ$(OII) index is positive when the line is in emission, while the $W_\circ(H\delta)$ index is positive when the line is in absorption.*

It must be noted that the indices defined above (or, indeed, any such indices) are not necessarily related simply or directly to physical quantities. The value of the $W_\circ(H\delta)$ index is very sensitive to the line and continuum definitions, and also on the spectral resolution and sampling. In particular, negative values of $W_\circ(H\delta)$ do not always indicate emission, since absorption lines in the continuum regions (especially in galaxies with old stellar populations) may result in negative $W_\circ(H\delta)$ index values. Thus, caution must be taken when comparing these measurements with those of other authors; in fact, the index definition here differs slightly from that used by our own collaboration in Abraham et al. 1996.

4.2.2.1 Index Uncertainties

Errors on the spectral indices are determined from the noise vector generated from the optimal IRAF extraction. The D4000 index is simply a flux ratio and, hence, the error is determined from standard propagation techniques. Errors on equivalent width measurements are computed from equation A8

in Bohlin et al. 1983; this makes use of the uncertainties of the weighted, linear continuum fit, and the uncertainties of each pixel defined as comprising the line itself. Often, spectral regions contaminated by bright night sky line emission are very noisy, or interpolated over by hand. Since the computed error vector reaches very large values at the wavelengths of night sky lines, this effect will be reflected in the index uncertainties. Excluding from the sample all galaxies in which either of the lines at 5577 Å, 5890 Å, or 6300 Å lands within the index definitions of $H\delta$ or [OII] does not significantly change our main results.

Since spectra were obtained with up to three masks for each cluster and, also, since adjacent fields overlap by about 15″, some galaxies were deliberately observed more than once. This allows us to test the reliability of our error estimate, by comparing the difference between two measurements $(x_1 - x_2)$ with the quadrature sum of their errors, $\sqrt{\sigma_1^2 + \sigma_2^2}$. In Figure 4.3 we plot the distribution of the ratio of these two numbers, $\epsilon = (x_1 - x_2)/\sqrt{\sigma_1^2 + \sigma_2^2}$, for each of the three indices. If the true errors are Gaussian distributed with a variance given by our error estimate, the distribution of ϵ should be Gaussian with a mean of zero and variance of unity; this is shown as the solid curve for reference. All of the ϵ distributions have a variance greater than 1, and are inconsistent with the solid curves. This implies that our raw uncertainties are underestimated, which may reflect the small but inevitable systematic error resulting from the subtraction of incorrect sky levels in some cases. The 3σ clipped variance of each ϵ distribution is 1.44 for W_o(OII), 1.42 for $W_o(H\delta)$ and 1.96 for D4000. The distributions are better represented by a Gaussian of the corresponding, wider variance,

shown as the dashed lines. To compensate for this effect, we multiplied all error estimates by the appropriate value. The final index value adopted for multiply observed galaxies is the average, weighted by the square of the error, of all independent measurements (up to three).

4.2.3 The Data Sample

In order to carry out our analysis, statistical weights must be computed for all galaxies, to correct for the incompleteness of the spectroscopic sampling; this procedure is reviewed in §4.2.3.1. We then proceed to define a luminosity-limited sample, in §4.2.3.2, which will be considered for those analyses which are sensitive to such a limit. For the remainder of the analysis, for which the primary purpose is to compare properties in the cluster and field samples, we define a larger sample which is not luminosity limited, but in which the lowest quality data are excluded, in §4.2.3.3. Unless otherwise specified, this latter is the data sample that will be discussed in the remainder of the paper.

4.2.3.1 Data Weights

Since spectra are not obtained for all of the galaxies observed photometrically, we must correct for this incompleteness and any selection effects that may arise as a result. These effects, and the calculation of compensating statistical weights, are considered in detail in Yee et al. 1996; we review them briefly here. The main selection criterion is apparent magnitude; a smaller fraction of faint galaxies are observed spectroscopically, relative to brighter galaxies. The magnitude weight W_m compensates for this effect. A second order, geometric weight W_{xy} is computed which compensates for such effects as

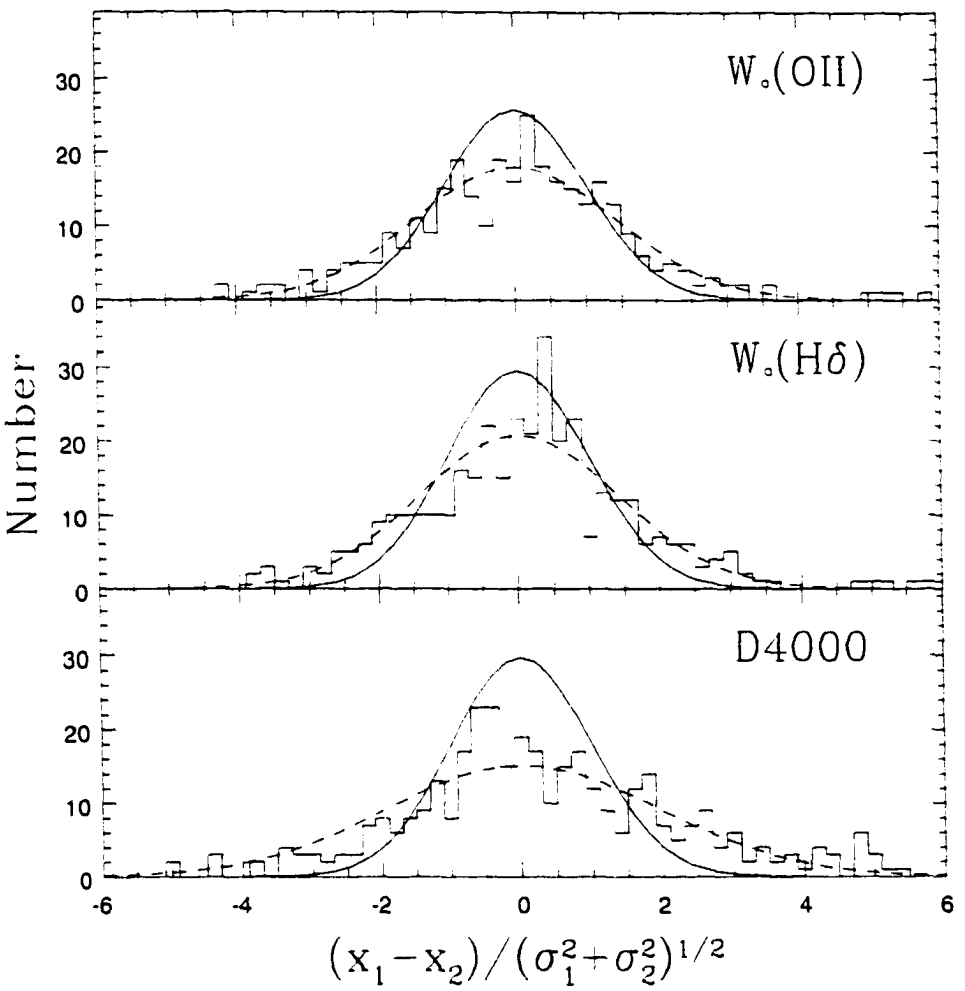

Figure 4.3: For multiply observed galaxies in the sample, we plot the ratio of the difference between two independent measurements of each index and the quadrature sum of the estimated index errors. If the true errors are normally distributed and well represented by the estimated errors, the distribution will be Gaussian with a mean of zero and variance of unity, shown by the *solid line*. The distributions are wider than this Gaussian, but consistent with one of variance 1.44 (W_o(OII)), 1.42 ($W_o(H\delta)$) and 1.96 (D4000), shown as the *dashed lines*.

the under-sampling of denser regions, and vignetting near the corners of the chip. Finally, a colour weight W_c is computed to account for the fact that bluer galaxies are more likely to show emission lines, facilitating redshift determination; however, this is a small effect, and we have checked that the inclusion of this weight does not significantly affect any of the results discussed in the present paper. Both W_{xy} and W_c are normalised so that their mean is 1.0 for the full sample. In all of our statistical analysis, each galaxy in our sample is weighted by $W_{spec} = W_m \times W_{xy} \times W_c$ to statistically correct for these selection effects[5]. We have also computed a "ring" weight, which is meant to correct for the fact that, due to the geometry of the cluster mosaics, the outer regions of clusters are less well sampled (in area) than the central regions. This correction is only important in the presence of radial gradients, if a globally averaged cluster quantity is sought. We will not use this weight in the present analysis, though we have verified that its use does not change any of the results (recall that we restrict the cluster sample to those galaxies within $R < 2R_{200}$).

4.2.3.2 Luminosity Limited Sample

We will first define a sample limited only in luminosity. Absolute r magnitudes (M_r) are calculated from the photometry, and k–corrections are made based on the g-r colours and the model spectral energy distributions of Coleman, Wu and Weedman 1980, convolved with the filter response function, for four, non–evolving spectral types (E/S0, Sbc, Scd and Im). We also correct

[5]All uncertainties in this paper that are based on $\sqrt{N}$ Poisson statistics are computed from the unweighted number of galaxies under consideration.

M_r for redshift evolution by assuming galaxies brighten by a factor (1+z) (Lilly et al. 1998; Abraham et al. 1998); thus, we correct all luminosities to the corresponding $z = 0$ values by dividing them by (1+z), though this does not significantly affect our results. We chose an absolute magnitude limit of $M_r = -18.8 + 5 \log h$, since this excludes most of the galaxies with large magnitude weights, $W_m > 5$; this limit corresponds to 1.8 mag below M* in r (King and Ellis 1985). The absolute magnitude distribution of the cluster sample (weighted by W_{spec}) is compared with that of the field in Figure 4.4. There are 1125 galaxies in this sample (omitting the BCGs and cluster members beyond $2R_{200}$), including 710 cluster members, 343 field galaxies and 72 near field galaxies.

The absolute magnitude distributions of the low ($z \leq 0.33$) and high ($z > 0.33$) redshift galaxies in this sample are shown in Figure 4.5. As a result of the fainter apparent magnitude limit in the high redshift cluster samples (Yee et al. 1996), and the luminosity evolution correction, the two distributions are comparable.

4.2.3.3 The Maximal Sample

For the purposes of comparing cluster and field galaxy populations, it is desirable to use as much of the data as possible, excluding only that of the poorest quality, and ensuring that the luminosity distributions of the cluster and field samples remain similar. From the 1823 galaxies for which both [OII]λ3727 and Hδ lie within the observed redshift range (excluding the BCGs and cluster members beyond $2R_{200}$), we first select the 1572 which have $W_m \leq 5$, so that the lowest quality data do not dominate our results; this is equivalent to

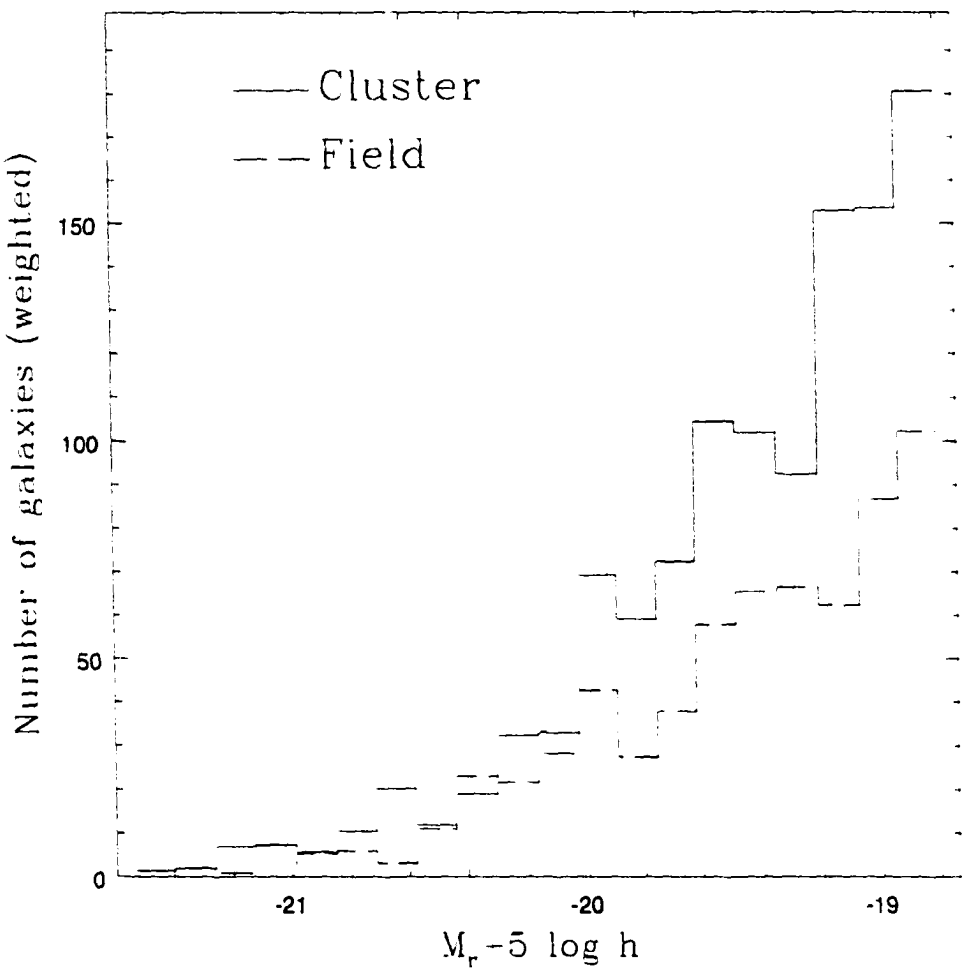

Figure 4.4: The evolution and k–corrected, absolute Gunn r magnitude distributions of the cluster (*solid line*) and field (*dashed line*), luminosity limited galaxy samples. Each bin is weighted by W_{spec}, discussed in §4.2.3.1; thus, the height of each bin represents the number of galaxies in the photometric sample, as determined from the spectroscopic sample.

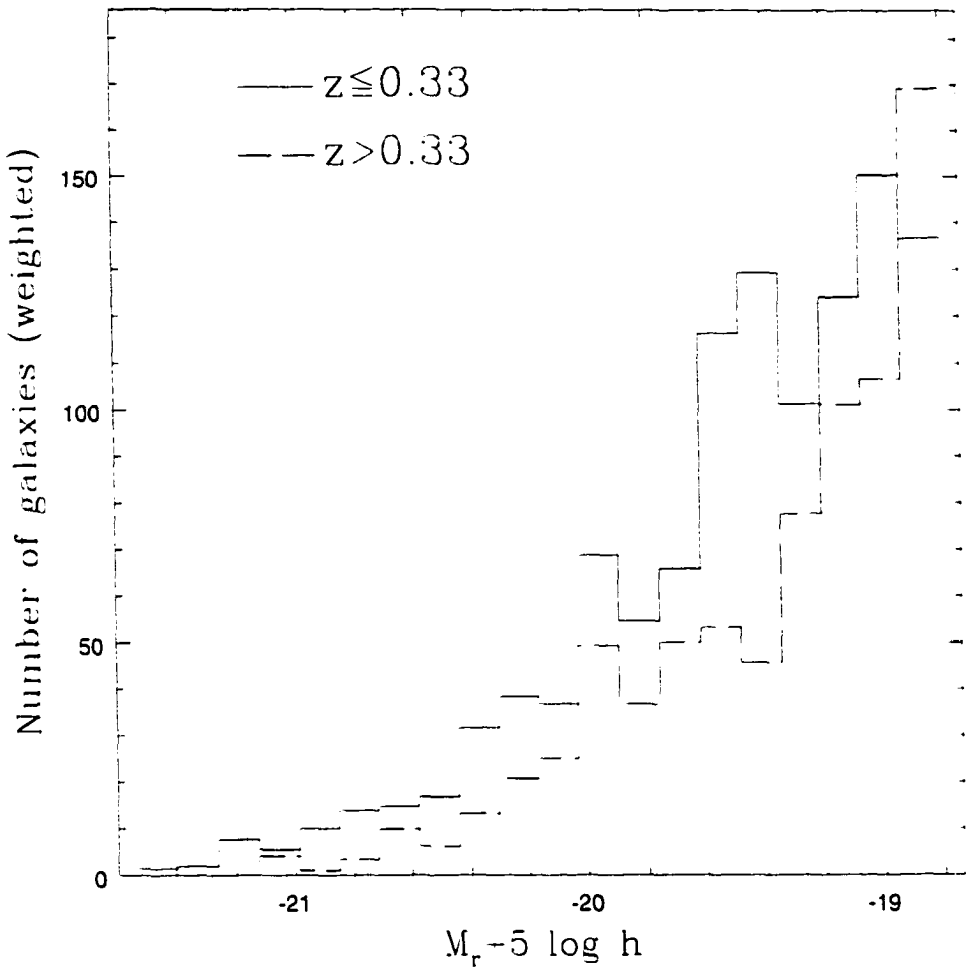

Figure 4.5: The evolution and k-corrected, absolute Gunn r magnitude distributions of the low redshift (*solid line*) and high redshift (*dashed line*), luminosity limited galaxy samples. Due both to the luminosity evolution correction, and to the fact that longer exposure times were used for the higher redshift clusters, the two distributions are similar. The histograms are weighted by $W_{\rm spec}$; see the caption of Figure 4.4.

imposing a magnitude limit which varies from cluster to cluster. It is further desirable to remove those galaxies from the sample which have extraordinarily large uncertainties in the measured spectral indices, which often result from poor subtraction of bright night sky lines. The distribution of the error estimates for each index, scaled as discussed at the end of the previous subsection, are shown in Figure 4.6. Based on these distributions, we have chosen to exclude an additional 159 galaxies with errors greater than 15Å, 5Å, and 0.5 for $W_\circ$(OII), $W_\circ(H\delta)$ and D4000, respectively. This selection introduces another second order correction to $W_{\rm spec}$, as galaxies with index errors exceeding our limit tend to be fainter. We calculate, in bins of absolute luminosity, the fraction of galaxies, weighted by $W_{\rm spec}$, removed from the sample by this selection. The remaining galaxies are weighted by the inverse of this number, which we will call $W_{\rm err}$, multiplied by $W_{\rm spec}$. $W_{\rm err}$ varies from 1 for galaxies with $M_r < -19.8 + 5\log h$, to ~ 2 for galaxies with $M_r \approx -17.1 + 5\log h$. The maximal sample consists of 1413 galaxies: 924 cluster, 407 field and 82 near field. The absolute magnitude distribution of the cluster sample (weighted by $W_{\rm spec} \times W_{\rm err}$) is compared with that of the field in Figure 4.7. Although the two distributions are similar, the cluster sample is biased toward less luminous galaxies, and the weights do not sufficiently correct the spectroscopic numbers (to be representative of the photometric sample) below $M_r = -18.8 + 5\log h$, due to the removal of galaxies with $W_m > 5$.

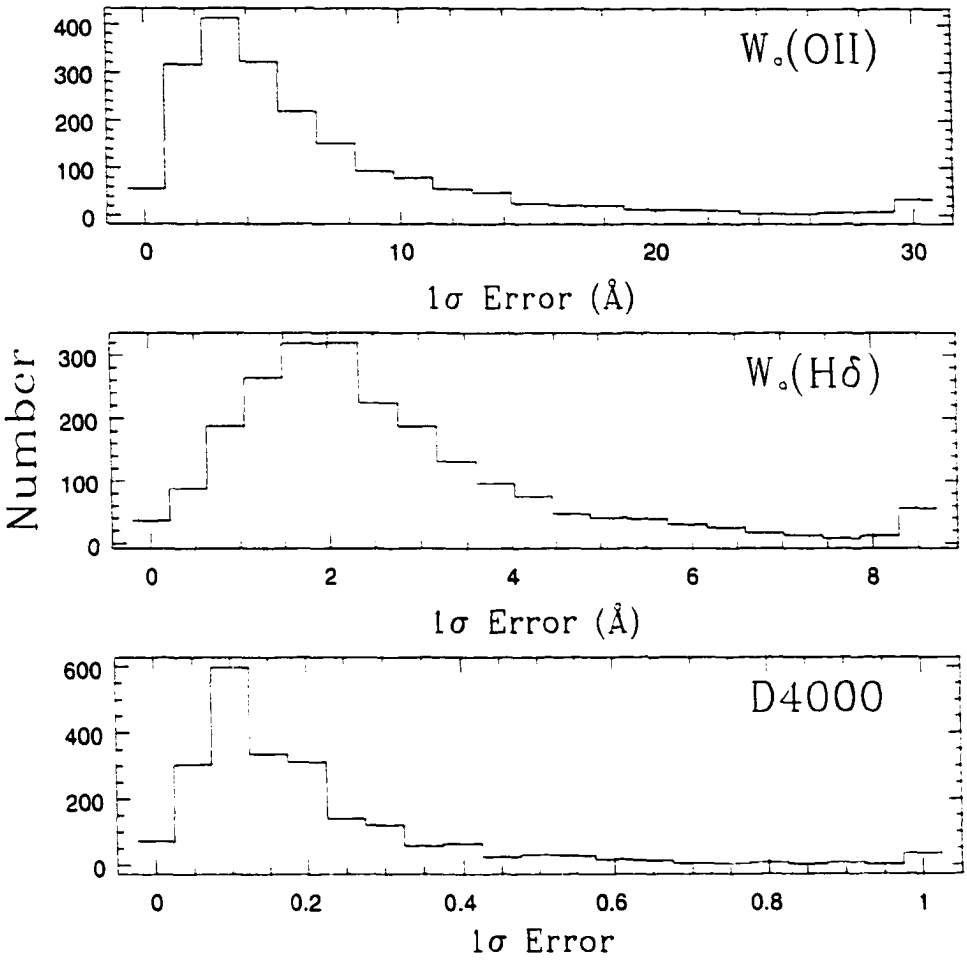

Figure 4.6: The distribution of 1σ errors on each of the three indices considered. In each case, the tail of the distribution extends to errors much greater than the mean. To avoid including data with very large uncertainties, we exclude the $\sim$ 10% of galaxies with errors greater than 15Å, 5Å, and 0.5Å for W_o(OII), $W_o(H\delta)$ and D4000, respectively, in the maximal sample. This selection criteria is compensated for by a statistical weight, $W_{\rm err}$, discussed in §4.2.3.3.

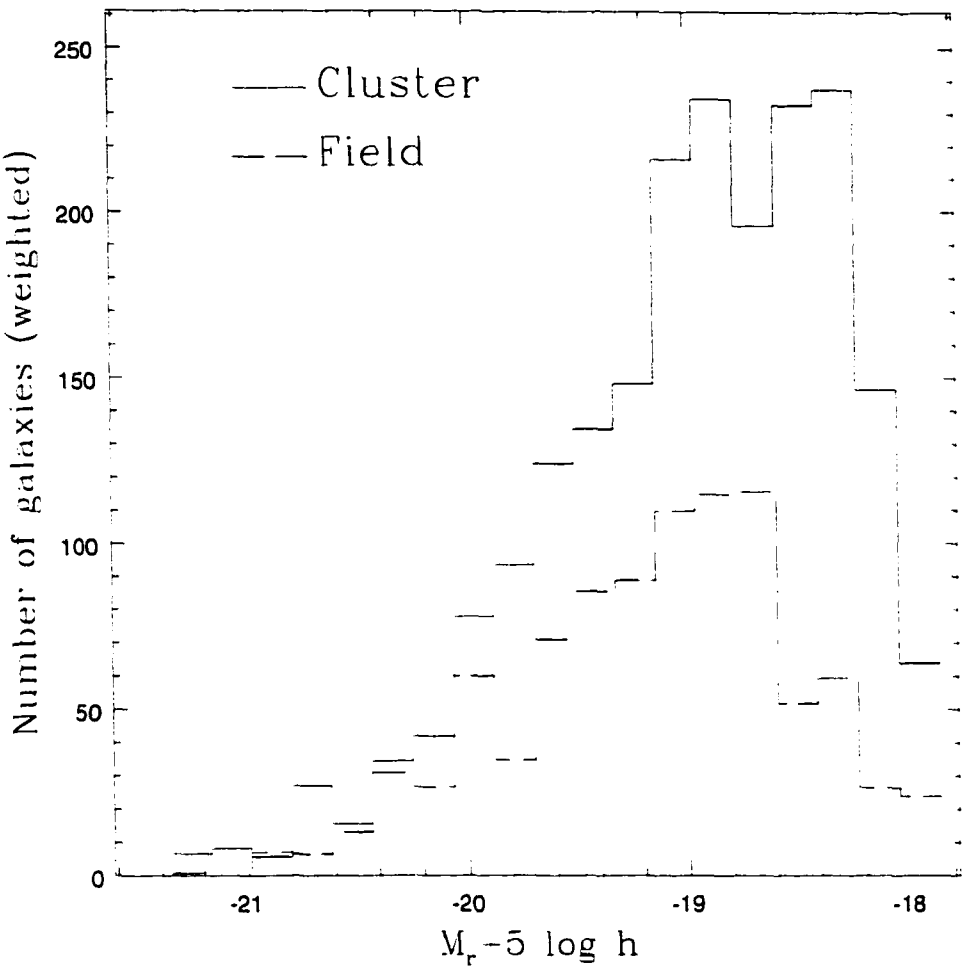

Figure 4.7: The evolution and k–corrected, absolute Gunn r magnitude distributions of the cluster (*solid line*) and field (*dashed line*) maximal galaxy samples (§4.2.3.3). The histograms are weighted by $W_{\rm spec} \times W_{\rm err}$, as discussed in the text. The cluster sample is biased to lower luminosities relative to the field sample, and a standard K–S test rejects the hypothesis that the two are drawn from the same population with $\sim 3\sigma$ confidence.

4.2.4 The PEGASE Model Parameters

As discussed in § 4.2.2, the $W_\circ(H\delta)$ index is sensitive to its definition and the manner in which it is measured. Thus, its interpretation depends on comparing it with models in which the index is measured in an identical manner. It is not possible to use model results published by other authors (e.g., Couch and Sharples 1987; Barbaro and Poggianti 1997) to interpret data unless it is shown that the indices defined for those models are comparable to those defined for the data. In light of this, we will reconstruct models in §4.3 which have been explored by other authors, but based on our index definitions.

The evolution of $W_\circ(H\delta)$ and D4000 with star formation history for solar metallicity galaxies is obtained from the PEGASE population synthesis code (Fioc and Rocca-Volmerange 1997), based on their UV to NIR spectral library. The PEGASE models predict results similar to those of the updated GISSEL96 models (Bruzual and Charlot 1993), but provide more freedom in constructing spectra with complex star formation histories; in particular, different initial mass functions (IMFs) are readily implemented. The drawback is that the models are solar metallicity; to investigate metallicity effects, we will consider the GISSEL96 models. The standard IMF adopted here is that of Salpeter (1955); the effect of adopting a truncated IMF model will be discussed in §4.4.4.

Spectral indices are determined from the model spectra in the same manner as from the CNOC1 data; that is, the same code, with the same line definitions, are run on the spectra output by PEGASE. We have not included Balmer-filling due to nebular emission; thus, the model $W_\circ(H\delta)$ indices rep-

resent an upper limit on the equivalent width one expects to observe when massive stars are present.

Care was taken to ensure that the line indices we obtain from the models correspond to the line indices measured on the data; in particular, the $W_\circ(H\delta)$ index is quite sensitive to both the resolution and the sampling of the spectra. The (rest frame) resolution of the model spectra is 10Å, comparable to the resolution of our data (about 15Å at z=0.3). However, the model spectra are more coarsely sampled than the CNOC1 data (every 10Å instead of every 2.6Å, rest frame), so we resample them to 2.6Å, interpolating using a fifth order polynomial fitting routine. We verified that each line index we measure on the CNOC1 spectra is unchanged if we first smooth the spectra by averaging every four pixels, and then resample using our interpolation algorithm.

4.3 Galaxy Classifications

There is, as yet, no clear consensus in the literature about what type of galaxy is called, for example, a "starburst", "Hδ-strong", "post-starburst", "E+A/K+A", etc. This is because the diagnostic indices are not all defined in the same way, the spectra used vary in terms of S/N and resolution, and the physical phenomena one is trying to isolate varies from author to author. In any case, such classifications are somewhat arbitrary, and there can be no objectively correct choice. For reasons discussed in §4.5, we have chosen not to use the most recent classification scheme (Dressler et al. 1999), and thus wish to state clearly how our classes are defined. These should be

compared and contrasted not only with that paper, but also, for example, the differing definitions in Couch and Sharples 1987, Barbaro and Poggianti 1997, Barger et al. 1996 and Morris et al. 1998. In most cases, the differences in classification are ones of detail, and refined precision of the evolving nomenclature.

4.3.1 Determination of the Hδ Threshold

One of the main goals of this paper is to identify a population of galaxies which were forming stars a short time (< 1 Gyr) ago, but have since stopped. These must be distinguished from galaxies which are currently undergoing star formation, and those which have not done so for a long time. We will make this distinction partly based on the spectra of local galaxies (see §4.3.2), and partly on model predictions, which is the purpose of this subsection.

In Figure 4.8 we show, as the dashed line, the evolution of the $W_\circ(H\delta)$ index for a galaxy with a constant star formation rate. As long as massive stars are present, nebular emission filling of Hδ will reduce the index by between about 1Å and 3.5Å (Barbaro and Poggianti 1997); thus, such a spectrum will not reach $W_\circ(H\delta) \gtrsim 5$Å. All normal, star-forming galaxies are therefore expected to have $W_\circ(H\delta) \lesssim 5$Å, and nebular emission lines. This is confirmed by the line indices of normal, spiral galaxies, as we show in §4.3.2.

To reach $W_\circ(H\delta) > 5$Å, the spectral light of a galaxy must be dominated by A- and early F-type stars. The presence of O- and B-type stars, which have weak intrinsic Hδ absorption and can dominate the galactic light, is the reason why the dashed line in Figure 4.8 does not reach $W_\circ(H\delta) > 6.5$Å, even without considering nebular emission contributions. For illustrative

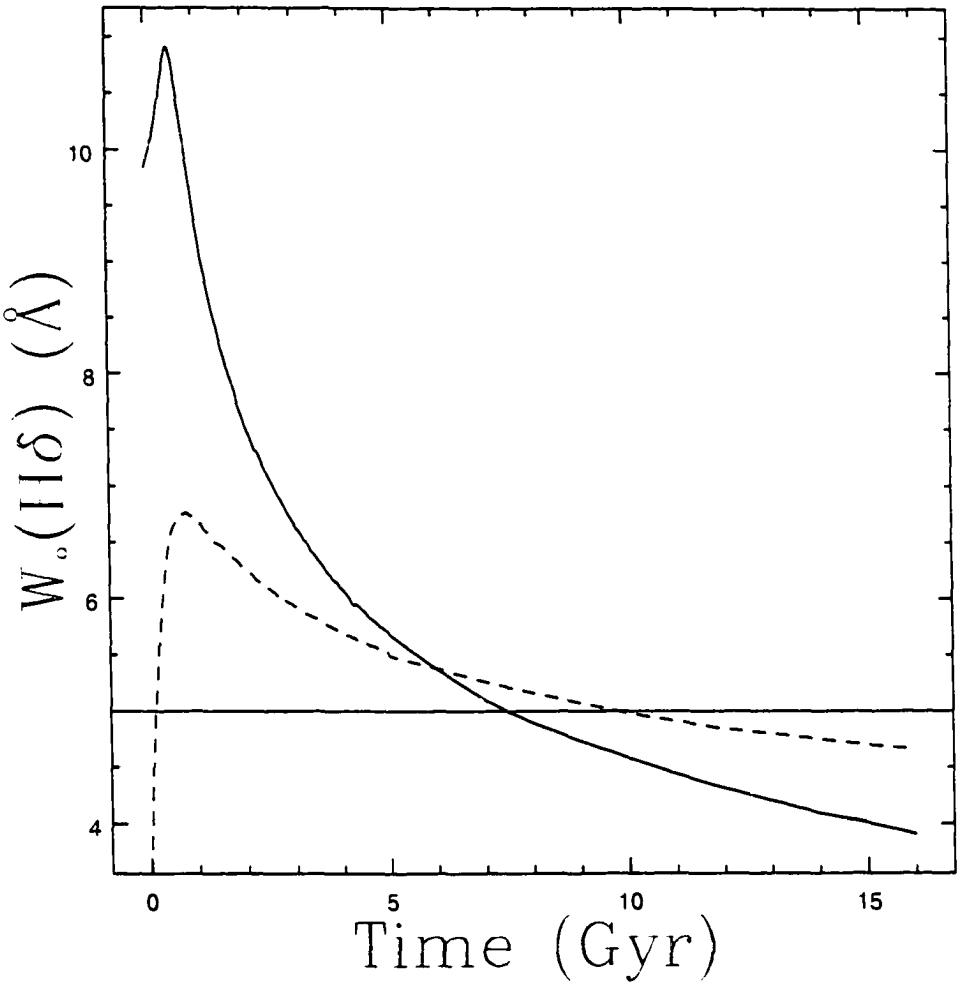

Figure 4.8: The evolution of $W_o(H\delta)$ with time, as determined from PEGASE models. The *dashed line* traces the evolution of a galaxy with a constant star formation rate, neglecting nebular emission, which will reduce $W_o(H\delta)$ by $\sim 1 - 3.5$ Å. The *solid line* is the same model, but without stars more massive than $2.7M_\odot$; there will be no emission contribution in this case. The horizontal line at $W_o(H\delta)$=5Å is the lower $W_o(H\delta)$ limit for our K+A galaxy definition.

purposes, we show the evolution of $W_\circ(H\delta)$ in Figure 4.8 for a model galaxy with a constant star formation rate, but with no stars more massive than $2.7M_\odot$ (corresponding to an A0 star, Böhm–Vitense 1992). There will be no emission contribution to such a spectrum, which therefore has $W_\circ(H\delta)> 5$Å for up to 7 Gyr; after that the accumulation of less massive stars, which have weak $W_\circ(H\delta)$ absorption, begins to contribute significantly to the light. Clearly the absence of OB–stars allows $W_\circ(H\delta)$ to reach much higher levels. As we will discuss in more detail in §4.3.3, strong $W_\circ(H\delta)$ indices may be observed following the abrupt termination of star formation, due to the almost immediate death of the O– and B–type stars. This can be visualised in Figure 4.8 as follows. A constantly star–forming galaxy will evolve at least ~ 1 Å below the dashed line; as soon as star–formation terminates, $W_\circ(H\delta)$ will increase approximately to the height of the solid line (which is an A–star dominated spectrum). For this reason, terminating star formation after 3 or 4 Gyr results in only a weak increase in $W_\circ(H\delta)$, while terminating a short burst of a few hundred Myr results in a much larger increase. In either case, emission lines will be absent in the spectrum.

Based on the results of these models, we adopt a threshold of $W_\circ(H\delta)$=5 Å as an acceptable division between galaxies with normal rates of star formation, and those with recently truncated (or otherwise anomalous) star formation. This threshold is confirmed by the line indices of normal local galaxies, as discussed in the following subsection, and may be lowered to $W_\circ(H\delta)$=3Å for the reddest galaxies, as we demonstrate in §4.3.3.

4.3.2 Definitions Based on $W_\circ$(OII) and $W_\circ(H\delta)$

We will classify the galaxies in our sample based principally on their position in the $W_\circ$(OII)–$W_\circ(H\delta)$ plane relative to the PEGASE models, and to local galaxies. We show this plane in Figure 4.9. The data plotted are indices measured by running our code with our line definitions on the local data of Kennicutt (1992b, open symbols) and Kinney et al. (1996, filled symbols). The different symbols represent the different morphological classifications as shown on the figure. The diamonds include any galaxy classified as peculiar, irregular or starburst; all other points correspond to "normal", local galaxies. The plane is divided into five regions, each of which we will discuss separately.

- **Passive Galaxy:** This is a galaxy that is not currently undergoing significant star formation, and thus evolves passively. Spectrally, we identify such a galaxy as one with $W_\circ$(OII)$<$ 5Å, which is roughly our detection limit, and $W_\circ(H\delta)<$ 5Å. The local galaxies in this category are mostly elliptical, S0 or early type spirals; the presence of these normal galaxies with $W_\circ(H\delta)$ as large as nearly 5Å justifies the need for a threshold of at least this strength to clearly isolate galaxies with anomalous star formation histories.

- **Star Forming (SF) Galaxy:** This is a galaxy that has been undergoing significant star formation for at least several hundred million years. Unless heavily obscured by dust, the [OII]λ3727 emission line should be prominent, so $W_\circ$(OII)$>$ 5Å. Furthermore, models show that $0 < W_\circ(H\delta) <$ 5Å; the lower limit is determined from the results of Poggianti and Barbaro 1996 and Barbaro and Poggianti 1997, which show

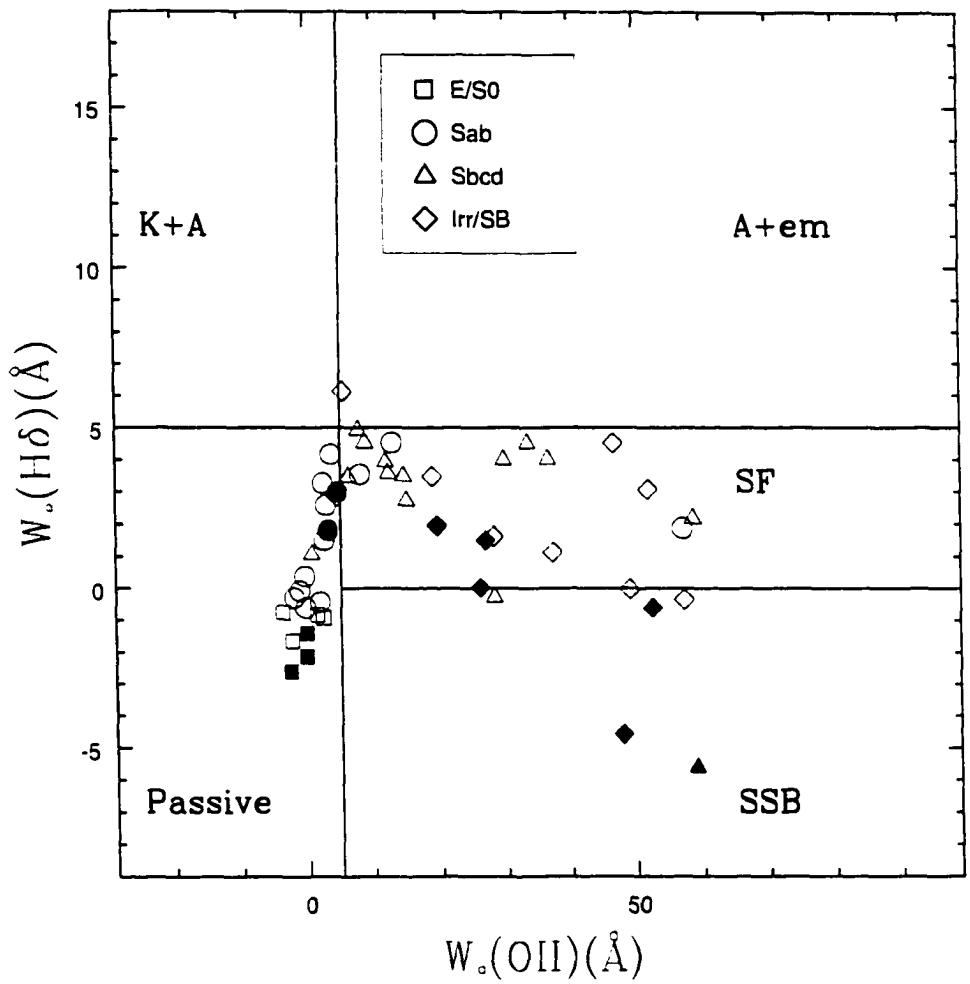

Figure 4.9: Local data of Kennicutt (1992b, *open symbols*) and Kinney et al. (1996, *filled symbols*) presented in the W_o(OII)-$W_o(H\delta)$ plane. Positive values of W_o(OII) and negative values of $W_o(H\delta)$ represent emission in these indices. The plane is divided into five regions according to the definitions in §4.3.2: Star-forming (SF) galaxies are those which have undergone significant star formation for at least several hundred Myr, while star formation in short starburst (SSB) galaxies has begun within about 200 Myr. The origin of A+em galaxies, which exhibit a strong A-star spectrum with emission lines, is uncertain; some may be dusty starbursts, or host an AGN. Of galaxies with W_o(OII)$<$ 5Å, K+A galaxies may have recently had their star formation truncated, while those galaxies with weaker $W_o(H\delta)$ indices are evolving passively, with little or no star formation.

that, if star formation has been ongoing for at least several hundred million years, the stellar absorption will dominate any nebular emission of this feature. Local galaxies that lie in this category are both late Spirals (Sc) and some galaxies that have been classified "starburst", based on the presence of strong emission lines.

- **Short Starburst (SSB):** We define a short starburst as a *short lived (< 200 Myr), large increase* in star formation rate. A galaxy that has had a high star formation rate for more that a few hundred Myr will be considered a SF and *not* a SSB galaxy. In this case, nebular emission will dominate the $W_\circ(H\delta)$ feature and, hence, both $W_\circ$(OII) and $W_\circ(H\delta)$ will be emission features (Poggianti and Barbaro 1996; Barbaro and Poggianti 1997).

- **K+A Galaxy:** This type of galaxy is one with no detectable [OII]λ3727 emission (defined as $W_\circ$(OII)$<$ 5Å), but strong Hδ absorption ($W_\circ(H\delta)>$ 5Å). Such a spectrum, which requires the presence of spectral type–A stars *without* more massive stars (which would give rise to [OII] emission lines), may be the result of a recently terminated episode of star formation, most likely following a short starburst (see, for example, Dressler and Gunn 1983, and §4.3.3). Alternatively, some of these galaxies may be extreme examples of the dust–obscured starburst scenario advocated by Poggianti et al. 1999 to describe the A+em galaxies (see below). This simple classification is based on only two line indices, and our K+A galaxies do not comprise a completely homogeneous class in terms of other spectral features, including the strength of other Balmer lines, or

the CaII H and K lines. This must be kept in mind when comparisons are made with other work in which these features are considered.

- **A+em Galaxy:** Our final category consists of galaxies with $W_\circ$(OII)> 5Å and $W_\circ(H\delta)$> 5Å. This corresponds to a galaxy with Balmer absorption lines as strong as those found only in A– and early F–type stars, but with [OII]λ3727 emission lines indicating the presence of more massive O– and B–type stars. There is not yet a clear interpretation of these spectra; the presence of OB–stars should keep $W_\circ(H\delta)$<5Å due both to emission–filling and the weaker, intrinsic $W_\circ(H\delta)$ absorption of these luminous stars. It is possible that some of the observed emission lines are due to an active nucleus; the useful diagnostic emission lines (Hα,Hβ,[NII],[OIII]λ5007) are generally redshifted out of our spectral range, so that we are unable to confirm this possibility. Alternatively, Poggianti et al. 1999 suggest that these galaxies (which they call e(a)) may be dust–obscured starbursts; we discuss this point further in §4.6, and note that the same interpretation may hold for the previously discussed K+A class of galaxy. The lone point in the Kennicutt 1992b sample which lies in this region, shown on Figure 4.9, is NGC 3034, which is in fact a very dusty, star–forming galaxy. It has been classified "starburst" (e.g., Rieke et al. 1993) based on its strong Hα emission, but has long been known to have an integrated stellar spectrum analogous to A–stars (e.g., Humason 1956); this galaxy would thus seem to be of the type advocated by Poggianti et al. 1999.

4.3.3 Additional Definitions Based on D4000

To investigate the physical origin of the K+A galaxies, we will compare our observations with the PEGASE spectrophotometric models to predict how $W_\circ(H\delta)$ evolves with galaxy colour, as determined by the D4000 index. This largely follows the method outlined by Couch and Sharples 1987 and Barger et al. 1996, applied to the PEGASE models with our current index definitions.

Barger et al. 1996 divided their sample into red and blue halves at *B*-*R*=2 (observed at $z = 0.31$). To convert this to an equivalent cut in D4000, we calculate observed-frame ($z = 0.3$) *B*-*R* and rest frame D4000 for two different star formation histories, using the PEGASE models. We show the results in Figure 4.10; the models are described in the caption. From this figure, we adopt D4000=1.45 as the value corresponding to *B*-*R*=2; this value is fairly independent (within 0.05) of the model considered.

We now plot the output of five different models in the D4000–$W_\circ(H\delta)$ plane, shown in Figure 4.11 and described briefly in the caption; we defer detailed discussion of these models to the Appendix. The local data plotted on this Figure are the same as those shown in Figure 4.9. The plane is divided into five regions similar to those defined by Barger et al. 1996, with the help of the D4000=1.45 division justified above. We have also renamed some of the classifications to correspond with our present terminology. The Passive, SF and SSB regions are expected to contain galaxies similar in star formation history to those of the same name defined in §4.3.2. Galaxies with unusually strong $W_\circ(H\delta)$ indices are defined as either red or blue Hδ–

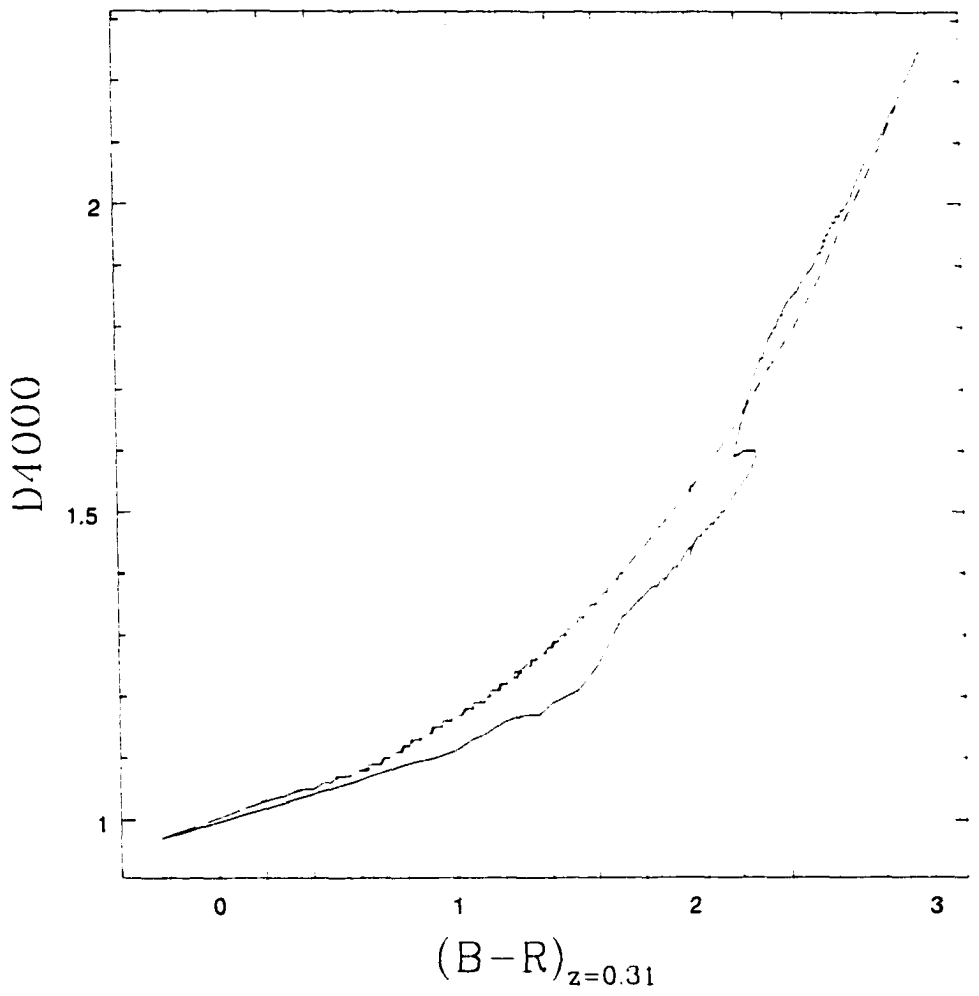

Figure 4.10: Observed frame *B-R* is plotted against rest frame D4000 for two different PEGASE models. The *solid line* represents the evolution of a galaxy which formed all its stars in an initial, instantaneous burst. The *dashed line* corresponds to a galaxy with an exponentially decaying star formation rate, with an e-folding timescale $\tau = 2$ Gyr. The vertical line represents the division adopted by Barger et al. 1996, at *B-R*=2; we find this corresponds to D4000$\approx$ 1.45.

strong (rHDS or bHDS); these will include both K+A galaxies and A+em galaxies. Furthermore, normal galaxies in the red half of this plane generally show little or no sign of star formation; both the models and real data of galaxies redward of D4000=1.45 have $W_o(H\delta)< 3$Å, and any contribution from nebular emission should be small. Therefore, we lower our $W_o(H\delta)$ threshold to 3Å for the rHDS galaxies, as only the truncated star formation models pass through this part of the plane.

Both HDS categories will contain A+em galaxies, which have W_o(OII)> 5Å. We discuss the suggestion by Poggianti et al. 1999, that these are dusty starbursts, in §4.6; whatever their origin, the A+em galaxies are not the result of truncated star formation, since such activity is still present. To isolate those spectra which most likely result from truncated star formation, we define two more galaxy classes, subsets of the rHDS and bHDS types:

- **Post-Starburst (PSB) Galaxies:** We define these to be bHDS galaxies with W_o(OII)< 5Å. The PEGASE models shown in Figure 4.11 demonstrate that such a spectrum requires the termination of a short burst of star formation. Following this event, the galaxy spectrum will remain of the PSB type for about 300 Myr. Truncated star formation without a burst (the solid line) causes the spectrum to evolve quickly ($\lesssim$ 100 Myr) through this region, and during much of this time emission lines will be present, reducing $W_o(H\delta)$ to values less than 5 Å. Thus, few (if any) bHDS galaxies are expected to result from truncated star formation without an initial starburst.

- **Post-Star Formation (PSF) Galaxies:** These are rHDS galaxies

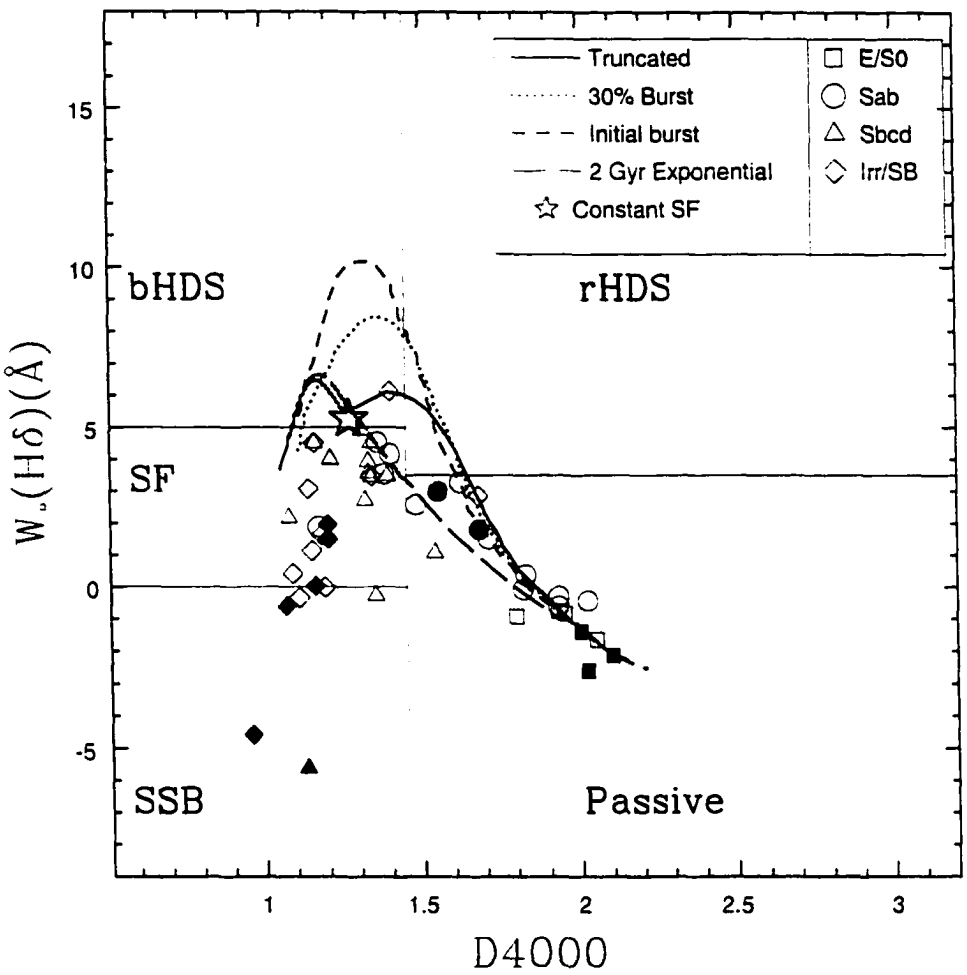

Figure 4.11: PEGASE models in the D4000–$W_0(H\delta)$ plane, for four different star formation histories which are discussed in the Appendix. Nebular emission contribution, not included in the models, will lower the $W_0(H\delta)$ index of any track with ongoing star formation, by at least 1Å. A galaxy with a constant star formation is at the locus indicated by the *star*; an exponentially declining SFR gives rise to the evolutionary track traced by the *long-dashed line*. Truncating star formation in a galaxy with constant star formation at 4 Gyr causes it to evolve along the *solid line*. The *dashed line* shows an initial, instantaneous burst of star formation, while the *dotted line* represents a 200 Myr burst, involving 30% of the stellar population of a constantly star forming galaxy (all star formation is truncated following the burst). The plane is divided into SSB (short starburst), rHDS (red Hδ–strong), blue HDS (blue Hδ–strong), SF (star-forming), and Passive. The local data are from Kennicutt (1992b, *open symbols*) and Kinney et al. (1996, *filled symbols*).

Table 4.2: Definitions of Unusual Galaxy Types

Type	$W_\circ$(OII) (Å)	$W_\circ(H\delta)$ (Å)	D4000	Interpretation
K+A	< 5	> 5	—	T,TSB
A+em	> 5	> 5	—	U
bHDS	—	> 5	< 1.45	TSB,U
rHDS	—	> 3	> 1.45	T,TSB,U
PSB	< 5	> 5	< 1.45	TSB
PSF	< 5	> 3	> 1.45	TSB,T

with $W_\circ$(OII)$<$ 5Å, and their spectra can be matched with either a recently terminated starburst episode, *or* through the abrupt cessation of longer term star formation. Galaxies evolving along either model track will spend about 300 Myr as a PSF galaxy; from the D4000 and $W_\circ(H\delta)$ indices alone, it is not possible to distinguish between these two possibilities.

4.3.4 Summary of Definitions

We have now defined six different types of "unusual" spectral types, based on models and the indices of local galaxies. All six of these types are rare, and can usually be matched by models in which star formation is truncated (T), sometimes following a short starburst (TSB); the galaxies with emission lines are not matched by either of these models, and are of uncertain origin (U). These six types, their definitions and interpretations are summarised in Table 4.2.

4.4 Results

4.4.1 Spectral Index Dependence on Cluster–Centric Radius

The measured values of $W_o(H\delta)$, D4000 and W_o(OII) in the maximal sample (§4.2.3.3) are shown in Figure 4.12, as a function of cluster–centric radius, R/R_{200}. Field galaxies are shown in the right hand panel of each graph, plotted against an arbitrary abscissa. The solid lines in each graph are the weighted median value for the field (right panel) and every 150 cluster points (left panel), with 2σ jackknife errors (Efron 1981; Efron and Tibshirani 1986). In the central regions, all three indices are inconsistent with the corresponding field value with at least 2σ confidence, and they become increasingly field-like with increasing radius. The $W_o(H\delta)$ index shows a small increase from the centre of the cluster out to R_{200}, significant at about the 2σ level; the decrease in D4000 over this range is measurable with about the same confidence. The median value of W_o(OII) is roughly constant throughout the cluster, within 2σ limits, but clearly the total distribution changes more strongly; particularly striking is the near total absence of galaxies with W_o(OII)$>$ 20Å within 0.1 R_{200}, as shown previously in Balogh et al. (1997; 1998). These trends are consistent with those observed in the individual clusters Abell 2390 (Abraham et al. 1996) and MS1621.5+2640 (Morris et al. 1998), and are qualitatively consistent with a model in which most cluster galaxies evolve passively, and the mean age of the galaxy stellar population decreases with increasing distance from the cluster centre.

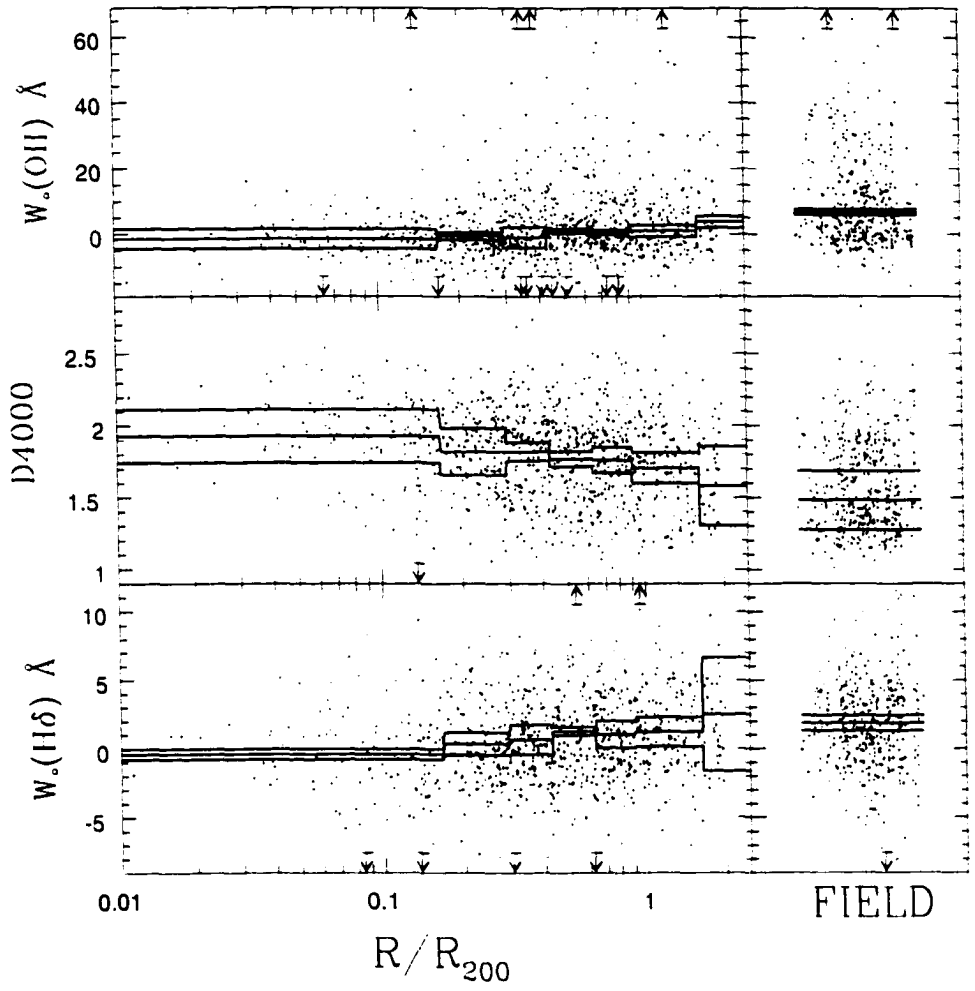

Figure 4.12: Spectral indices plotted as a function of cluster–centric radius. The sample displayed in the right hand panels is the field galaxy sample, plotted against an arbitrary abscissa for display purposes. Positive values of $W_\circ$(OII) and negative values of $W_\circ(H\delta)$ represent emission in these indices. The *solid lines* are the median index value for every 150 cluster galaxies, and the 2σ jackknife error estimates. The range of data shown is restricted to clarify the characteristics of the bulk of the data; arrows indicate data which lie outside the plotted regions.

4.4.2 Galaxies in the $W_\circ$(OII)–$W_\circ(H\delta)$Plane

We plot $W_\circ$(OII) and $W_\circ(H\delta)$ for the cluster and field (maximal) samples separately, in Figure 4.13. Each panel is divided into the same regions shown in Figure 4.9 and discussed in §4.3.2. The weighted percentage of galaxies in each region is shown, and the error associated with each number is determined assuming Poisson statistics. This error does not account for the uncertainty due to unequal scatter in this figure; we will address this issue in §4.4.2.1

The fraction of galaxies undergoing *some* type of star-formation (whether SF, SSB or A+em type) is $57 \pm 4\%$ in the field and only $29 \pm 2\%$ in the clusters. Despite the established B–O effect, the mean star formation rate in these clusters is less than that in the field, as discussed in Balogh et al. (1997; 1998). There is an apparent excess of K+A galaxies in the clusters compared with the field, significant at almost the 3σ level. As we will show in the next subsection, most or all of this difference can be attributed to the scatter in this figure, and to the slightly different absolute magnitude distributions of the cluster and field samples. In particular, the systematic effects of scatter result in an overestimation of the K+A fraction; thus, we interpret the cluster fraction of $4.4 \pm 0.7\%$ as an upper limit. This is consistent with the results of other similarly defined samples at these redshifts, as we show in §4.5.

4.4.2.1 Determining the True K+A fraction

The large errors on both indices plotted in Figure 4.13 spread the data out in this plane; this results in non-uniform scatter since galaxies from the most populated regions (Passive and SF) will preferentially scatter into neighbour-

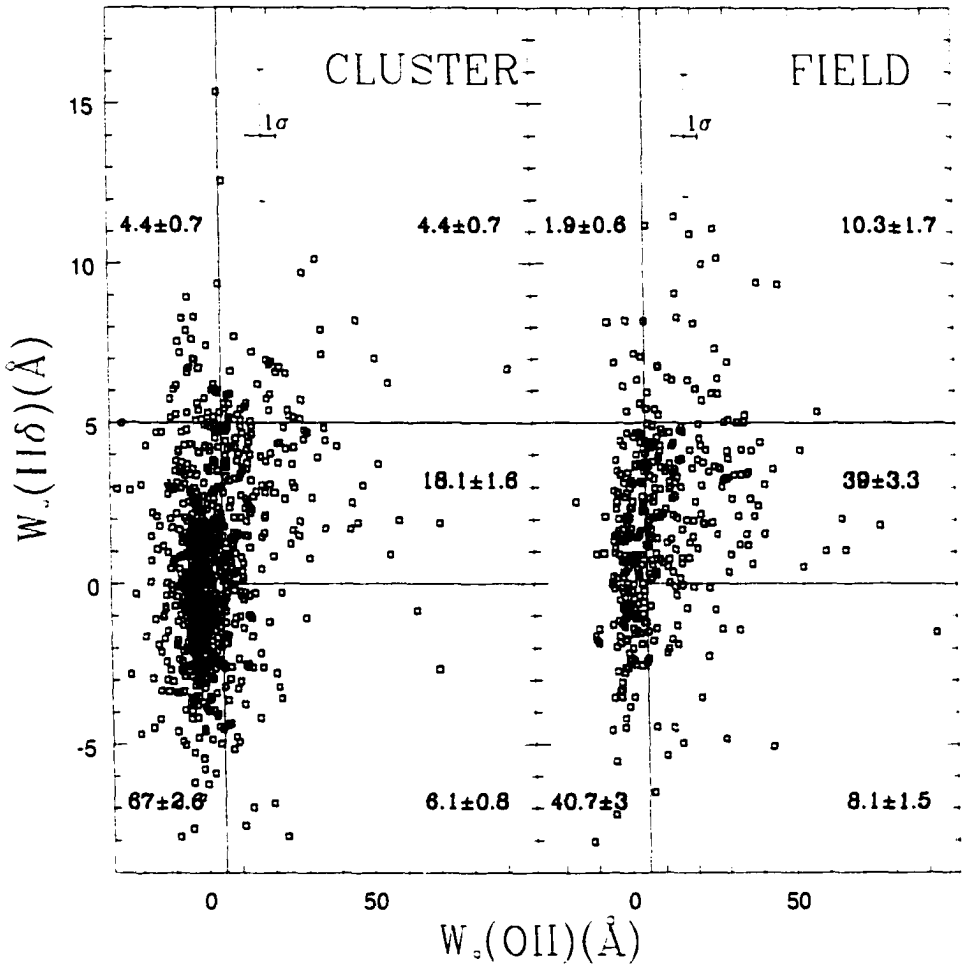

Figure 4.13: The cluster and field data presented separately in the W_o(OII)-$W_o(H\delta)$ plane, which is divided into regions defined in Figure 4.9 and discussed in §4.3.2. Positive values of W_o(OII) and negative values of $W_o(H\delta)$ represent emission in these indices. The sample error bars represent the mean 1σ error, and the number in each region represents the weighted percentage of galaxies in that region. The errors assume Poisson statistics, and do not account for the nonuniform scatter of data points throughout the plane; see §4.4.2.1 for details of this effect.

ing areas, biasing the fractions in these regions to larger values. In particular, the fraction of K+A galaxies, which occupy the high-end tail of the $W_\circ(H\delta)$ distribution, will be overestimated, and we can expect this effect to be larger in the cluster sample, where the Passive galaxy population is more dominant than in the field. We can demonstrate this by assuming that the true distribution of Passive galaxies is the same in both the cluster and the field though the absolute number of such galaxies in each environment is different. Thus, the $W_\circ(H\delta)$ distribution of galaxies with $W_\circ$(OII)$<$ 5Å should be the same if the fraction of K+A galaxies is also identical. In Figure 4.14, we show these distributions normalised to unit area in the top (field) and middle (cluster) panels. Subtracting the cluster bins from the field bins yields the distribution shown in the lower panel. This allows easy comparison of the shapes of the $W_\circ(H\delta)$ distribution in the cluster and field samples: a relative excess of cluster galaxies with a given $W_\circ(H\delta)$ would result in a negative value in the bottom panel of this figure. Instead, we see that the fraction of galaxies with $W_\circ(H\delta)>$ 5Å, corresponding to the K+A galaxies, is not significantly different in the two samples. That is, the difference between the (normalised) cluster and field samples in the two bins with $W_\circ(H\delta)>5$ Å is equal to zero within the 1σ errors. There is a 1σ excess of field galaxies with $W_\circ(H\delta)\approx$ 3 Å, which suggests that even "passive" galaxies in the field may have somewhat younger stellar populations than similar galaxies in clusters.

We will now estimate a correction for the fractions in each of the regions of Figure 4.13. The only way that a precise correction can be made is if the *a prior* distribution is known, which is not the case here; therefore, some assumptions about this distribution will have to be made. We will consider two

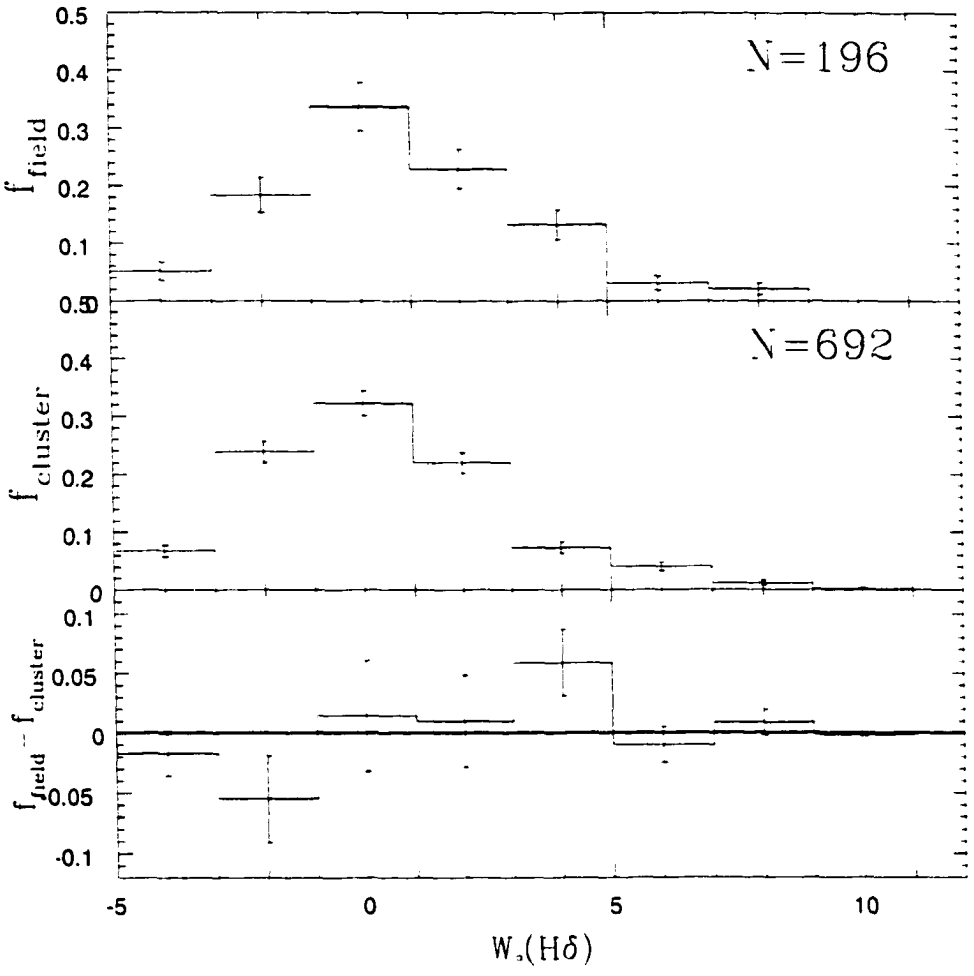

Figure 4.14: The distributions of $W_o(H\delta)$ for the subsample of galaxies with W_o(OII)< 5Å are shown for the field (*top panel*) and cluster (*middle panel*), normalised to unit area. The number of galaxies in each sample is shown in the top right corner; all error bars are 1σ, assuming Poisson statistics. The difference between these two distributions is shown in the *bottom panel.* There is no excess of cluster galaxies with $W_o(H\delta)$> 5Å, which correspond to the K+A galaxies, relative to the field.

different methods of obtaining this correction: the first is applicable to each galaxy class, but requires stronger assumptions, while the second method provides a more robust estimate but is only valid for the K+A galaxies.

Method 1: Monte Carlo Simulations: We could estimate the effects of scatter by adding appropriate noise to a "pure" sample with no scatter. We attempt to approximate such a sample by selecting galaxies with reasonably high signal-to-noise measurements (S/N> 5) and errors in both indices which are below the 25th percentile ($\Delta W_\circ$(OII)< 2.5Å and $\Delta W_\circ(H\delta)$< 1.5Å). Admittedly, this is not quite what we want, as it is quite possible that this subsample (generally with higher luminosities) is not distributed like the full sample; however, it should give an approximately accurate correction, as confirmed by the second method described below. These data are shown in the bottom panel of Figures 4.15 and 4.16 for the cluster and field samples, respectively.

We now simulate noisy cluster and field samples by adding Gaussian random noise, with a variance chosen randomly from the 1σ uncertainties of the full (cluster or field, as appropriate) data sample. We then generate several realizations, each one containing a number of points equal to the number in the true cluster or field sample. One such simulation is shown in the top panels of Figures 4.15 and 4.16. From twenty realizations, we determine, for each galaxy class, the average difference between the fraction of such galaxies in the noisy (simulated) and true (low-error sample) distributions, and the variance of that difference. We will refer to this value as the "scatter correction".

In Table 4.3, we show the measured fraction of each galaxy type, from

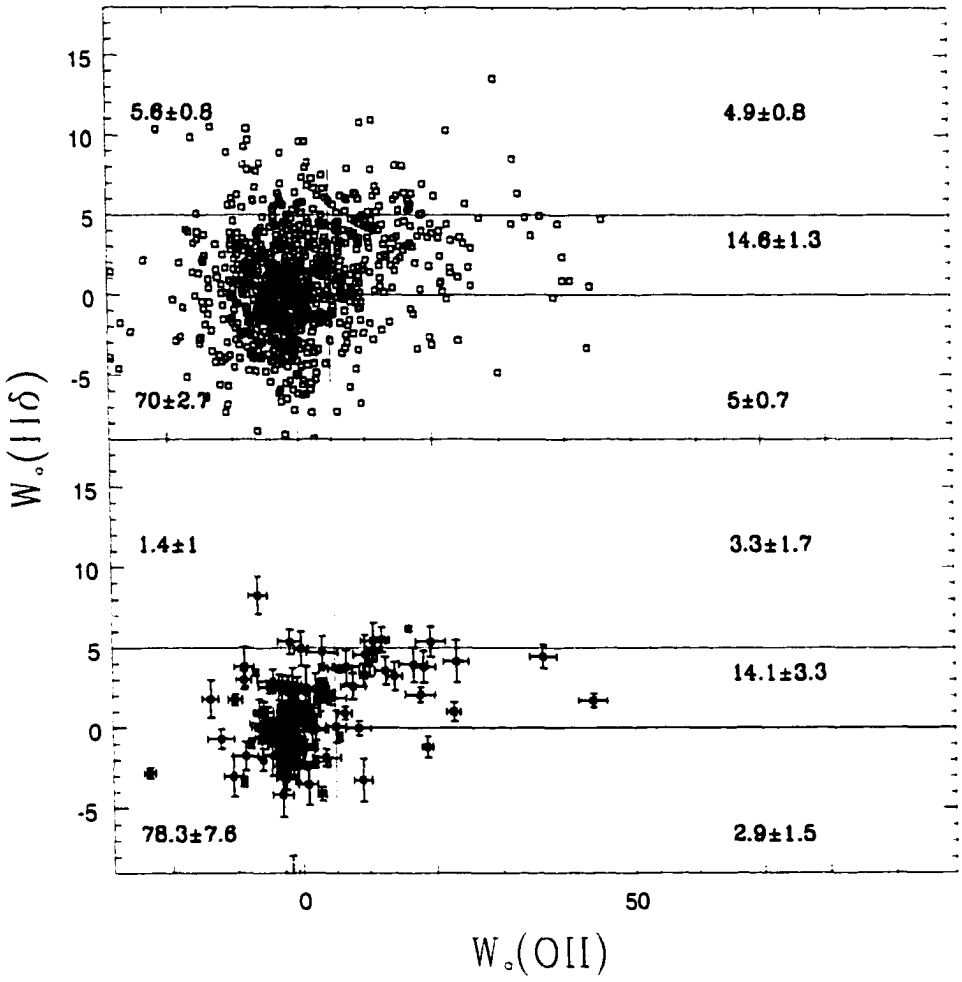

Figure 4.15: The *bottom panel* shows cluster data with S/N> 5, and errors in $W_o(H\delta)$ and W_o(OII) less than 1.5Å and 2.5Å, respectively. Error bars are 1σ. We add noise, characteristic of the full sample error distribution, to each point, and generate twenty realizations containing the same number of data points as the full cluster sample. One such realization is shown in the *top panel.* The plane is divided into the same regions defined in Figure 4.9; the numbers in each panel are the weighted percentage of objects in that bin. This experiment is used to calculate the scatter correction given in Table 4.3.

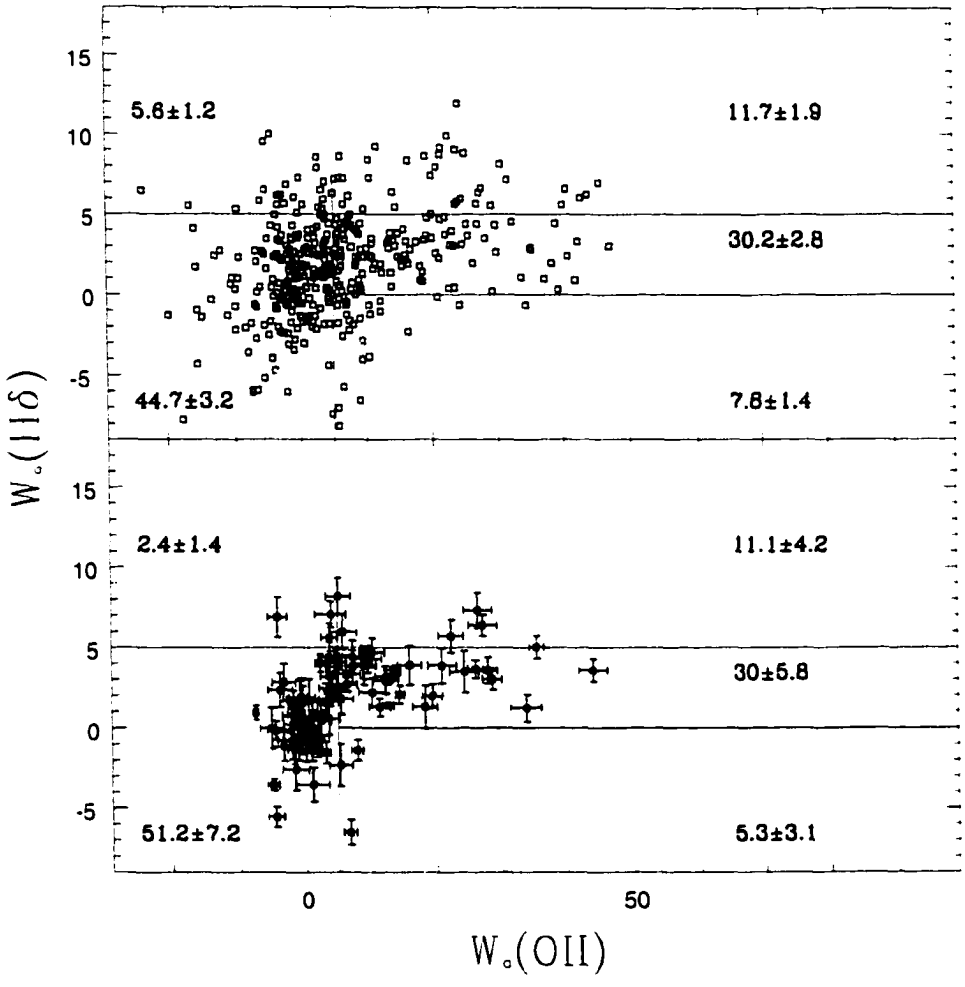

Figure 4.16: This is the same as Figure 4.15, but for the field sample. Again, the results are tabulated in Table 4.3.

Table 4.3: Scatter Corrections in the W_o(OII)–$W_o(H\delta)$ Plane

Object	Cluster (%)			Field (%)		
	Measured	Scatter	Corrected	Measured	Scatter	Corrected
K+A	4.4 ± 0.7	2.8 ± 0.5	1.6 ± 0.9	1.9 ± 0.6	2.2 ± 0.9	-0.3 ± 1.1
A+em	4.4 ± 0.7	1.4 ± 0.5	3.0 ± 0.9	10.3 ± 1.7	4.0 ± 1.3	6.3 ± 2.1
SF	18.1 ± 1.6	-2.4 ± 0.6	20.5 ± 1.7	39.0 ± 3.3	-3.3 ± 2.2	42.3 ± 4.0
Passive	67.0 ± 2.6	-7.1 ± 1.0	74.1 ± 2.8	40.7 ± 3.0	-6.2 ± 1.4	46.9 ± 3.3
SSB	6.1 ± 0.8	5.0 ± 0.8	1.1 ± 1.1	8.1 ± 1.5	3.4 ± 1.4	4.7 ± 2.1

Figure 4.13, in columns 2 (cluster) and 5 (field). Columns 3 and 6 show the estimated scatter correction. Subtracting these numbers from the appropriate measured value, including the error in this correction, yields the corrected fractions in columns 4 and 7.

We note that, in Table 4.3, the corrected K+A fraction is equal to zero within 2σ uncertainties. However, this does *not* mean that K+A galaxies are not present in the sample; to provide concrete examples we show, in Figure 4.17, sample spectra for two K+A galaxies: one found in the field and one in the cluster. Note that the CaII K line, prominent in the bottom spectrum, is weak/absent in the top spectrum; this is an example of two galaxies which are assigned the same classification (K+A), though their spectra are not identical.

Method 2: Gaussian Cloud Analysis: An alternative way to determine the overestimate of the K+A fraction is to assume that it is due only to scatter in the $W_o(H\delta)$ direction from the Passive galaxies, i.e. those with $W_o(H\delta) < 5$Å and W_o(OII)< 5Å. We can represent the $W_o(H\delta)$ index of each galaxy as a Gaussian probability function, with variance given by the 1σ index uncertainty. For each galaxy in the Passive sample, we calculate

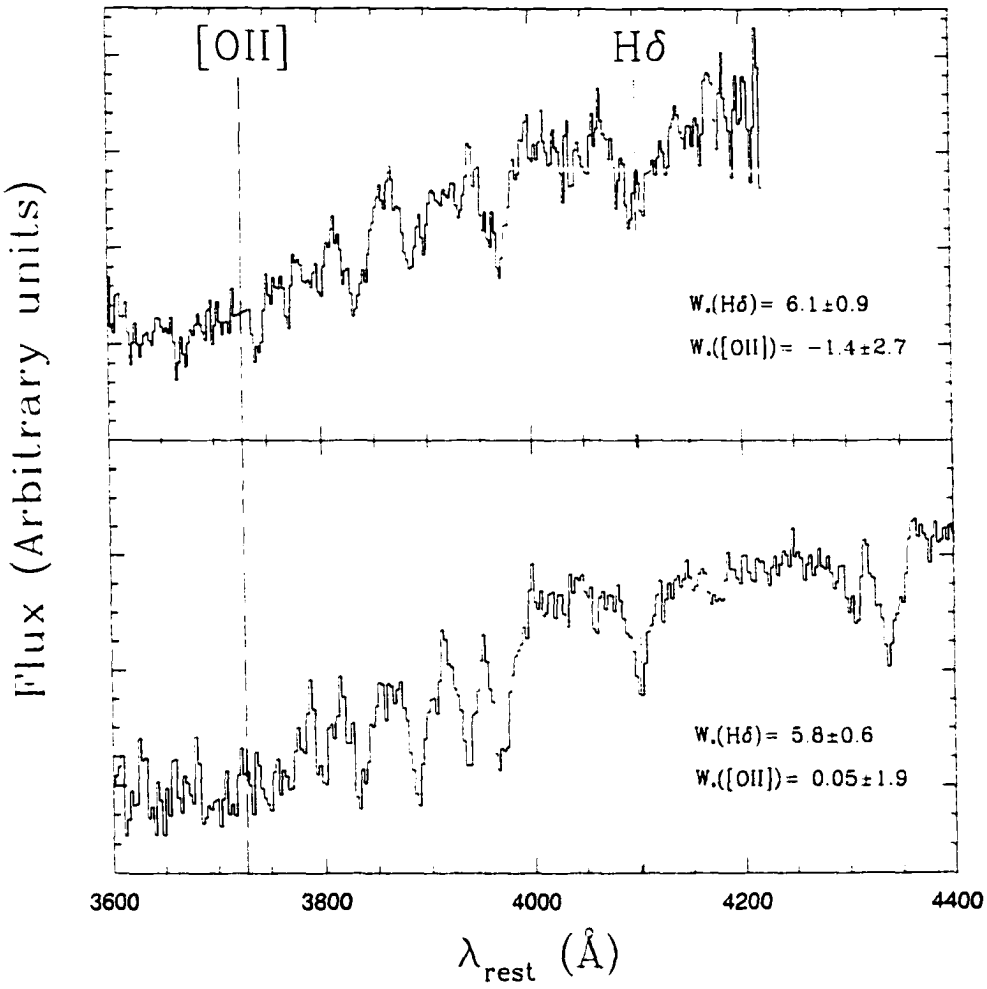

Figure 4.17: Two high S/N examples of galaxies in our sample with a K+A type spectrum, in the rest frame. The *bottom panel* shows a cluster member in Abell 2390 at $z = 0.2211$ (S/N=22, ppp #100537); the *top panel* shows a field galaxy in the field of MS1512 at $z = 0.4926$ (S/N=7, ppp #200607). These are good quality spectra, and not characteristic of typical spectra in the CNOC1 sample. Note that, although both galaxies are classified as K+A, the top spectrum lacks the strong CaII K line present in the bottom spectrum.

the probability that $W_o(H\delta) > 5$Å, and then compute the weighted sum of all these probabilities. A smaller amount of "backscatter" (from the K+A region to the Passive) will also take place, and this must be subtracted off in an analogous manner. This difference would give the total fraction of galaxies which have scattered from the Passive region into the K+A region, if the distribution of data in this plane was representative of the error-free distribution; since the uncertainties significantly blur this distribution, this difference results instead in the *maximum* amount of K+A "contamination" expected. Following this procedure, we determine that the maximum correction to the K+A fraction should be 2.8% for the cluster, and 2.5% for the field (appropriate for the maximal data sample of §4.2.3.3).

We can now estimate the *minimum* correction required by counting the weighted number of Passive galaxies with $W_o(H\delta) < -5$Å. Since the mean $W_o(H\delta)$ in the Passive region is greater than zero, and we expect few if any Passive galaxies to actually have $W_o(H\delta) < -5$, this fraction of galaxies represents the minimum amount of scatter into the K+A region (without a backscatter correction). For the maximal cluster sample, this minimum correction is 1.9%; for the field, it is 1.2%.

If we adopt the average of the minimum and maximum corrections, and half the difference to represent (arbitrarily) a 2σ uncertainty, we determine the best correction to be 2.3 ± 0.25% for the cluster, and 1.8 ± 0.3% for the field, resulting in corrected K+A fractions of 2.1 ± 0.7% and 0.1 ± 0.7%, respectively. These corrections are somewhat smaller than the ones in Table 4.3, but equivalent within the uncertainties. Although we take this method to be the more robust estimate for the K+A correction, it confirms that the

corrections listed in Table 4.3 are likely to be reasonable estimates.

Luminosity Limit: In Figure 4.18 we show the M_r distribution of the K+A sample, compared with the overall distribution of the maximal sample. This figure shows that many of the K+A galaxies lie below $M_r = -18.8 + 5 \log h$, where the magnitude weights are large, and the maximal sample is not statistically representative of a complete photometric sample. Thus, any absolute evaluation of the K+A fraction will be sensitive to the magnitude limit and statistical correction. In consideration of this, we show the results for the luminosity limited sample (§4.2.3.2) in Figure 4.19. For this restricted sample, the fraction of K+A galaxies is equal to $3.3 \pm 0.7\%$ in the cluster, and $2.7 \pm 0.8\%$ in the field; the two are equivalent within 1σ uncertainties. Adopting the Gaussian cloud scatter correction (Method 2), we find that these two numbers are overestimated by $1.8 \pm 0.4\%$ and $1.5 \pm 0.3\%$, respectively; thus, the true fraction is reduced to $1.5 \pm 0.8\%$ in the cluster, and $1.2 \pm 0.8\%$ in the field.

Summary of Corrected Values: Although the amount of scatter correction necessary cannot be precisely determined (since the true distribution of the data is unknown), the uncorrected, cluster K+A fraction of $4.4 \pm 0.7\%$ is a secure upper limit. Our best estimate of the true K+A fraction is thus obtained by applying the corrections determined by the Gaussian cloud estimate. For the maximal galaxy sample, we find the fraction of K+A galaxies is $2.1 \pm 0.7\%$ in the cluster, and $0.1 \pm 0.7\%$ in the field. For the luminosity limited sample, the fraction is $1.5 \pm 0.8\%$ (cluster) and $1.2 \pm 0.8\%$ (field). We conclude that, once scatter and luminosity effects are accounted for, there is no significant difference between the frequency of K+A galaxies

in the cluster and field environments. We will compare these numbers with the results of other surveys, both locally and at similar redshifts, in §4.5.

4.4.2.2 The Radial Dependence

The fraction of each galaxy type is plotted as a function of distance from the centre of the cluster, normalised to R_{200}, in Figure 4.20. The three "active" classes SF, A+em and SSB have been grouped together for clarity. We have corrected each value for the estimated effects of scatter, using Method 1 in §4.4.2.1, and included the uncertainty of this correction in the error bars. The galaxy population within the cluster exhibits a steadily increasing fraction of passively evolving galaxies and a steadily decreasing fraction of star forming galaxies with decreasing radius. This is at least partly expected from the morphology–density relation (Dressler 1980) but, as shown in Balogh et al. (Balogh et al. 1998) this relation cannot completely account for the decrease in star formation rate toward the centre of the cluster. The fraction of K+A galaxies within the cluster is never significantly in excess of the field value, at any radius.

4.4.2.3 The Redshift Dependence

The fifteen clusters in the CNOC1 sample cover a large range in redshift, from 0.18 to 0.55 and, thus, it is of interest to investigate the possible redshift dependence of the populations. To ensure an equitable comparison, we consider the luminosity limited sample (§4.2.3.2) here (recall that an evolution correction is applied to the luminosities). First, we show in Figure 4.21 the redshift distribution of this sample, separately for the cluster and

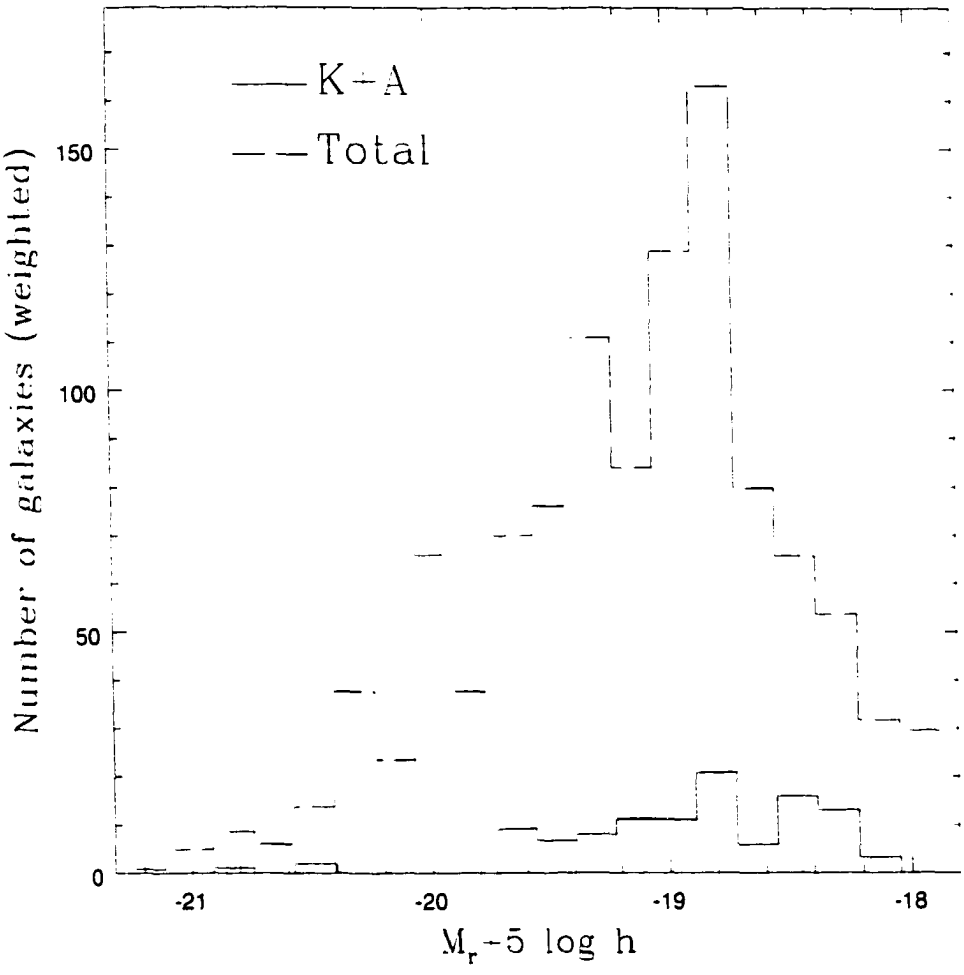

Figure 4.18: The k- and evolution-corrected absolute magnitude distribution for the K+A galaxies (*solid line*) and the full maximal sample (*dashed line*). Many of the K+A galaxies are less luminous than $M_r = -18.8 + 5\log h$, where the statistical corrections are large and the maximal sample is not representative of a complete photometric sample; the abundance of K+A galaxies is therefore sensitive to the magnitude limit and statistical correction used.

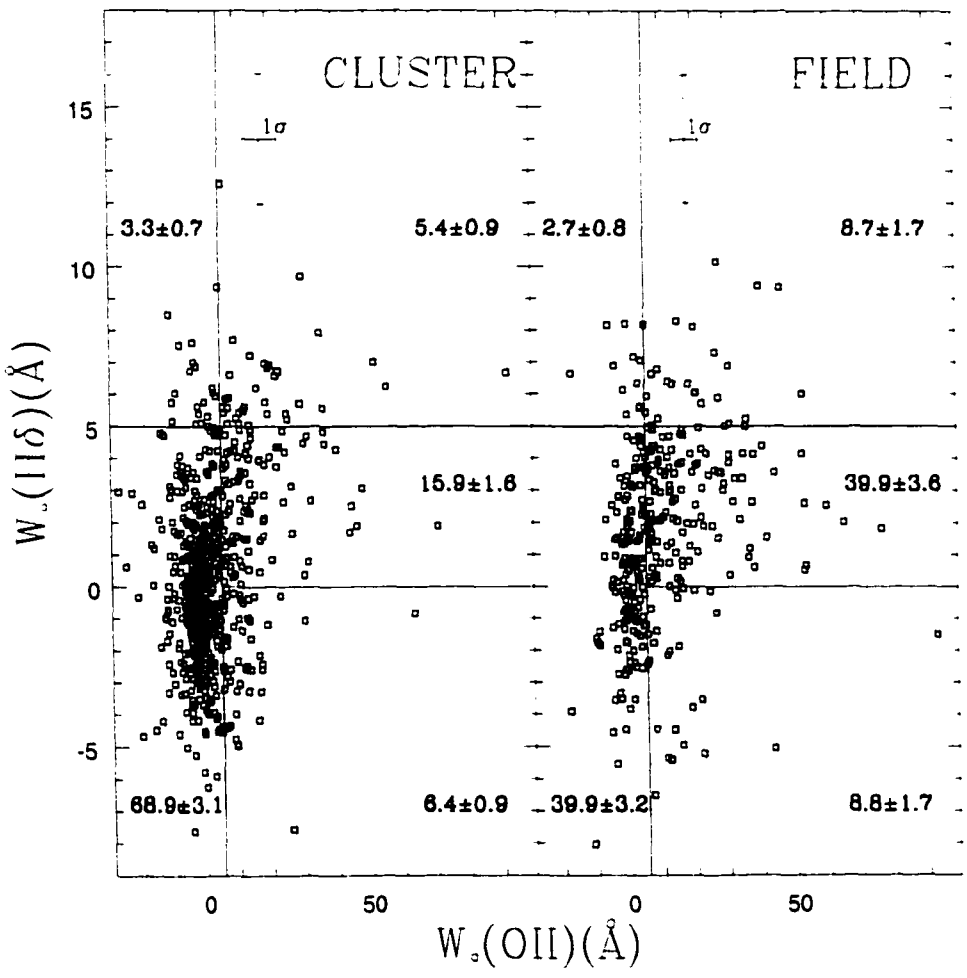

Figure 4.19: The same as Figure 4.13, but for the luminosity limited sample described in §4.2.3.2. The fraction of K+A galaxies in the cluster and field samples are equivalent within 1σ uncertainties.

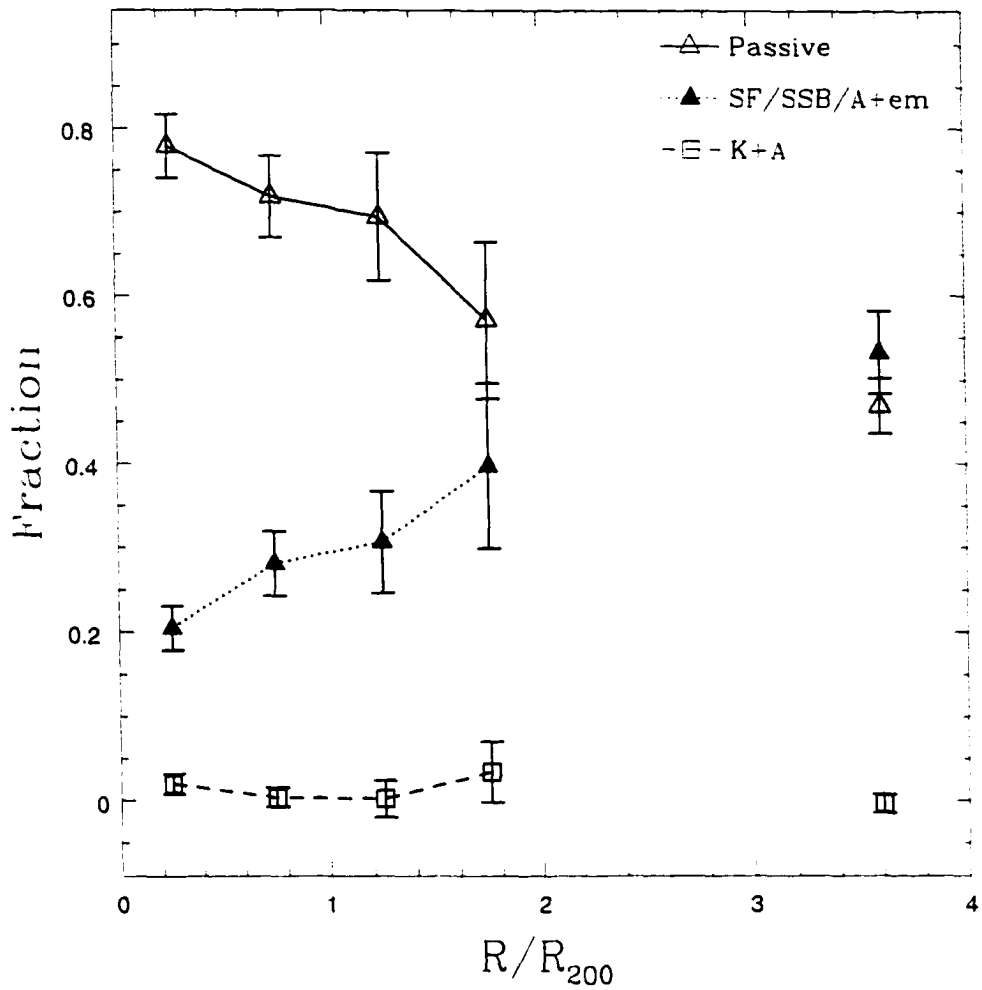

Figure 4.20: The weighted fraction of each type of galaxy, as selected based on its position in the W_o(OII)-$W_o(H\delta)$ plane shown in Figure 4.13, as a function of projected radius. The fractions and 1σ error bars are corrected for the systematic effects of nonuniform scatter, as discussed in §4.4.2.1. The connected points represent the cluster sample; the isolated points at $R/R_{200} = 3.6$ represent the values in the field sample, plotted at an arbitrary radius for display purposes only.

field. This figure shows that the cluster observations are well divided into three, well populated redshift bins: $0.15 < z < 0.28$; $0.28 < z < 0.35$; and $0.35 < z < 0.7$.

In Figure 4.22 we plot the fraction of each galaxy type, as defined in §4.3.2 and Figure 4.13, in each of the three redshift bins described above. Again, we have grouped all star-forming galaxies together (SF, A+em and SSB) for clarity, and corrected the values for the systematic effects of scatter using Method 1 of §4.4.2.1. The cluster sample is shown in the bottom panel, and the field in the top panel. A small increase in the fraction of star forming galaxies with redshift is observed, though only significant at about the 1σ level. Importantly, the abundance of K+A galaxies does not show an increase with redshift, which shows that the smallness of the fraction we observe is not just due to the fact that our sample is dominated by low redshift $z \approx 0.2$ galaxies.

4.4.2.4 The Near–Field Galaxies

In Figure 4.23 we show the W_o(OII)-$W_o(H\delta)$ relation for the near–field galaxies in the luminosity limited sample (§4.2.3.2). The near–field galaxies are a subset of galaxies with velocities intermediate between our cluster and field definitions (between 3 and 6 times the cluster velocity dispersion), and will include both galaxies that are far from the cluster ($\approx$ 50 Mpc), with velocity differences that reflect the Hubble flow, and infalling galaxies with peculiar velocities in excess of three times the cluster velocity dispersion. None of the galaxy abundances are significantly different from the field (c.f. Figure 4.19). Thus, even considering galaxies which may be in the infall regions

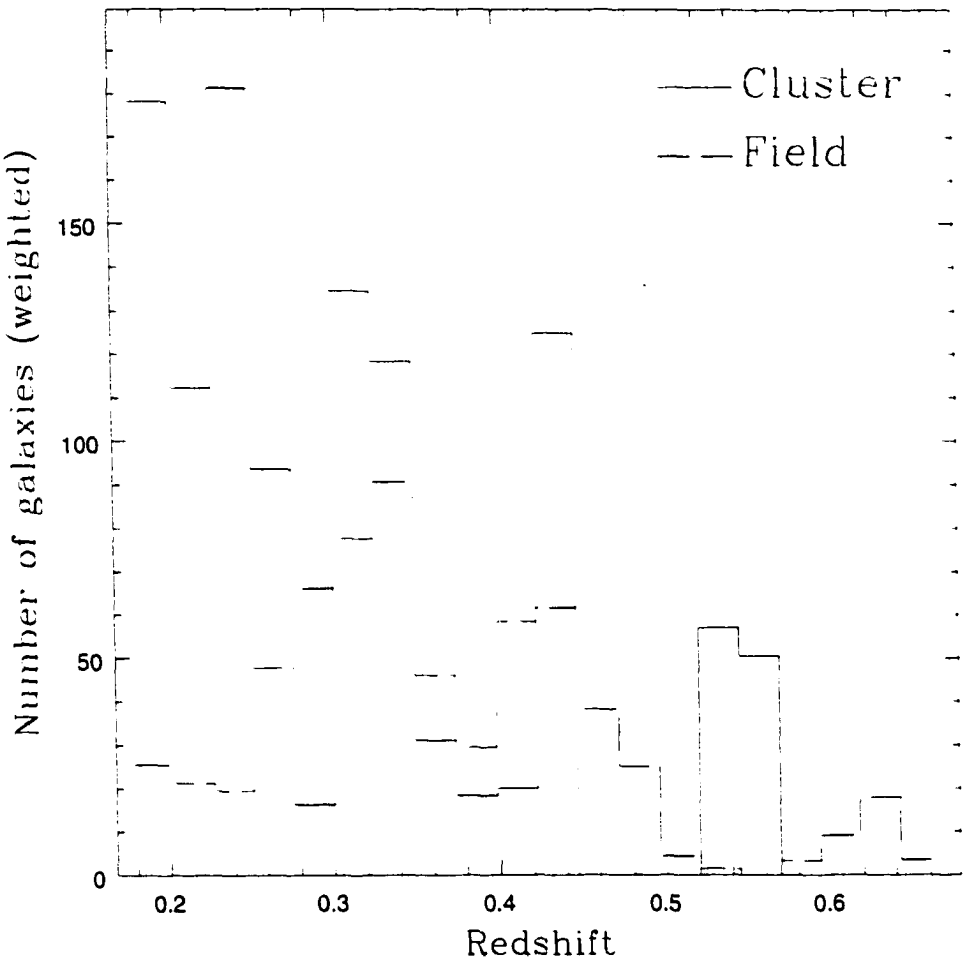

Figure 4.21: The redshift distribution of the cluster *(solid line)* and field *(dashed line)* samples, limited to galaxies more luminous than $M_r = -18.8 + 5 \log h$ (corrected for band shifting and evolution).

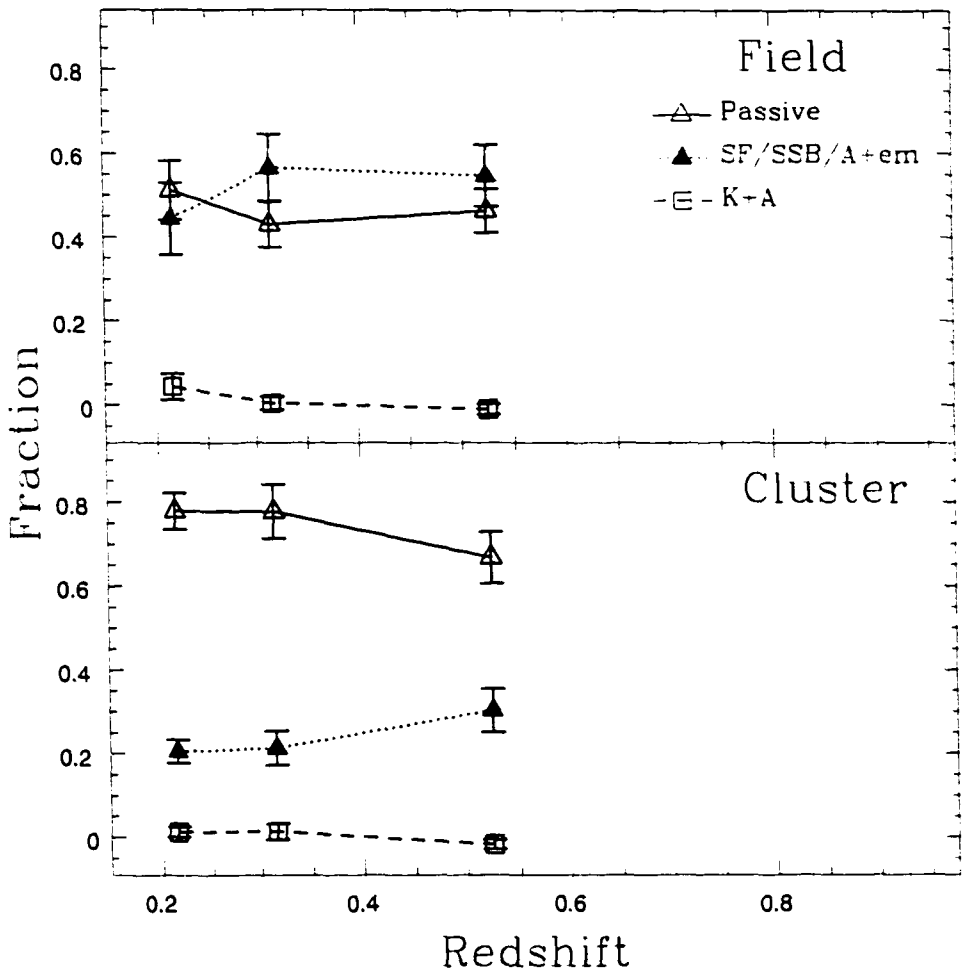

Figure 4.22: This figure shows the fraction of each galaxy population defined in §4.3.2 and Figure 4.13, as a function of redshift. Only galaxies more luminous than $M_r = -18.8 + 5 \log h$ are considered. The field galaxy sample is shown in the *top panel*, and the cluster sample in the *bottom panel*. The statistically weighted data are corrected for the systematic effects of scatter in the $W_o(H\delta)$-W_o(OII) plane, as discussed in §4.4.2.1. All error bars are 1σ. The K+A fraction is low in all three redshift bins.

of clusters, we do not detect evidence for an excess of star forming or K+A galaxies, relative to the field.

4.4.3 HDS and PSF Fractions

The measurements of $W_o(H\delta)$ and D4000 for the maximal sample (§4.2.3.3) are shown in Figure 4.24, for the cluster and field, separately. Each plane is divided into the five regions shown in Figure 4.11; the number in each panel is the weighted percentage of galaxies within it. The numbers in brackets, for the cluster sample, are from Barger et al. 1996, corrected for small differences in region definitions. We will compare these numbers in §4.5.2.

We can correct the fraction of galaxies in each region of this figure for the effects of scatter in a manner analogous to the Monte Carlo method described in §4.4.2.1; the results are shown in Table 4.4. After this correction, both bHDS (at 1.0±1.2%) and rHDS galaxies (3.6±1.4%) in clusters are not more common than they are in the field (2.7±1.8% and 9.4±2.2%, respectively).

As discussed in §4.3.3, the HDS galaxies include emission line galaxies; populations with recently truncated star formation should fall into either the PSB or PSF subclasses. In Table 4.5 we show, for the cluster and field separately, the "raw" PSB and PSF measurement, the estimated scatter correction (assuming that the relative scattered fraction is the same for the PSF/PSB classes as for the rHDS/bHDS classes) and the corrected estimate of the "true" fractions. Again, the fractions of PSB and PSF galaxies are not significantly more common in clusters than they are in the field. In both cases, the PSF galaxies are more abundant, relative to the PSB galaxies, by a factor of $\sim 5 - 10$. Though this number is quite uncertain, if the large

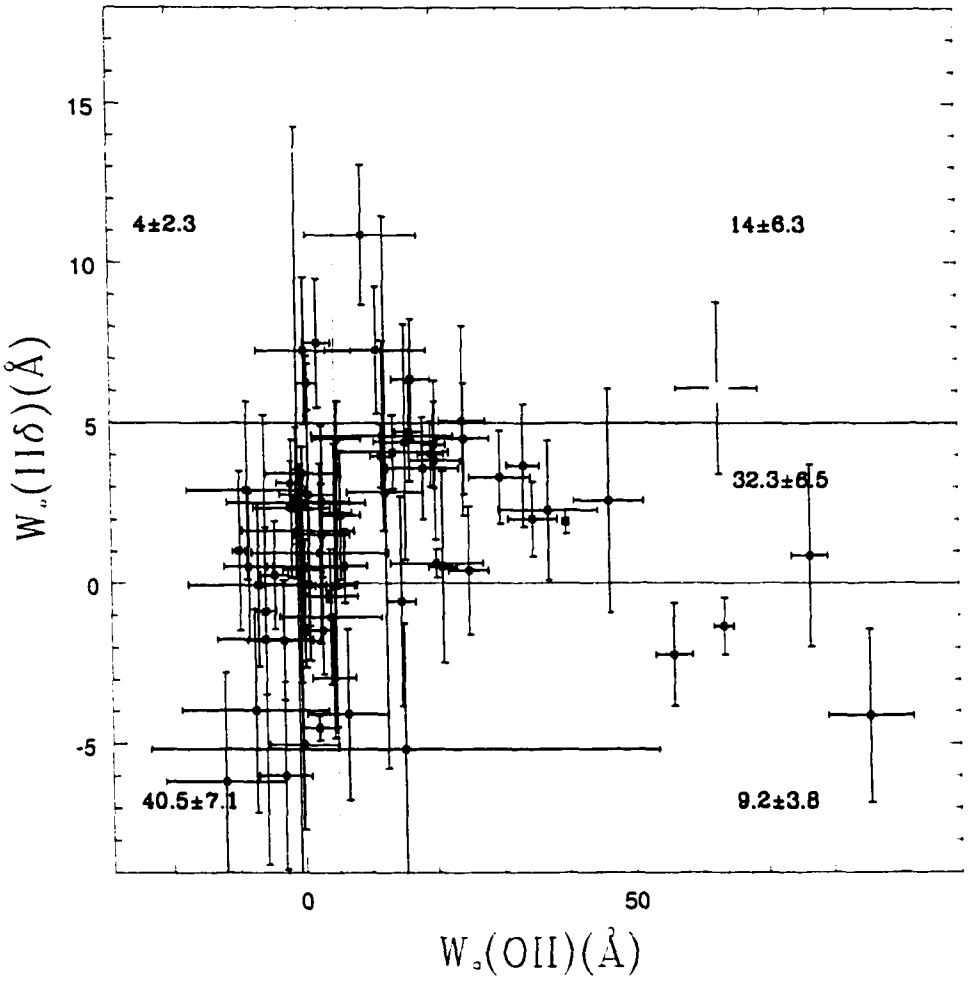

Figure 4.23: Selected from the luminosity limited sample, we show the near-field galaxy population, which has velocities intermediate between our cluster and field definitions, in the W_o(OII)-$W_o(H\delta)$ plane, with 1σ error bars. The regions are the same as in Figure 4.9, and the number shown in each region represents the weighted percentage of galaxies within that region. The error is estimated assuming Poisson statistics. The fraction of galaxies in each class is not significantly different from the field values shown in Figure 4.19.

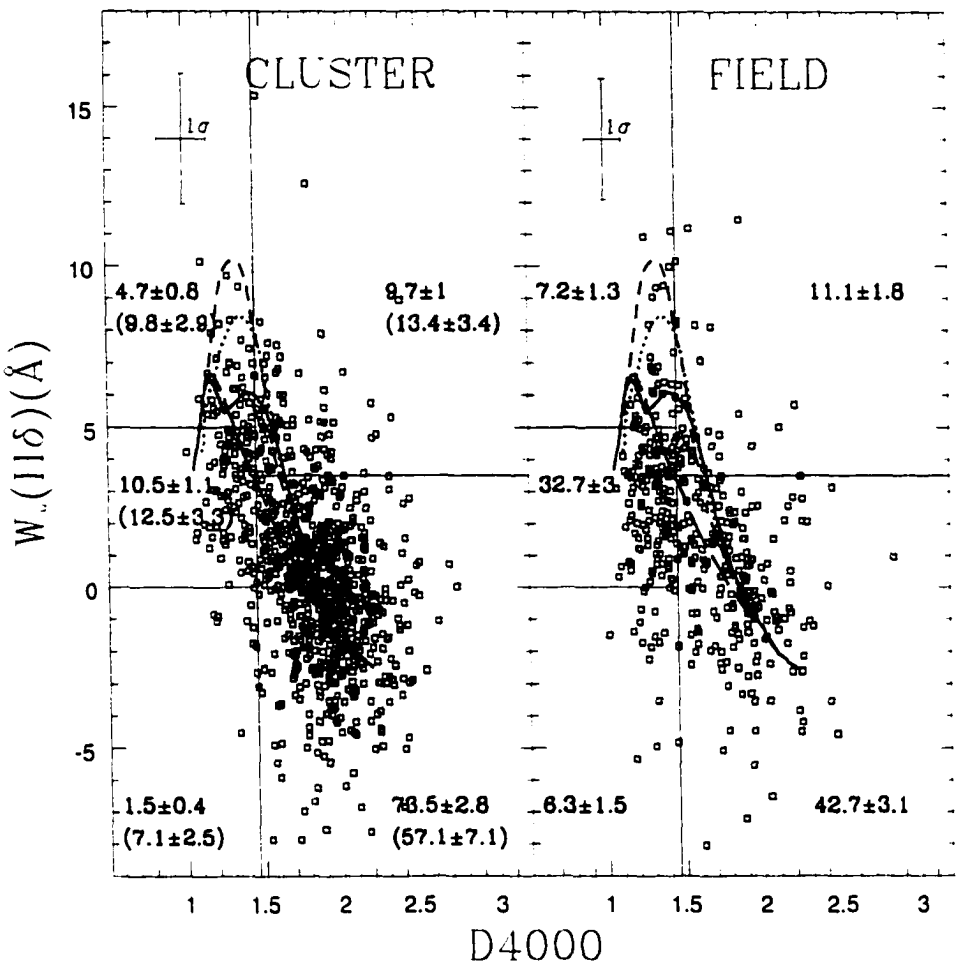

Figure 4.24: The data presented in the D4000-$W_o(H\delta)$ plane, divided into a field and cluster sample. The models and region delineations over-plotted are the same ones shown in Figure 4.11. The number in each region is the weighted percentage of galaxies in that region, and the errors assume Poisson statistics. The numbers in brackets, for the cluster sample, are from Barger et al. 1996, corrected for the small differences in region definitions. Our results are compared with those of Barger et al. in §4.5.2. The sample error bars represent the mean 1σ error.

Table 4.4: Scatter Corrections in the D4000–$W_\circ(H\delta)$ Plane

Object	Cluster (%)			Field (%)		
	Measured	Scatter	Corrected	Measured	Scatter	Corrected
bHDS	4.7 ± 0.8	3.7 ± 0.9	1.0 ± 1.2	7.2 ± 1.3	4.5 ± 1.3	2.7 ± 1.8
rHDS	9.7 ± 1.0	6.1 ± 1.0	3.6 ± 1.4	11.1 ± 1.8	1.7 ± 1.3	9.4 ± 2.2
SF	10.5 ± 1.1	-12.1 ± 1.1	22.6 ± 1.5	32.7 ± 3.0	-11.3 ± 2.2	44.0 ± 3.7
Passive	73.5 ± 2.8	-0.8 ± 1.2	74.3 ± 3.0	44.7 ± 3.1	1.7 ± 1.6	43.0 ± 3.5
SSB	1.5 ± 0.4	3.1 ± 0.7	-1.6 ± 0.8	6.3 ± 1.5	3.2 ± 1.4	3.1 ± 2.0

Table 4.5: Abundances of PSB and PSF Galaxies

Object	Cluster (%)			Field (%)		
	Measured	Scatter	Corrected	Measured	Scatter	Corrected
PSB	1.3 ± 0.4	1.0 ± 0.2	0.3 ± 0.4	0.7 ± 0.3	0.4 ± 0.1	0.3 ± 0.3
PSF	4.9 ± 0.6	3.0 ± 0.5	1.9 ± 0.8	3.6 ± 0.9	0.5 ± 0.5	3.1 ± 1.0

excess is real it may have significant consequences, as we discuss in §4.6.

4.4.4 Reddening, Metallicity and IMF Effects

A striking feature of Figure 4.24 is the abundance of galaxies, both cluster and field, with D4000 $\gtrsim 1.9$ and $W_\circ(H\delta) \gtrsim 2$Å, which are not matched by any of the models in Figure 4.11. This problem has also been pointed out by Couch and Sharples 1987, Morris et al. 1998 and Poggianti and Barbaro 1996, among others, and persists if photometric colours are considered instead of D4000. The problem has been substantially alleviated by considering the narrower D4000 index, but it still persists.

In Figure 4.25, we plot only the data with S/N >15 and uncontaminated by bright night sky lines near the $W_\circ(H\delta)$ and $W_\circ$(OII) indices. For reference, we plot the initial burst, Salpeter IMF model shown in Figure 4.11, with a

solid line. Using the *deredden* task within IRAF, we redden this model by a large amount, E_{B-V}=0.5; this moves the model to the right by about 0.15, as represented by the dotted line. This reddened model extends in D4000 nearly to the full extent of the data, and the scatter in $W_\circ(H\delta)$ at the red end is fairly uniform about it.

We also consider two other model variations. The short-dashed line in Figure 4.25 represents an initial burst model for a galaxy with super-solar metallicity, Z=2.5$Z_\odot$, generated from the updated Bruzual and Charlot 1993 models. Although this model does indeed extend to very large D4000, the $W_\circ(H\delta)$ index is always negative[6] for D4000> 1.9 and, thus, lies below the bulk of the data. Secondly, we consider the effects of an extreme IMF model, after Rieke et al. 1993, in which no stars less massive than $2M_\odot$ are formed. An initial burst of star formation with this IMF is shown in Figure 4.25 as the long-dashed line. This model is also able to match the strongest $W_\circ(H\delta)$ indices of our data with D4000> 1.9. However, the stellar population resulting from such a burst is very short lived, about 300 Myr; thus, it is unlikely that many of these red galaxies can be undergoing such a burst, and we expect that significant dust reddening is the best explanation of the data. This supports the finding of Poggianti et al. 1999, that dust obscuration in galaxies at these redshifts plays an important role in the appearance of their spectra.

[6]Recall, from §4.2.2, that a negative $W_\circ(H\delta)$ index does not necessarily imply an emission feature.

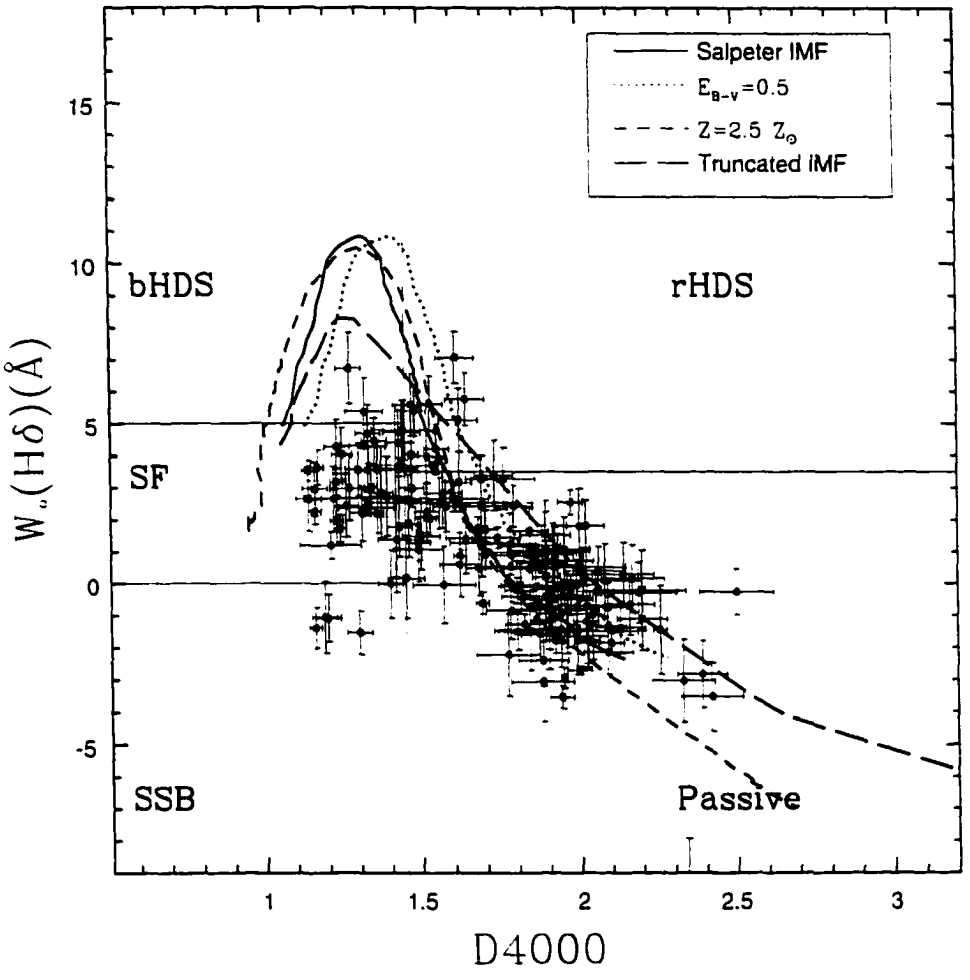

Figure 4.25: PEGASE star formation models presented in the D4000–$W_\circ(H\delta)$ plane, with regions delineated as in Figure 4.11. The *solid line* is the standard, Salpeter IMF initial burst model, also shown in Figure 4.11. This model, reddened by E_{B-V}=0.5, is shown as the *dotted line*. A truncated IMF initial burst (Rieke et al. 1993) is shown as the *long-dashed line*, and a high metallicity (GISSEL96) model is the *short-dashed line*. The data plotted are only those with high signal-to-noise ratios (S/N>15) and uncontaminated by bright night sky lines; the error bars are 1σ.

4.5 Comparison With Previous Work

4.5.1 The Low Redshift Universe

The Las Campanas Redshift Survey (LCRS), as presented in Zabludoff et al. 1996, is a large ($\sim 24,000$ galaxies), unbiased sample of relatively nearby galaxies ($0.05 < z < 0.13$) for which good quality spectra and line indices are available. Zabludoff et al. identify 21 of their 11,113 galaxy subsample ($M_r \gtrsim -19 + 5\log h$) as E+A (renamed here K+A) types, based on $W_\circ$(OII) and an average equivalent width of Hδ, Hγ, and Hβ ($< H\delta\gamma\beta >$). They estimate that 1785 galaxies in their sample lie within the infall radius of a rich cluster, and five of these are identified as K+A types; therefore, $0.28 \pm 0.12\%$ of the cluster population are K+A galaxies, compared with $0.17 \pm 0.04\%$ in the field. These fractions are equivalent within 1σ uncertainties. The definition of a K+A galaxy adopted by Zabludoff et al. differs slightly from the one we have adopted here (§4.3.2) in two respects. First, they use a minimum Balmer index of $< H\delta\gamma\beta >$=5.5Å. From the PEGASE models we find that, for $W_\circ(H\delta) \approx$ 5Å, $< H\delta\gamma\beta > - W_\circ(H\delta) \approx 0.7$; thus, our limit of $W_\circ(H\delta)$>5 Å is nearly equivalent to theirs. Secondly, Zabludoff et al. require $W_\circ$(OII)< 2.5Å; our lower S/N requires us to use a more generous definition of $W_\circ$(OII)< 5Å. Adjusting for this difference allows the inclusion of an additional $\sim$ 13 K+A galaxies in the LCRS sample, raising the total K+A fraction to $0.30 \pm 0.05\%$. Since the uncertainties on the LCRS line indices are small (due to the high S/N of the data), a scatter correction like the one discussed in §4.4.2.1 is not made.

In our luminosity limited sample (§4.2.3.2), which most closely matches

the luminosity range of the Zabludoff et al. sample, the "raw" K+A fraction in the field is 2.7±0.8%, which we regard as an upper limit. Our best estimate of this fraction, corrected for scatter using the Gaussian cloud method (§4.4.2.1), is 1.2±0.8%. Thus, the evolution in the K+A fraction over this fairly small redshift range (from $z \sim 0.1$ to $z \sim 0.3$) amounts to a factor of only about 4±2.7, and the two fractions are actually consistent at about the 1σ level.

4.5.2 Couch and Sharples (1987) and Related Work

Much of the original work in this field was done by Couch and Sharples 1987, whose dataset of 152 galaxies more luminous than about $M_r = -20 + 5 \log h$ in three clusters at $z \approx 0.31$ was later analysed in more detail by Barger et al. 1996. As shown in Figure 4.24, we find somewhat fewer rHDS and bHDS galaxies than Barger et al., though the difference is significant at less than the 2σ level, and may be partly due to an imprecise mapping of *B-R* to D4000 (which was determined in §4.3.3). Barger et al. performed a useful and detailed analysis of the distribution of galaxies in this figure, and compared it with model simulations to determine the importance of starbursts to cluster galaxy evolution. They suggest the data are well represented by a model in which $\sim$ 30% of cluster galaxies have undergone a 0.1 Gyr starburst (which produces 10–20% of the the galaxy's final stellar mass) in the last $\sim$2 Gyr. Given the small number of galaxies and the considerable uncertainties on the line indices, these numbers are uncertain, as the authors acknowledge. In §4.6 we will argue from the fraction of K+A galaxies in the CNOC1 sample that the importance of such short-lived starbursts in clusters is unlikely to

be this large.

The Couch and Sharples data are also considered by Poggianti and Barbaro 1996, who conclude from their modelling that strong starbursts are required to match the K+A galaxies in that sample. However, the comparison between the data and models may be compromised by a difference in index definition. The Couch and Sharples data have $W_\circ(H\delta)$ indices as large as 9 Å, with many points around 5 $<W_\circ(H\delta)<$ 6 Å, while the post-starburst models of Poggianti and Barbaro struggle to reach $W_\circ(H\delta)=$ 6 Å (see their fig. 4), and then only for short periods of time. By dividing the data and models into broad categories (i.e. $W_\circ(H\delta)>$ 3 and $(B-R)<2$) it is possible to misinterpret the results if the models do not match the data *within* a given category, as may be the case here.

4.5.3 Cl1358+62 and CFRS

Fisher et al. 1998 analysed spectra for 232 galaxies within a ~4 Mpc region around the $z \approx 0.32$ cluster Cl 1358+6245, with a magnitude limit of $M_r \approx -19.1 + 5\log h$. This improves on the preliminary work presented by Fabricant et al. 1991, which used only 70 spectra in the central regions of this cluster. These authors define K+A (which they term E+A) galaxies in a manner similar to Zabludoff et al. 1996, but with more generous limits in $< H\delta\gamma\beta >$ and $W_\circ$(OII). They find 11 (4.7±1.9%) of their cluster galaxies show K+A type spectra, remarkably similar to our total cluster fraction, before the necessary scatter correction. Since their uncertainties are also comparable to ours, we expect this correction also to be similar, resulting in a reduced, true K+A fraction.

A similar comparison can be made with the work of Hammer et al. 1997, who find a K+A fraction of 4.9±1.5% in the CFRS field galaxy sample, with a less precise K+A definition, roughly similar to that of Fisher et al. Again, this number should be reduced due to the overestimation resulting from unequal scatter and, thus, the amount of evolution implied relative to the low redshift (LCRS) sample will be significantly less than the order of magnitude implied by the raw fraction alone. This number is similar to our raw cluster K+A fraction, but somewhat larger than our field value. Thus, it supports our conclusion that K+A galaxies are not preferentially found in clusters; however, we note that the mean redshift of the CFRS, $z \approx 0.6$, is considerably higher than that of the CNOC1 sample, and evolutionary effects may be important.

4.5.4 The MORPHS Collaboration

After this paper was submitted, the MORPHS collaboration published a similar study based on ten clusters at $0.37 < z < 0.56$, including 657 galaxies brighter than $M_r \approx -19 + 5\log h$. (Dressler et al. 1999; Poggianti et al. 1999). These authors conclude that galaxies without detectable [OII] emission but $W_o(H\delta) > 3$Å (which they call k+a/a+k) are significantly more common in the cluster sample than the field, (21±2% compared with 6±3%). Both the largeness of these fractions, and the significance of their difference, are apparently in conflict with the results we have presented in §4.4.2. This difference warrants a detailed comparison of the data and analysis, which we present in this subsection.

We will first show that our data are of comparable quality to the MORPHS

data, and then suggest that the differences in our conclusions may result from (1) different selection criteria (both of galaxies and of clusters); (2) different treatment of uncertainties; and (3) differences in galaxy classifications and definitions.

4.5.4.1 A Comparison of Data Quality

We have obtained the publicly available MORPHS data from http://www.ociw/~irs, and computed our indices from their data directly. However, the MORPHS data do not include error vectors, and uncertainty estimates of their indices are unpublished; thus care must be taken before quantitative comparisons are made with our results. In particular, S/N ratios cannot be computed in the same way as we have done in §4.2.1. Instead, we define an alternate estimate as the mean flux per pixel divided by the *r.m.s.* in the wavelength region $4050 < \lambda/\text{Å} < 4250$. This underestimates the true S/N, especially for high S/N spectra, due to real features in the spectrum. In Figure 4.26 we show how this "alternate" value of S/N, computed for the CNOC1 galaxies, compares with our definition in §4.2.1. The correlation is evident, though the scatter is large, and the underestimation of S/N at high S/N values is clear. Based on this correlation, we will assume that our alternative definition can hold as a reasonable proxy for the more realistic measurement used to qualify the CNOC1 data.

In Figure 4.27, we compare the S/N distribution of the CNOC1 sample to that of the MORPHS sample (excluding from the latter galaxies that have a quality index of 4, which are defined as those with S/N sufficient only for a redshift determination). In both cases, S/N is computed in the "alternative"

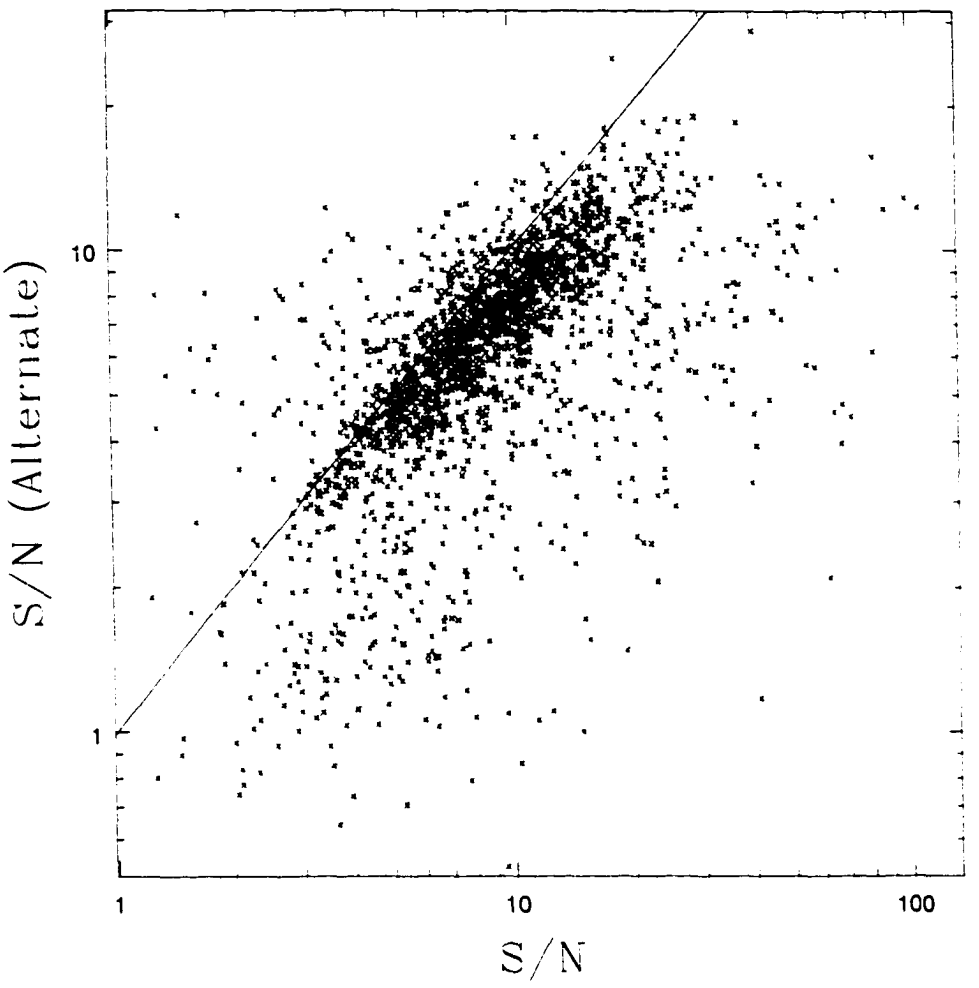

Figure 4.26: Using the CNOC1 sample, we compare the S/N measured in the manner defined in § 4.2.1 (on the x-axis) to the alternate definition described in § 4.5.4.1. The *solid line*, drawn for reference, is where the points would like if both S/N measurements were equal. Most of the data show a strong correlation, though there is significant scatter. The alternate definition underestimates the S/N, especially at high values, where real features in the continuum add to the *r.m.s.* which is used instead of the noise.

manner described above. Both samples have similar distributions, apart from a small excess of low S/N objects in the MORPHS sample[7]. We can crudely assign an uncertainty to the index measurements made on the MORPHS sample by correlating the errors on the CNOC1 data with our alternative S/N measurement. From the S/N measured on the MORPHS data, we can then determine approximate index uncertainties. Representing the uncertainties in $W_o(H\delta)$ and W_o(OII) by $\Delta H\delta$ and Δ[OII], respectively, we find $\Delta H\delta = 9.2 \times (S/N)^{-1.08}$ and Δ[OII]$= 32.8 \times (S/N)^{-1.22}$.

The uncertainty of a line index will be reduced if the resolution is improved, and the continuum S/N ratio is fixed. The MORPHS spectra were obtained using different telescopes and instruments, and are not all of the same resolution; the best resolution spectra (obtained with the COSMIC spectrograph) have a dispersion of 3.1 Å per pixel, and are smoothed to the instrumental resolution of $\sim$ 8 Å, and rebinned to 10 Å per pixel. Thus, the average FWHM of emission lines is comparable to that of the CNOC1 spectra, $\sim$ 16.5 Å, as confirmed by the measurement of several [OII] lines.

A second property which must be tested is the equivalence of the CNOC1 line indices to those measured by the MORPHS collaboration. In Figure 4.28 we show the values of our $W_o(H\delta)$ index, defined in §4.2.2 and measured on the MORPHS spectra, compared with those of Dressler et al. 1999. We exclude galaxies with quality indices of 4, or flagged as uncertain. The latter were usually computed by interactively fitting the continuum and then

[7]These S/N ratios are computed *per pixel*, and the CNOC1 spectra are sampled at 3.45 Å per pixel, while many of the MORPHS spectra are more coarsely sampled (for example, the COSMIC spectra are rebinned to 10 Å per pixel).

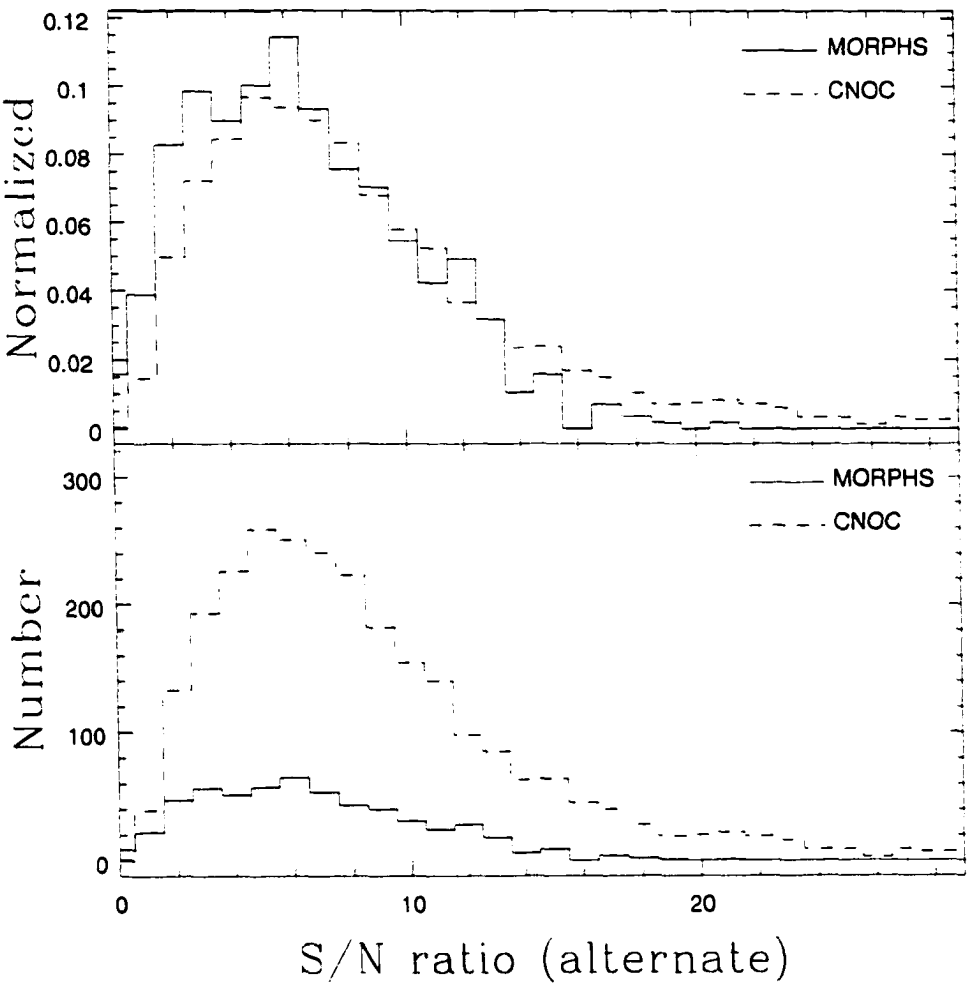

Figure 4.27: We compare the S/N distribution for galaxies in the MORPHS sample with quality indices less than 4*(solid line)* to that in the CNOC1 sample *(dashed line)*. In this case, S/N is measured as the ratio of the mean flux per pixel in the range $4050 < \lambda/\mathring{A} < 4250$ to the *r.m.s.* in the same range. The *bottom panel* shows the number of galaxies in each bin; in the *top panel* both samples are normalised to unit area.

fitting a Gaussian profile to the absorption or emission lines. Given the noisy nature of the data, and the generally complex region of the spectrum under consideration, we find that such an interactive approach is difficult to duplicate, and makes uncertainty estimates difficult to determine reliably. Nonetheless, the correlation between our Hδ index and that of Dressler et al. is fairly good. In particular, we recover the large $W_\circ(H\delta)$ indices measured in many cases by Dressler et al., showing that our index is not insensitive to spectra of this type. The scatter in this figure reflects the fact that both of these indices have considerable uncertainties.

4.5.4.2 Reanalysis of MORPHS Data

In Figure 4.29 we show the MORPHS data in the $W_\circ$(OII)-$W_\circ(H\delta)$ plane, with our region delineations from §4.3.2, and the measurements we have made using our index definitions (§4.2.2). We exclude data of quality index 4, and mark as open circles those galaxies which are either flagged as having uncertain $W_\circ(H\delta)$ measurements, or for which no $W_\circ(H\delta)$ measurement is listed in the MORPHS catalogue (i.e., they are listed as either INDEF, or 0). Furthermore, no magnitude limit is imposed. The sample error bars represent the mean error in each index. The field sample is somewhat biased to lower S/N galaxies and, hence, results in larger mean index errors.

We will not attempt to evaluate the fractions of each type of galaxy (K+A, SF etc.) that we have defined for galaxies in this plane, due to the difficulty in correcting for the morphologically based selection (see Smail et al. 1997). There is clearly, however, a strong presence of K+A galaxies in the cluster sample that is not observed in the field. For most (20/24) of the

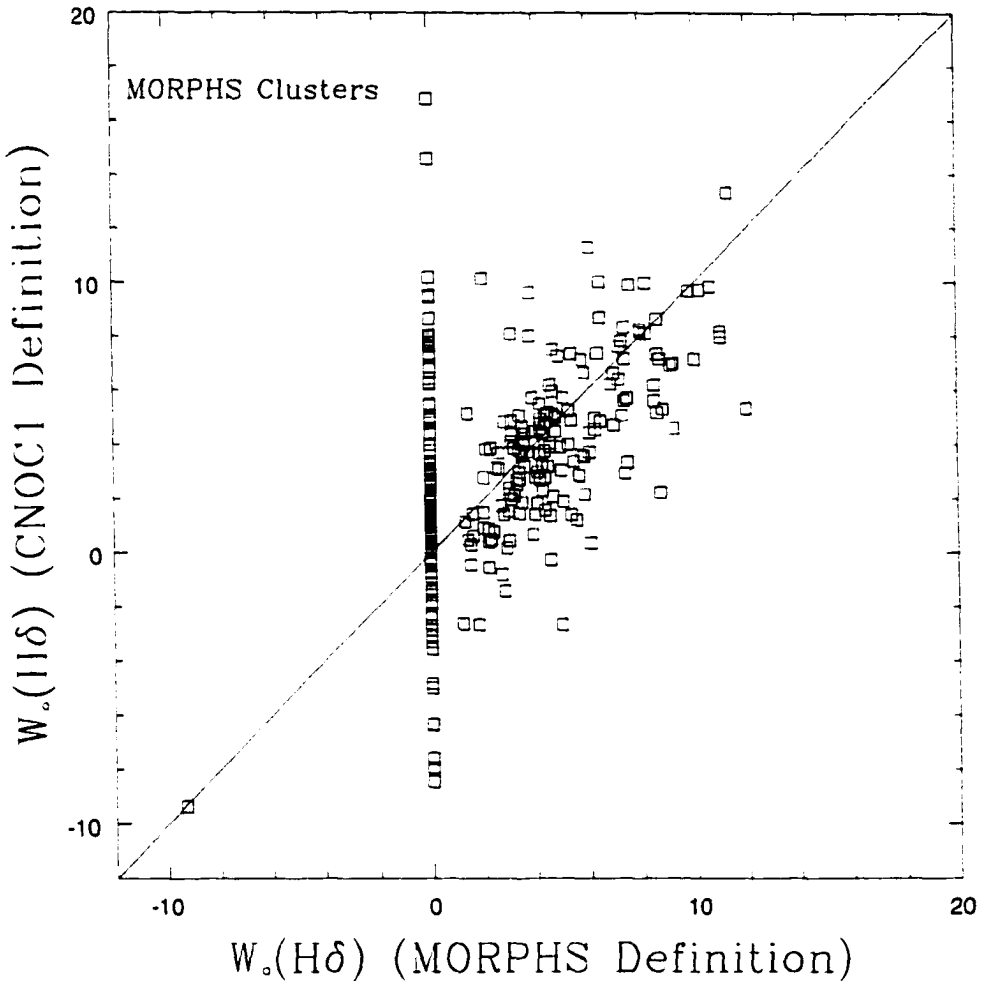

Figure 4.28: Our measurements of $W_\circ(H\delta)$ for galaxies in the MORPHS galaxy sample (on the y-axis) are compared with the equivalent widths published in Dressler et al. (1999, on the x-axis), excluding galaxies with low quality indices ($q = 4$) or flagged as uncertain in the catalogues. Although the two indices are defined in very different ways, they are correlated. The *solid line* shows where the two indices are equal; it is not a fit to the data. The scatter in this figure reflects the uncertainty in both indices, which arises from low S/N data and uncertainty in continuum placement.

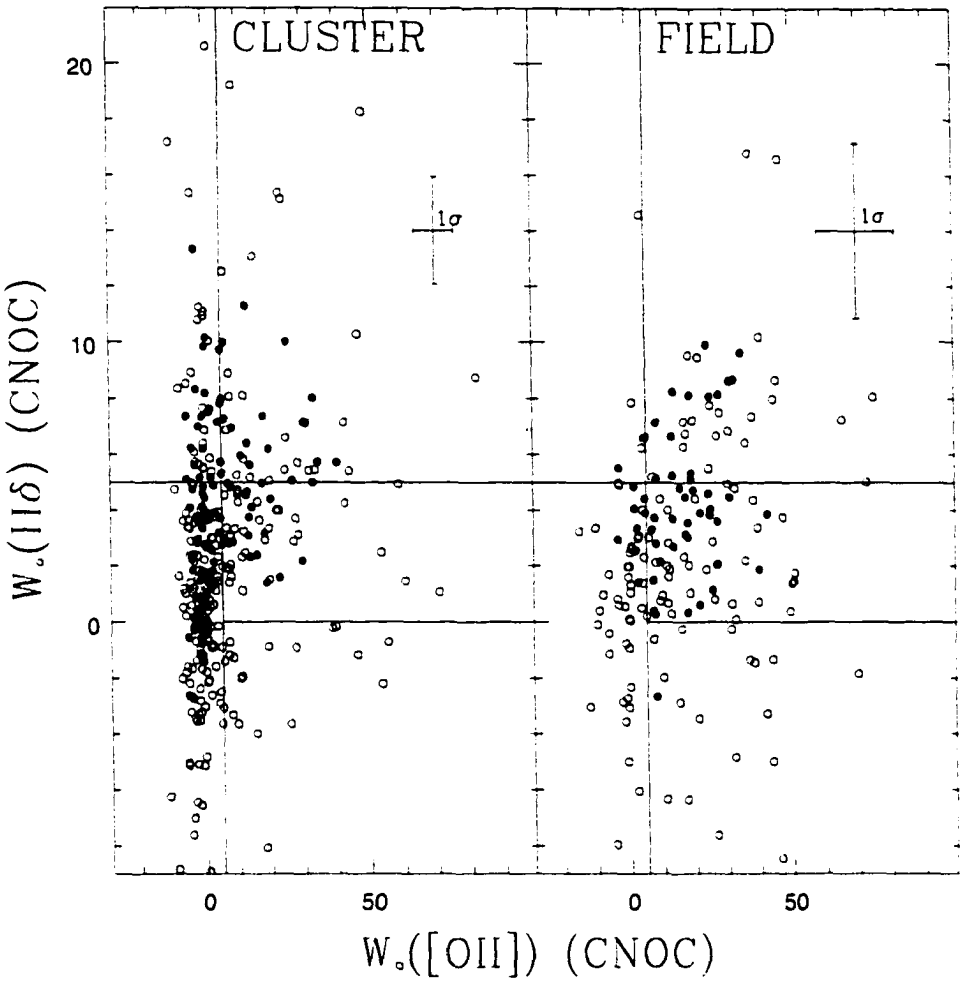

Figure 4.29: Our measurements of W_o(OII) and $W_o(H\delta)$ on the MORPHS cluster and field samples. Data which are of quality index 4 have been excluded. *Open circles* are data for which either no $W_o(H\delta)$ measurement is presented in the MORPHS catalogue, or the measurement is flagged as uncertain. The sample error bars represent the mean, 1σ uncertainty, computed assuming the CNOC1 correlation between S/N and index uncertainty holds for the MORPHS sample. This figure may be compared with the CNOC1 data presented in Figure 4.13, but note that the selection criteria are different in that the MORPHS data are biased toward late type galaxies (which will generally have stronger W_o(OII) and $W_o(H\delta)$ indices). There is a clear excess of K+A galaxies in the MORPHS clusters, relative to their field sample. Although the absolute fraction of K+A galaxies in this sample is difficult to determine reliably, this excess suggests that the MORPHS clusters may have different galaxy populations than the X-ray luminous clusters considered in the present work.

galaxies with $W_\circ(H\delta)>$ 10 Å, Dressler et al. 1999 either did not measure $W_\circ(H\delta)$ or the measurement was flagged as uncertain (open circles). Often, this is due to poor sky subtraction near the line, which should result in large index uncertainties that justify their removal from the sample (as we do for our maximal sample in §4.2.3.3). However a large population of cluster K+A galaxies with $W_\circ(H\delta)<$ 10Å persists. This strong population is clearly not as abundant in the MORPHS field sample, in contrast with the results found in our sample (Figure 4.13). Due to the unusual selection criteria, however, the absolute fraction of K+A galaxies in the two samples cannot be easily compared in a quantitative way.

4.5.4.3 Possible Sources of Differences Between MORPHS and CNOC1

Given that the CNOC1 resolution, S/N distribution and line index definitions are comparable to those of the MORPHS collaboration, what is the source for the difference in results? We discuss three possibilities below.

Cluster Selection: Given that galaxy clusters are a very heterogeneous class of objects, with differing galaxy populations, some or all of the difference between the MORPHS and CNOC1 results may be in cluster selection. The CNOC1 clusters are among the most X-ray luminous at these redshifts, often containing cooling flows, and are mostly dynamically relaxed (Lewis et al. 1999). It is quite possible that, as a class, these clusters differ from the more heterogeneously selected clusters in the MORPHS sample (though we confirm K+A fractions of $\lesssim 5\%$ for the two clusters in common with both samples). Furthermore, the MORPHS clusters are generally at higher redshifts than

the CNOC1 targets; all but four of the CNOC1 clusters lie at redshifts less than that of the lowest redshift MORPHS cluster, A370.

Galaxy Selection: The selection of spectroscopic targets from the photometric sample differs in the two surveys. The MORPHS sample was primarily selected based on galaxy morphology; Sd/Irregular galaxies are oversampled relative to earlier types. Since late–type galaxies were targeted preferentially, the detection of a large population of starburst and/or post–starburst galaxies may not be surprising. Dressler et al. 1999 attempt to correct for this by comparing the morphological distribution of their spectroscopic sample with the photometric sample, but this correction is not completely reliable since the statistical correction for late type field galaxies is uncertain (Smail et al. 1997). Alternatively, the primary selection criterion in the CNOC1 sample is apparent magnitude, with small corrections for galaxy colour and position. In particular, we note that any colour selection effect is quite small, and there does not seem to be a significant bias to our results as a function of galaxy spectral type at these apparent magnitudes. As discussed in section 4.2.3.1, we used weighting functions to correct our sample of line indices to be representative of the full photometric sample in the cluster fields.

We also note that the CNOC1 survey includes galaxies at much larger distances from the cluster centre, as shown in Figure 4.30. However, the lack of an observable gradient in the K+A fraction (Figure 4.22) makes it unlikely that this can have a strong effect.

Uncertainties: No uncertainties are published for the line indices presented in Dressler et al. 1999 or Poggianti et al. 1999. As we have shown

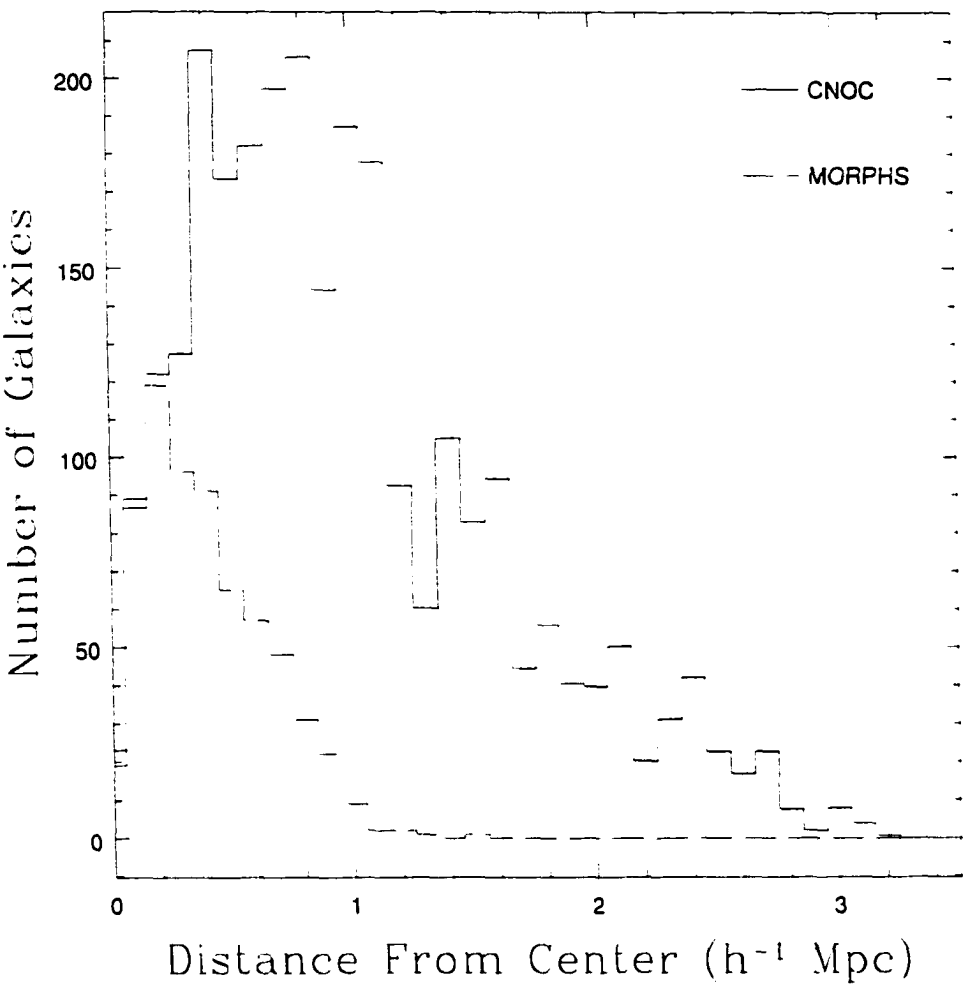

Figure 4.30: Radial Distributions of Galaxies in the CNOC1 and MORPHS Samples

The distribution of distances from cluster centres, for galaxies in the CNOC1 (*solid line*) and MORPHS (*dashed line*) samples. The CNOC1 distribution is weighted by W_{spec} (see §4.2.3.1), but renormalised so that the total number of galaxies represented in this figure corresponds to the number in the spectroscopic sample. On average, galaxies in the CNOC1 sample come from radii about 3 times larger than galaxies in the MORPHS sample.

in § 4.4.2.1, the large uncertainties of our indices result in an overestimate of the K+A fraction; since we believe the MORPHS index uncertainties to be comparable to ours, the same holds true for their sample, and some correction for this effect must be made. Index measurements for galaxies with undetectable or hard to measure lines are not listed in Dressler et al. and, thus, the scatter in the measurements that do exist does not accurately reflect the average uncertainty of the data.

Galaxy Classifications: Based on unpublished recomputations of the Barbaro & Poggianti 1997 models, using their new $W_\circ(H\delta)$ definition, Poggianti et al. 1999 have chosen a threshold of $W_\circ(H\delta)>$ 3 Å for their classification of k+a/a+k galaxies. This is considerably lower than we have adopted for our K+A definition, and clearly leads to the identification of a larger population of "unusual" galaxies. We have justified our limit not only by comparison with the PEGASE models, but also by comparison with the local data of Kennicutt et al. 1992b and Kinney et al. 1996. From Figure 4.9 alone, it is clear that galaxies with $W_\circ(H\delta)>$ 3Å and no detectable [OII] emission are *not* exclusively K+As, but include normal S0 and early spiral galaxies. Since the Dressler et al. $W_\circ(H\delta)$ threshold is significantly lower than previously adopted by many other authors (e.g., Dressler and Gunn 1983; Fabricant et al. 1991; Zabludoff et al. 1996; Abraham et al. 1996; Morris et al. 1998), we chose not to adopt their lower limit. Adopting 3Å instead of 5Å as our lower limit for the classification of K+A galaxies would increase the fraction of galaxies that satisfy this definition[8]. To some ex-

[8]For reference, 7.6±1.1% of cluster galaxies, and 9.1±1.6% of field galaxies in our luminosity limit sample have $W_\circ(H\delta)>$ 3Å, and $W_\circ$(OII)< 5Å (uncorrected for scatter).

tent, of course, the choice of limiting $W_o(H\delta)$ is quite arbitrary and of little consequence as long as it is interpreted as such, and accounted for when comparisons with other work is made.

4.5.5 Summary

With the exception of the MORPHS results (Dressler et al. 1999), the surveys discussed above are not inconsistent out our principal results, which are: (1) the fraction of K+A galaxies (as defined in §4.3.2) in the field and X-ray luminous clusters at $z \approx 0.3$ is less than 5%; (2) it has not been shown conclusively that the $z \approx 0.3$ K+A fraction is significantly larger than the fraction at $z \approx 0.1$; and (3) there is no strong evidence yet that K+A galaxies are more common in cluster environments than in the field. We suggest that the higher fractions of K+A galaxies found by the MORPHS group may come from the very different methodologies used, especially in the selection of the galaxy sample. We suggest that the simpler CNOC1 sample and weighting functions are likely to produce a fair sampling of the cluster populations. In addition, there may be an actual difference in the populations of our two differently selected cluster samples. In that case, it remains to be seen whether clusters at these redshifts are better typified by the X-ray luminous CNOC1 sample, or the more heterogeneous MORPHS sample.

4.6 Discussion

It was shown in Balogh et al. 1997 that the star formation rate (determined from [OII] emission lines) at all radii within CNOC1 clusters is always less

than that in the field galaxy population. However, if a substantial fraction of cluster galaxies have undergone massive but very short starbursts, as postulated for example by Barger et al. 1996, the short duration of these bursts ($\approx$100 Myr) would mean that only a small fraction of cluster galaxies would be observed in the burst phase at a given epoch.

According to the results of the PEGASE models, following a short burst a galaxy will appear as a PSB or PSF type for between 0.75 and 1 Gyr. Thus, the starburst rate can be determined from the abundance of these "remnants". For our maximal sample (§4.2.3.3), the fraction of these galaxies in the cluster is less than 6.2$\pm$0.7%; this is an upper limit because it does not include the correction for non-uniform scatter. This implies that, in the last 2 Gyr, less than approximately 15$\pm$2% of the galaxy population may have undergone a starburst. Using our best estimate for the scatter correction from Table 4.5, the corrected fraction of cluster PSB and PSF galaxies is 2.2$\pm$0.9%, which reduces the estimated starburst population to only $\sim$ 6% in the last 2 Gyr. This is much less than the 30% estimated by Barger et al. 1996. Part of this difference is due to the factor of two difference between the abundance of HDS galaxies in our respective samples, as shown in Figure 4.24 (significant at the $\sim 2\sigma$ level). Secondly, our fractions are reduced due to the scatter correction, though Barger et al. include their uncertainties in their models, which should account for this effect if their error bars are reliable. Finally, Barger et al. actually model the HDS galaxies (which comprise 4.6$\pm$1.8% of our cluster sample, after scatter correction) with post–starburst tracks; however, some of these have [OII] emission (the A+em galaxies), and cannot therefore be truly post–starburst.

Poggianti et al. 1999 have recently suggested that the A+em galaxies are dusty starbursts which may later evolve into K+A types; the strong Balmer lines arise because the OB-stars responsible for the emission lines are heavily obscured by dust, while the longer lived A stars have migrated out of their birthplaces and are more widespread throughout the galaxy, so that their light dominates the spectrum. In our cluster sample, we find 3.0±0.9% of the galaxies have A+em spectra, after scatter correction. This is almost two times larger than the K+A galaxy fraction and implies that the A+em phase must last at least twice as long as the K+A phase if the two types are evolutionarily linked, and if *all* A+em galaxies evolve into K+A types. Thus, these dusty starbursts should either be fairly long-lived, with lifetimes of more than 1.5 Gyr, or a large fraction of them never evolve into K+A types. The fraction of field galaxies classified A+em, $6.3 \pm 2.1\%$, is twice as large as the cluster fraction. Thus, the cluster environment does not appear to be responsible for preferentially generating these galaxy types, whether or not they are starbursts. It is also possible that, if this interpretation of A+em spectra is correct, some K+A galaxies are just a more extreme example, in which the [OII]λ3727 line is completely obscured, as pointed out by Poggianti et al. In this case, A+em and K+A galaxies are not evolutionary counterparts, but representative of the same, starburst phenomenon.

Assuming that K+A galaxies are the result of recently terminated star formation, we can use the fractions of PSF and PSB galaxies in our sample to assess the relative contribution of starbursts and truncated star formation to this scenario. In general, PEGASE models of post-starburst galaxies spend roughly an equal amount of time in both PSB and PSF stages, while

truncated star formation leads only to PSF galaxies, lasting about 300 Myr after the star formation activity ceases (see §4.3.3). Thus, if starbursts are the dominant mechanism for generating HDS galaxies, there should be (roughly) an equal number of PSB and PSF galaxies. As shown in §4.4.3, the PSF fraction in both cluster and field environments may be much higher ($\sim 5-10$ times) than the PSB fraction. If this overabundance is real, it suggests that at least some of the galaxies may have had their star formation truncated without a burst, as supported, for example, by recent simulations (Fujita et al. 1999).

The lack of a marked excess of K+A or A+em galaxies relative to the field may suggest that the cluster environment does not actively truncate *or* induce star formation, but merely inhibits it from regenerating once it has ceased. For example, in the galaxy formation model of Baugh, Cole and Frenk 1996, after a merger of two spiral galaxies succeeds in producing an elliptical galaxy, halo material may recollapse to form a new disk. This reformation of a stable disk could conceivably be inhibited in the cluster environment, due to the presence of strong tidal fields and galaxy harassment. Furthermore, the halo of gas surrounding a spiral galaxy, which may continually cool onto the disk, forming new stars, may be easily stripped away when a galaxy falls into a cluster (Larson et al. 1980). The conditions for this to happen are much less stringent than those for stripping all the gas out of the galactic disk. In either of these cases, K+A galaxies will generally evolve to become Passive within the cluster once they have exhausted their gas supply, whereas, in the field, many will again become star-forming galaxies. Starbursts and K+A phases are then interpreted as natural stages in galaxy evolution (i.e., galaxies

form stars in bursts, not continuously), and the cluster merely prevents a galaxy from recommencing its star formation once the activity has stopped of its own accord. We are currently analysing dark matter simulations of clusters to link a galaxy's star formation history to the time elapsed since it was accreted. Preliminary analysis shows that a gradual reduction of SFR following galaxy accretion adequately reproduces the radial gradient of star formation (Balogh et al., in preparation).

There are several caveats which may alter the conclusions described above, and there are several ways in which future observations may address these issues; we list these caveats below:

1. Once statistical correction weights are included, our spectroscopic sample is representative of a photometric sample complete to $M_r = -18.8 + 5 \log h$. When star formation is truncated in the more numerous, faint galaxy population, they will fade and many will drop below this limit. Indeed, the K+A galaxies in our sample appear to be of intrinsically low luminosity. It is also known that the less luminous galaxies evolve more significantly with redshift (Lilly et al. 1995; Lin et al. 1997), and thus contribute more to the Butcher–Oemler effect. Thus, it is possible that there exists a large number of faint K+A galaxies which we are not detecting, and these may show an environmental preference.

2. Whether or not an equal fraction of K+A galaxies in the cluster and field necessarily implies an equal production rate of starbursts in both environments is somewhat model-dependent, as it may only be a subset of the total population that is ever engaged in starburst activity.

For example, the results of Ellis et al. 1997 and Barger et al. 1996 suggest that most cluster ellipticals formed from a single burst many Gyr ago, and have since evolved passively. If we assume that the Passive type galaxies play no part in cluster evolution, then the fraction of "active" galaxies in clusters that have a K+A spectrum is $6 \pm 3\%$, (corrected for scatter effects). However, it is not yet clear how many of the Passive galaxies are safely excluded in this manner; many of our Passive galaxies have spectra consistent with those of early type spirals and S0 galaxies. Furthermore, it is not clear what fraction of the field galaxies are also "primordial" (e.g., Kelson et al. 1997; Kodama et al. 1998).

3. The [OII] index is metallicity dependent, which affects star formation rates derived from its measurement; however, this dependence is fairly weak (Kennicutt 1992a) and unlikely to strongly affect our results. More important is the fact that this blue feature is quite sensitive to dust obscuration, and many of the PSB or PSF galaxies with $W_o(\mathrm{OII}) \lesssim 5$Å may have significant, but dust-obscured, star formation (e.g., Poggianti et al. 1999). Infrared spectroscopy and imaging, and measurements of Hα emission, will be helpful in constraining this effect.

4. The K+A population is known to be morphologically heterogeneous (Couch et al. 1998; Caldwell et al. 1998). If high resolution HST imaging reveals that K+A galaxies in clusters are morphologically distinct from those in the field, this may support models in which the mechanisms which are responsible for generating K+A galaxies are

environment–dependent.

5. Kauffmann 1995 and Andreon and Ettori 1999 have suggested that the X–ray luminous clusters observed at moderate redshifts are not the evolutionary predecessors of the less luminous, low redshift clusters to which they are often compared. In particular, the CNOC1 sample is composed of the most X–ray luminous clusters in the universe and, hence, may have unique or unusual galaxy populations; this may be responsible for some of the discrepancy between our results and those of Dressler et al. 1999. We note, however, that Andreon and Ettori find no dependence of the blue galaxy fraction on X–ray luminosity, specifically.

6. Finally, the field sample drawn from the foreground and background of these rich clusters may be unusual in some way, though results are generally consistent with the field samples of other groups (Lin et al. 1997). Work is currently being undertaken to address this issue using the CNOC2 field galaxy sample (Ellingson et al., in preparation).

4.7 Summary and Conclusions

We have presented a detailed analysis of the spectral characteristics of a large sample of galaxies in X–ray luminous clusters between z=0.18 and z=0.55, and of an identically selected field galaxy sample. We focus on three spectral indices: D4000, which traces the old stellar population; $W_\circ(H\delta)$, which indicates the presence of A–type stars and is sensitive to star formation that

took place up to 1 Gyr ago; and the $W_\circ$(OII) index, which indicates current star formation activity. We compare our data to the model predictions of Fioc and Rocca-Volmerange 1997 and Bruzual and Charlot 1993, and draw the following conclusions:

- The radial trends within the cluster sample are consistent with a continuous age sequence, in the sense that the last episode of star formation occurred more recently for the outermost galaxies than for the central galaxies.

- We define K+A galaxies as those with $W_\circ$(OII)$<$ 5Å, and $W_\circ(H\delta)>$ 5Å. Our measured K+A galaxy fraction is $4.4 \pm 0.7\%$ in the cluster and $1.9 \pm 0.6\%$ in the field, but this is only an upper limit due to the large index errors which tend to overestimate these numbers. Attempting to correct for this effect, we find the true fraction of K+A galaxies to be only 2.1±0.7% in the cluster environment, and 0.1±0.7% in the field. For our luminosity limited sample (galaxies brighter than $M_r = -18.8 + 5 \log h$), these corrected values are 1.5±0.8% (cluster) and 1.2±0.8% (field). Our field results are consistent with the LCRS $z = 0.1$ fraction of 0.30% (Zabludoff et al. 1996) at the $\sim 1\sigma$ level.

- The fraction of cluster galaxies which are undergoing, or have recently undergone, a short burst of star formation is not significantly greater than the field fraction, at any redshift or distance from the cluster centre. From the fraction of PSB and PSF galaxies, we conclude that less than ~10% of the galaxies in both the cluster and the field may have undergone short starbursts in the last 2 Gyr.

- If all the A+em galaxies are dusty starbursts and progenitors of the K+A galaxies, then these must be undergoing fairly long-lived episodes of star formation (> 1.5 Gyr). These galaxies are two times more common in our field sample than in the cluster.

- We find that PSF galaxies may outnumber PSB galaxies by a factor of 5-10, in both cluster and field environments (though the samples are small). Comparison with models suggests that truncated star formation *without* a short starburst phase may play a significant role in galaxy evolution.

- More photometry of the CNOC1 fields is still needed; particularly K-band to constrain the total stellar mass, and U-band to independently measure star formation rates. Infrared imaging and spectroscopy is needed to determine the amount of dust-obscured star formation, and HST images are required to sub-classify the various galaxies types morphologically.

Keeping in mind the caveats listed at the end of §4.6, we can discuss some of the implications of our results. The general trend for higher redshift clusters to be bluer (the B–O effect) has not yet been linked to a population of galaxies unique to the cluster environment. The simplest explanation consistent with the current data is that the B–O effect in clusters largely reflects the increased level of star formation in the field at larger redshifts. Secondly, there is no evidence that recent (<1 Gyr) cluster-induced star formation is responsible for driving the differential evolution between cluster and field within the virial radius, since there is no tell-tale population of starburst or

post–starburst cluster galaxies that does not exist in the field. We speculate that the presence of bursting galaxies, and the possible increase of such galaxies with redshift, reflects the general nature of star–forming galaxies, independent of environment. However, galaxies in dense environments are eventually *prevented* from bursting, perhaps because their halo gas reservoir has been stripped. This, coupled with a population of "primordial" ellipticals and perhaps some truncation due to ram pressure stripping of disk gas, could be responsible for the older stellar populations which inhabit cluster environments.

Chapter 5

Hα Observations of Abell 2390

5.1 Introduction

In Chapters 2-4, evidence for star formation has been based on the presence of the [OII]λ3727 emission line in a galaxy's spectrum. Though Kennicutt (1992a) has shown that the strength of this emission line correlates well with star formation rate (SFR), it is also sensitive to the metallicity and excitation of the gas. More importantly, the [OII] feature lies in the blue part of the optical spectrum, and is thus easily obscured by dust. Without a good estimate of the internal extinction, this can result in a serious systematic underestimate of the SFR.

Star formation rates are much more reliably estimated from the strengths of Balmer recombination lines, which result from the re-emission of incident flux blueward of Lyα. The Hα line (λ = 6563 Å) is particularly useful as it is strong, and only weakly sensitive to underlying stellar absorption and dust extinction. However, it is redshifted into the near-infrared spectrum at moderate redshifts, and is thus generally not available in spectra obtained in

redshift surveys, like the CNOC1 cluster survey (Carlberg et al. 1996).

Since only short-lived (< 20 Myr), massive stars contribute enough flux blueward of Lyα to give rise to nebular emission, the emission line flux provides a measure of the instantaneous SFR, nearly independent of previous star formation history. However, the derivation of a total SFR from the presence of only the most massive stars results in sensitivity to the adopted initial mass function (IMF). Kennicutt (1983) has shown that this function can be constrained from measurements of the Hα equivalent width and galaxy broad band colours, which confirm that a Salpeter IMF is appropriate for normal, local disk galaxies. Assuming this IMF for stellar masses ranging from 0.1 to 100 $M_{\odot}$, Kennicutt et al. (1994) find the following relationship between Hα luminosity, L(Hα) and SFR (for solar metallicity):

$$\mathrm{SFR}(M_{\odot}yr^{-1}) = 7.9 \times 10^{-42} L(H\alpha)(\mathrm{ergs\ s^{-1}}), \qquad (5.1)$$

computed for Case B recombination, at T_e = 10000 K (Osterbrock 1989). As recently reviewed by Kennicutt (1999), other calibrations have been published by other authors, with a variation of about 30%, reflecting differences in the models used. In particular, the coefficient in Equation 5.1 is 13% smaller than that determined by Kennicutt (1992a, as used in Balogh et al. 1997) and 50% smaller than that determined by Barbaro and Poggianti (1997, used in Balogh et al. 1998).

Although the Hα line is much less sensitive to extinction than [OII], this effect is still the most important source of systematic error (Kennicutt 1999). Typical estimates of the mean extinction are A(Hα)=0.5–1.8 mag (Kennicutt 1983; Niklas and Wielebinski 1997; Caplan and Deharveng 1986; Kaufman

et al. 1987; van der Hulst et al. 1988; Caplan et al. 1996); however A(Hα) is certainly not the same for all galaxies, and it is likely correlated with galaxy type and SFR. A final difficulty with Equation 5.1 is that it usually requires measurements to be corrected for [NII]$\lambda\lambda$6548,6583 emission, which is not usually resolved from Hα in redshift surveys. Kennicutt (1983) found, for local galaxies, that the mean ratio of [NII]/Hα is approximately 0.5.

In Balogh et al. (1997, Chapter 2) we determined star formation rates for CNOC1 galaxies from the equivalent width of the [OII] emission line in their spectra. Based on this relation, we concluded that star formation is suppressed in cluster galaxies, relative to field galaxies, even beyond the virial radius of these clusters; Balogh et al. (1998, Chapter 3) showed that this effect is not completely accounted for by the morphology–density relation. These results are unlikely to be compromised by the presence of large amounts of dust, unless cluster galaxies have relatively more extinction than field galaxies. However, it is of interest to determine by how much the total star formation rate within rich clusters may have been underestimated. Furthermore, in Chapter 4, we used the abundance of K+A galaxies in these clusters to estimate the fraction of cluster galaxies that recently underwent a short starburst. This determination rests on the assumption that the absence of [OII] emission in these galaxies is due to the absence of star formation; Poggianti et al. (1999) have recently suggested instead that, in some cases, this type of spectrum could result from differential extinction effects, where the most massive stars only are heavily obscured. It is therefore important to determine how many of these types of galaxies show evidence for star formation in Hα, which is less sensitive to dust extinction.

In the present Chapter, we present Hα observations of galaxies in the CNOC1 cluster Abell 2390, which has been well studied previously by Abraham et al. (1996). We will attempt to determine the fraction of cluster galaxies undergoing strong star formation ($\dot{M} > 1 M_{\odot}/\mathrm{yr}$), and what fraction of these do not show [OII] emission lines in their CNOC1 spectrum. In §5.2 we describe the details of the observations made in 1998 at the Canada–France–Hawaii Telescope (CFHT). The reduction of this data, and the details of the photometry performed on it, is discussed in §5.3. Our results are presented in §5.4, and our findings are summarised in the final section, §5.5.

5.2 Observations

The data were taken with the *OSIS* (Optical Sub-arc second Imaging Spectrograph) instrument in imaging mode, over four half nights at CFHT from June 21–24, 1998. Twenty-one (19 reasonable quality) pointings were made, for a total areal coverage of about 270 □′. Figure 5.1 shows how the mosaic covers the cluster, relative to the CNOC1 observations. Note that only the central and extreme east/west portions of the CNOC1 strip were observed, due primarily to a night lost to cloudy conditions. The instrument choice of *OSIS* was made for its fast-guiding capabilities, which are capable of improving image resolution to as low as 0.″3 in ideal seeing conditions; however, as seeing was generally about 0.″7 and, more importantly, the fast-guiding option repeatedly caused the instrument control panel to crash, this option was only used for one field (e1c).

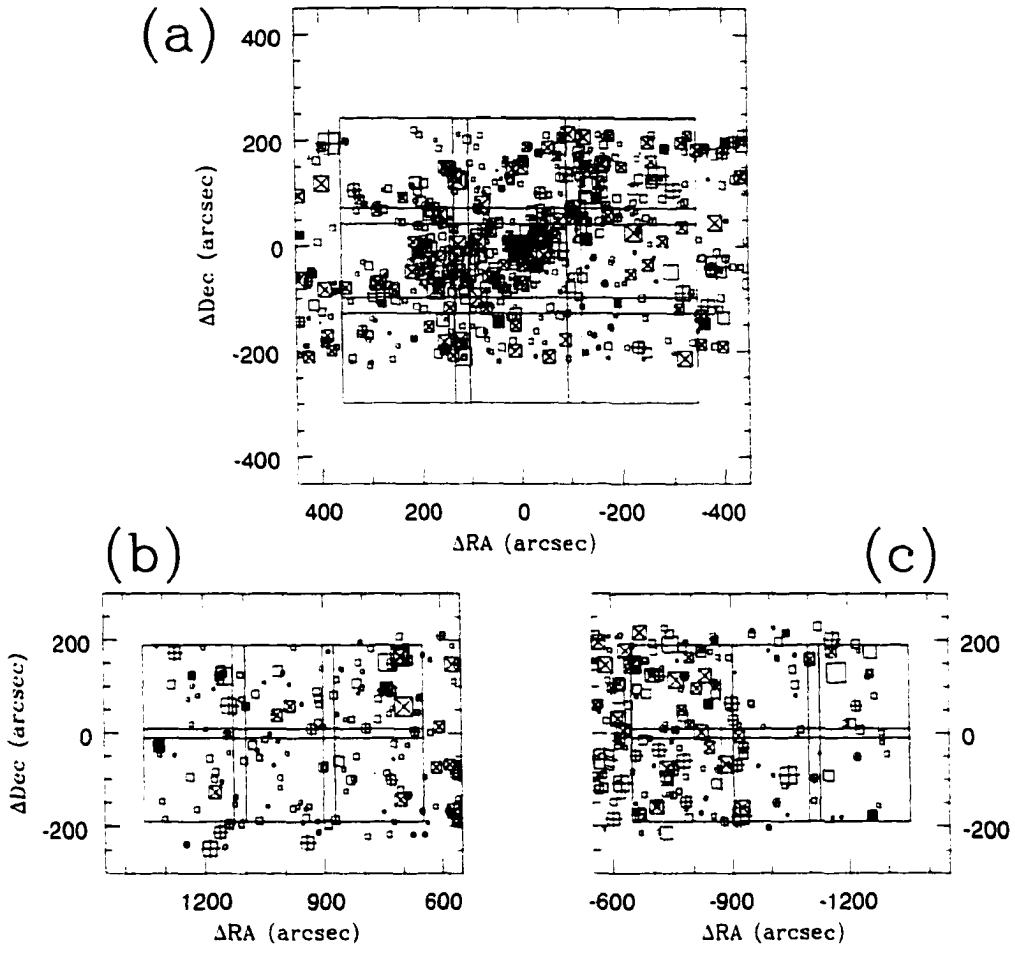

Figure 5.1: The *OSIS* mosaic used to cover A2390 in Hα, overlayed on the CNOC1 data. Coordinates are distance from the BCG, in arcseconds. The 9 central pointings are shown in (a); the 6 pointings in each of the east and west strips are shown in (b) and (c), respectively. Open symbols are galaxies in the CNOC1 catalogue without redshifts; crosses (+) are field galaxies; angled crosses (x) are cluster members with weak or absent [OII] emission (W_o(OII)< 20Å); filled squares are cluster members with strong [OII] emission (W_o(OII)> 20Å). Larger symbols correspond to brighter galaxies.

5.2.1 Filters

For each pointing, we obtained images through three narrow-band filters (the on-line, a red continuum (RC) and a blue continuum (BC)) and one broad band R filter. The three narrow–band filters were carefully chosen to isolate the Hα emission line at the mean cluster redshift of $z = 0.228$, $\lambda = 8059$ Å. To measure the flux in this line, an on–line filter is required that is broad enough to include the Hα line for most cluster members, and yet as narrow as possible to maximise the ratio of emission line flux to continuum flux. Secondly, continuum filters which lie to the blue and the red of Hα are required, such that (a) no cluster galaxies have a peculiar velocity great enough to shift their Hα emission into this band; and (b) they encompass as much continuum as possible, while avoiding other emission lines and ensuring that the continuum is roughly constant over its breadth. Using two continuum filters allows the determination of the continuum level at Hα in the presence of a continuum slope.

We had an appropriate on–line filter manufactured by Barr Associates, with $\lambda_o = 8037$ Å, $\Delta\lambda = 348$ Å FWHM and a peak transmission of ~90%. Adequate filters for the continuum observations were available from CFHT; we used #4701 for the blue and #1814 for the red. Figure 5.2 shows an example of a composite local starburst galaxy from the sample of Kinney et al. (1996) with strong Hα emission, redshifted to $z = 0.228$; the throughputs (calculated in §5.3.2.5) of the three narrow band filters and the broad band R filter are superposed. It is clear from this figure that the on–line filter will often be contaminated with [SII]$\lambda\lambda 6717, 6731$ emission, in addition to

[NII]. The red continuum filter is susceptible to contamination by the weak [ArIII]λ7136 line.

5.2.2 Exposure Times

Exposure times were calculated so that any cluster member with a star-formation rate $\dot{M} \gtrsim 1 M_{\odot} \mathrm{yr}^{-1}$ would be detected in Hα at roughly the 2σ level (assuming the relation in Equation 5.1, and a continuum magnitude of $r \approx 21$). Typical exposure times are 90 s for the R-band filter, 600 s for the on-line filter, and 300s for the two continuum filters. Longer exposure times were used in cloudy conditions; a summary of the observing log is presented in Table 5.1.

5.3 Data Reduction and Photometry

We have not reduced the data from fields w1n, w1c or e2s, for which observing conditions were poor, and the limiting magnitude is considerably brighter than for the rest of the fields. Thus, the final sample considered here consists of 19 pointings; the reduction and analysis of these images is described in this section.

5.3.1 Standard Reduction Procedure

Each image was reduced using the IRAF[1] *ccdproc* package, with the following steps (italicised words refer to IRAF tasks or packages):

[1]IRAF is distributed by the National Optical Astronomy Observatories which is operated by AURA Inc. under contract with NSF.

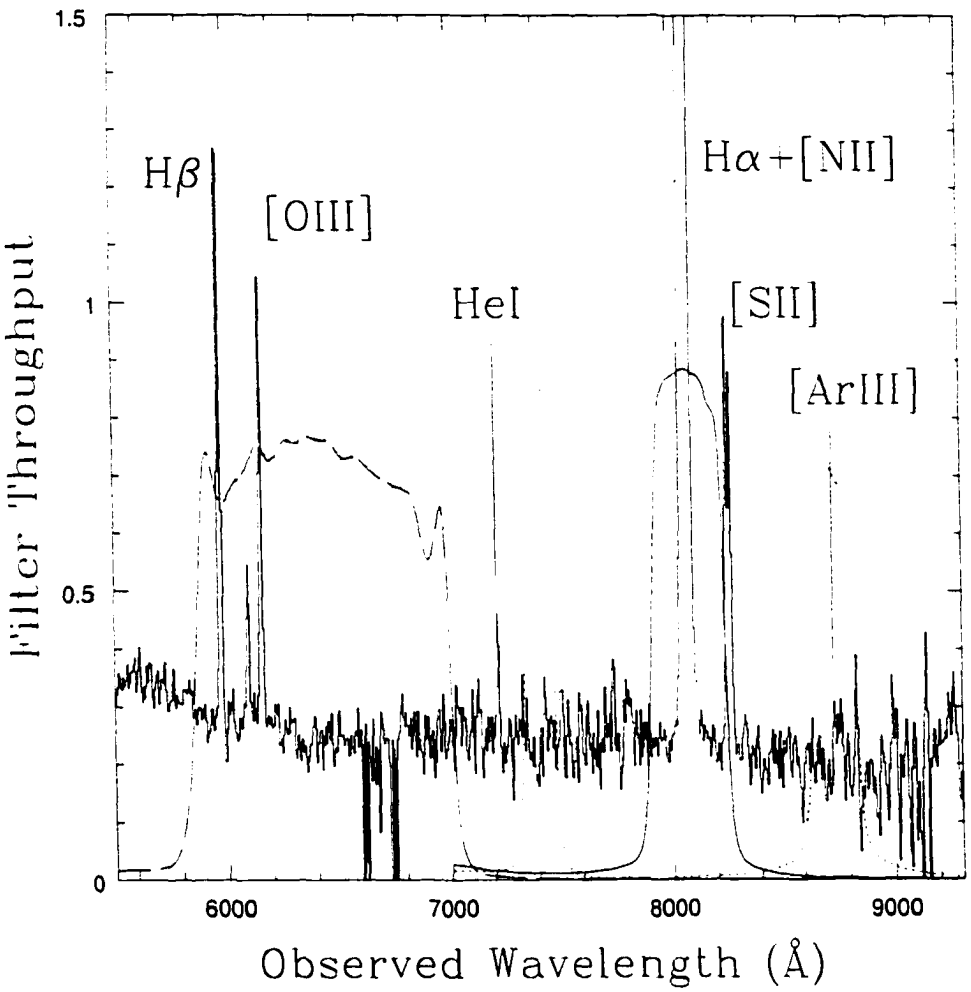

Figure 5.2: The throughputs of the on-line Hα filter (*solid line*), the red and blue continuum filters (*dotted lines*) and the broad-band R filter (*dashed line*) are overlayed on a composite local starburst spectrum from Kinney et al. (1996), redshifted to $z = 0.228$.

Table 5.1: Log of Hα Observations

Date (1998)	Field	Δ RA[a] (″)	ΔDec[b] (″)	*R* Time(s)	on-line Time(s)	Blue/Red cont. Time(s)	Comments
21/6	cc	0	0	90	600	300/300	Thin cirrus
21/6	e1c	225	0	90	600	300/300	Fast guiding
21/6	e1n	225	170	90	600	300/300	Thin cirrus
21/6	cn	0	170	90	600	300/300	Thin cirrus
22/6	w1n	-225	170	180	1200	600/2400	Thick cirrus
22/6	w1c	-225	0	180	2400	1200/2400	Thick cirrus
23/6	w1s	-225	-170	90	600	300/300	Clear all night?
23/6	cs	0	-170	90	600	300/300	
23/6	e1s	225	-170	90	600	300/300	
23/6	w4n	-900	90	90	600	300/300	
23/6	w3n	-675	90	90	600	300/300	
23/6	w2n	-450	90	90	600	300/300	
23/6	w2s	-450	-90	90	600	300/300	
24/6	w3s	-675	-90	90	600	300/300	Moderate cirrus
24/6	w4s	-900	-90	90	600	300/300	Moderate cirrus
24/6	e4n	900	90	90	600	300/300	Clear?
24/6	e4s	900	-90	90	600	300/300	Clear?
24/6	e3s	675	-90	90	600	300/300	Clear?
24/6	e3n	675	90	90	600	300/300	Clear?
24/6	e2n	450	90	90	600	300/300	Clear?
24/6	e2s	450	-90	90	600	300/300	Twilight

[a]Relative to RA 21:53:39.2 (J2000)
[b]Relative to Dec +17:41:16 (J2000)

1. **Overscan:** The mean value of the overscan region of each image, columns 1735 to 1756, was subtracted from each image. This value is typically about 1200 digital units (DUs).

2. **Bias Correction:** Five bias frames were obtained on nights 1 and 3; each of these sets were averaged using the *zerocombine* routine, with 3σ rejection around the median, after overscan correction. The combined bias from night 1 was applied to all images from nights 1 and 2, while the other was subtracted from images taken on nights 3 and 4.

3. **Flat Fielding:** For each filter, five dome flats were averaged using *flatcombine* with 3σ rejection around the median. A blank sky image was created for each filter by taking the 3σ clipped median of all good quality images in that filter, each scaled by the mode of the image. The *mkskyflat* task processes this sky image (for overscan, bias and flat field), smooths it with a boxcar average, and divides it into the original flat, to create a flat field image corrected for the large scale illumination gradient. Dome flats taken on night 1 were used to create the skyflat applied to night 1-2 data; flats taken on night 3 were used for nights 3-4. The flat field correction is good to about 1% over most of the image, with variations of up to 5% in the corners.

4. **Cosmetic Corrections:** Each image was trimmed to a region spanning columns 33 to 1718 and rows 360 to 1680. A bad column near 860 was interpolated over using the *fixpix* procedure (from within *ccdproc*), and cosmic rays were identified interactively and linearly interpolated

over, following a first pass with *cosmicray* to automatically remove most of the candidates.

5. **Alignment Procedure:** A candidate list of stellar objects in the on-line image were identified with the *starfind* algorithm, which detects objects from a Gaussian-convolved image, rejecting elliptical or extended objects that are most likely galaxies. This list is then manually cleaned of residual cosmic rays, galaxies, and stars with saturated pixels or otherwise corrupted isophotes. The centroids of these stars are then found on the other three images of that field using the *imcentroid* algorithm. The geometric transformation required to match pixel coordinates of the stellar centroids on each image is computed with *geomap*, and this solution is applied to the images with *geotran*, to align all four images of each field.

6. **Astrometry:** The astrometric solution of each image was computed by matching the list of stars with stars in the U.S. Naval Observatory (USNO) A2.0 catalogue[2]. An initial guess to the plate solution is made from the right ascension and declination in the image header, and the pixel scale of 0.″155 arcsec/pixel. This allows stars from the USNO catalogue to be matched with the closest stellar object on the OSIS images. After these identifications are checked, the plate solution is solved with *ccmap*, and applied to each image with *ccsetwcs*. Galaxy positions are generally good to 0.″5, though they are sometimes less

[2]The USNO SA2.0 catalogue is a product of the USNO Flagstaff Station and is distributed by the Astrometry Department.

accurate near the edges.

5.3.2 Catalogue Creation

Object detection, photometry and star/galaxy separation was done with the SExtractor photometry package (Bertin and Arnouts 1996). A review of the algorithms and a description of the chosen parameters is discussed here.

5.3.2.1 Background Estimation

The sky background is estimated in each mesh of a grid from a combination of $\kappa\sigma$ clipping and mode estimation. A bilinear interpolation between meshes of the grid is made to produce the final background map. For the present photometry, we have chosen a mesh size of 128 pixels, median filtered with a 5 pixel boxcar to suppress signal from bright stars. This mesh size was chosen to be as large as possible, while still matching the large scale variations in sky level which are primarily due to vignetting near the corners of the chip. Such a "global" background estimate is inadequate for objects found in the haloes of bright stars or near bright ghosts or reflections. These objects are excluded from the current catalogues; their photometry may be redone in the future, using background levels measured in an appropriate annulus.

5.3.2.2 Source Detection

Objects are detected using the thresholding algorithm of Lutz (1979) to identify objects as 5 contiguous pixels more than 1σ over the background, following convolution with a Gaussian (5 pixels FWHM). These detections are then passed through a deblending algorithm, which rethresholds each object

at 32 exponentially spaced levels, and identifies peaks that contribute at least 10^{-6} of the flux of the blended structure as distinct objects.

Sources were detected separately on all four images for each field; these detections were then matched, so the final catalogue contains only objects detected on all four images. This allows easy rejection of non-real detections due to noise spikes or residual cosmic rays.

5.3.2.3 Photometry

For each galaxy, SExtractor calculates the major and minor axes (A and B, respectively) as the second moment (i.e. *r.m.s.*) of the light profile; the galaxy size is then characterised by a bivariate gaussian with mean standard deviation σ. The first moment, r_1 is computed as:

$$r_1 = \frac{\Sigma r I(r)}{\Sigma I(r)}, \tag{5.2}$$

where $I(r)$ is the intensity profile as a function of position, and the summation is over all pixels within a radius of 6σ. The size of the aperture within which the photometry is measured is taken to be the largest of either $2r_1$ or $3.5\sqrt{AB}$; this is expected to contain about 94% of the total flux, independent of signal-to-noise, magnitude or PSF (Kron 1980). Within each aperture, the galaxy flux is the sum of the intensity of each pixel, less the background measured from the background image (§5.3.2.1). The adaptive aperture approach is taken to allow for the fact that the PSF can vary significantly between different images of the same field (in different filters).

5.3.2.4 Star–Galaxy Separation

SExtractor uses a neural network algorithm to distinguish between stars and galaxies, as described in detail in Bertin and Arnouts (1996). Ten parameters describing the object profile (peak intensity, seeing and eight isophotal areas) are input into the neural network, which has been trained on both artificial and real images. The classification of bright objects is at least reliable at the 95% level, though there is some tendency to classify compact members of deblended galaxy-galaxy pairs as stars. SExtractor assigns a "stellarity index" between 0 and 1 to each galaxy, where the larger number indicates increased likelihood that the object is a star. By inspecting objects on several of our OSIS images, we determined that objects with index greater than 0.97 are mostly stars, and we adopt this as our threshold.

5.3.2.5 Photometric Zero Points

A spectrophotometric standard star, BD+284211, was observed in all four filters on the first night. To determine the photometric zero point for each filter, we need to convolve the flux calibrated spectrum of this star from Oke (1990) with the response of the filter/detector combination. This response, as a function of wavelength, was determined by taking a long slit image of the flat field lamp through each filter. The overscan region was subtracted from each of these images, and the wavelength solution was found by identifying lines in an argon lamp spectrum with *identify* and mapping these wavelengths onto pixel coordinates with *fitcoords*. The average of all columns along the slit was taken to create a 1-dimensional, wavelength calibrated re-

sponse function. To determine the throughput of each filter (as plotted in Figure 5.2), we divide this function by that obtained without a filter in place. However, this division removes the detector response so, for the purposes of determining the zero point, we simply renormalise the response function to reach a maximum value of unity, so that the value of each pixel represents the relative contribution of flux at each wavelength, accounting for both filter and detector response; we call this function $S(\nu)$, expressed as a function of frequency rather than wavelength. This is not precisely correct, because the flat field lamp is not uniform in wavelength; however, it should be a suitable approximation since the wavelength ranges of the filters are fairly narrow.

The total standard flux of BD+284211 at the wavelengths sampled by each filter is then given by

$$F_{\rm tot} = \int_0^\infty F(\nu)S(\nu)d\nu, \tag{5.3}$$

where $F(\nu)$ is the flux (in ergs/s/cm^2/Hz) of BD+284211 as tabulated in Oke (1990). The frequency range of each filter is computed as

$$\Delta\nu = \int_0^\infty S(\nu)d\nu, \tag{5.4}$$

and the AB magnitude (Oke 1974) of the standard star in each filter is given by

$$m_{AB} = -2.5\log(F_{\rm tot}/\Delta\nu) - 48.6. \tag{5.5}$$

The observed flux in each filter of BD+284211 is computed with SExtractor using the same parameters described for object photometry in §5.3.2.3. The number of DU per pixel are multiplied by the gain (4.52 e-/DU) and

divided by the exposure time in seconds to yield an observed flux, $\mathcal{F}$, in units of electrons per second. The zeropoint for each filter i is then determined from

$$m_{o,i} = m_{AB} + A_i\chi + 2.5 \log \mathcal{F}_i, \tag{5.6}$$

where χ is the airmass, and m_{AB} is the standard star magnitude in the appropriate filter, from Equation 5.5. Coefficients for the airmass correction, A_i are taken from the OSIS manual[3]; we use A=0.08 (tabulated for R band) for the R and BC images, and A=0.05 (tabulated for I) for the on-line and RC images.

The results are shown in Table 5.2 where we list, for each filter, the measured flux of BD+284211 in DU (column 2), the exposure time in seconds (column 3), the airmass (column 4), standard magnitude (from Equation 5.5, column 5) and the photometry zero point calculated from Equation 5.6 (column 6). For each galaxy, then, we can determine the flux in each filter i, f_i, (ergs/cm^2/s/Hz) from the observed flux in electrons/s, $\mathcal{F}_i$, as

$$\log f_i = \log \mathcal{F}_i - \frac{1}{2.5}(m_{o,i} + 48.6 - A_i\chi) \tag{5.7}$$

5.3.2.6 Equivalent Widths

Since the nights were not photometric, the zeropoints determined in §5.3.2.5 are not reliable to within more than ~0.5 mag. However, Hα equivalent widths can be more precisely determined, since they only depend on the relative flux between the on-line and continuum images. We calibrate this by

[3]http://www.cfht.hawaii.edu/Instruments/Spectroscopy/SIS/Manual/chapter2_11.html

Table 5.2: Photometry Zero Points

Filter	Flux (DU)	Exp. Time (s)	Airmass	m_{AB}	m_o
on-line	177522	8	1.032	11.19	23.74
RC	140054	8	1.034	11.27	23.57
BC	126177	8	1.033	11.01	23.22
R	208817	1	1.030	10.76	25.78

assuming that stellar objects have no absorption or emission at $\lambda \approx 8100$Å, corresponding to the wavelength of our on-line filter; thus, an appropriate scaling can be found such that the mean equivalent width of stellar objects is equal to zero. We first calculated the continuum magnitude of each galaxy by averaging its flux (in ergs/s/cm^2/Hz) in each of the two continuum filters, RC and BC, to obtain f_c; this is appropriate because the central wavelengths of RC and BC are almost equally spaced on either side of the on-line filter in ν. We then selected a sample of stellar objects (with stellarity index >0.97) with uncorrupted photometry, and measured the ratio of the flux in the on-line filter, f_{on}, to f_c. An example of this relation is shown in Figure 5.3, where we compare these two fluxes for stars in the central field. The tight correlation suggests that it is fair to assume all stars in the field have a similar spectral shape in this wavelength range. We then multiplied f_c by the mean value of this ratio (1.30 in this case), to obtain a scaled continuum f_c' for all galaxies in the field, ensuring that the mean of $f_{on} - f_c'$ is zero for stellar objects. For all 19 fields, f_{on} is larger than f_c; we expect that the zeropoint of the on-line filter was underestimated due to cloudy conditions when the standard star was observed.

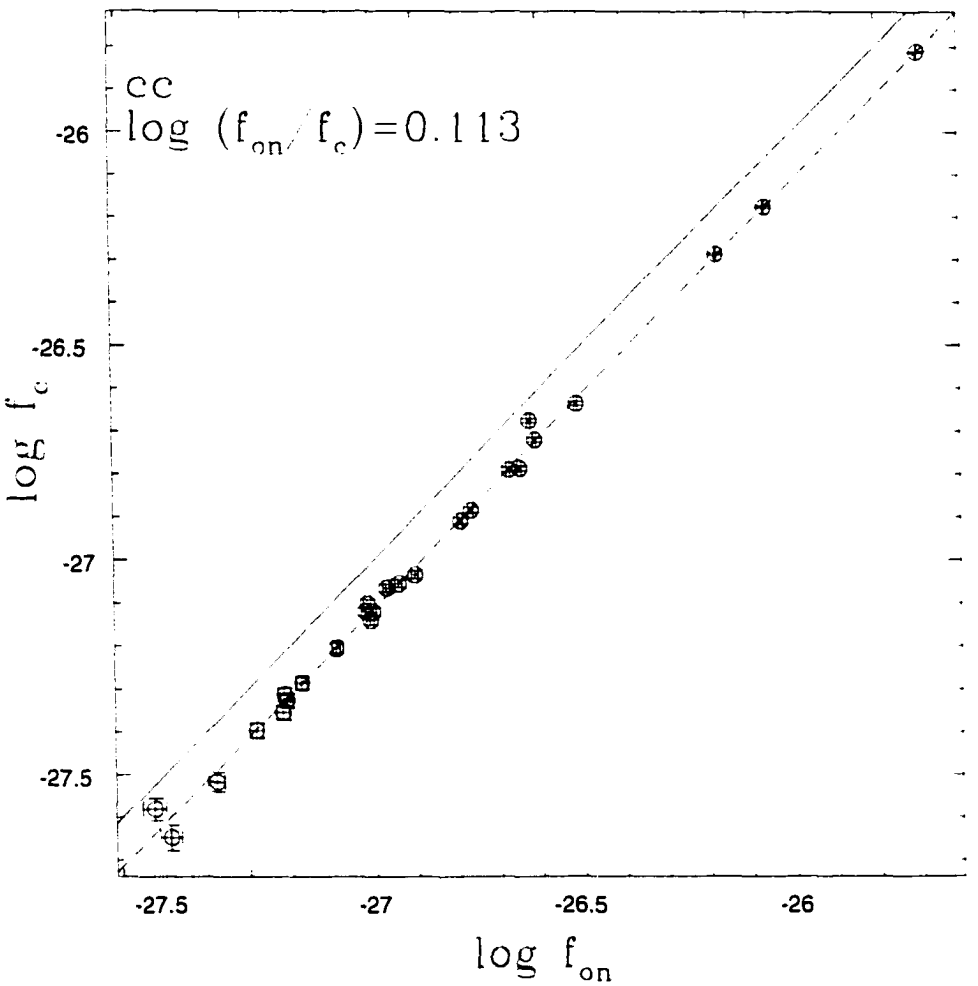

Figure 5.3: The logarithm of the flux in the averaged continuum (f_c) is plotted against the logarithm of the flux in the on-line filter, for stars in the central field; the two should be equal (indicated by the *solid line*), since stellar objects have no strong features at this wavelength. Due to incorrect zero point determination, the continuum flux in this case is a factor of 1.3 fainter than the on-line flux (*dashed line*). Thus, the continuum flux must be multiplied by this factor for all galaxies in this field.

The rest frame equivalent width of the Hα line is given by

$$W_\circ(H\alpha) = \Delta\lambda \frac{f_{on} - f'_c}{f'_c}, \tag{5.8}$$

where $\Delta\lambda$ is the *rest frame* width of the on–line filter, in Å, which we take to be the FWHM of the filter response function, 348 Å. In fact, the on-line filter also covers the adjacent [NII] emission line; all values of $W_\circ(H\alpha)$ presented in this Chapter include contribution from this line; a correction will only be made when star formation rates are considered.

5.3.2.7 The Final Catalogue

Since adjacent OSIS fields overlapped by up to 30″, some galaxies were observed on more than one field; from these duplicates, only the best quality image was used. Galaxies lying near the bad column (rows greater than 410, between columns 810 and 850), or in the haloes of bright stars were removed from the catalogue. The latter may be reintroduced into the catalogue at a later date, following more careful photometry which accounts for the strongly varying background intensity near these objects. Objects with stellarity index greater than 0.97 are considered stars, and were excluded from the galaxy sample. Finally, objects with corrupted photometry (due to nearness to an image boundary or saturated pixels) were also excluded. The final catalogue contains measurements for 1189 galaxies.

The on–line filter response is centred at $\lambda = 8071.5$Å, with a width (between 10% transmittance levels) of $\Delta\lambda = 398$Å. The Hα emission line lies within this wavelength range for galaxies at redshifts $0.200 < z < 0.260$. Hereafter, we refer to galaxies in this redshift range as cluster members;

from the CNOC1 spectroscopic catalogue (Abraham et al. 1996), 90.2% of galaxies in this redshift range lie within 3σ of the cluster redshift, and 96.7% lie within 6σ, where $\sigma = 1095$ km/s is the cluster velocity dispersion. The brightest cluster galaxy (BCG) right ascension and declination coordinates are (21:53:36.80, +17:41:43.8), and we take this to be the centre of the cluster, relative to which galaxy positions are measured. From Carlberg et al. (1996), R_{200} for this cluster is $1.51h^{-1}$ Mpc, where R_{200} is the radius at which the mean interior mass density is equal to 200 times the critical density, and within which it is expected that the galaxies are in virial equilibrium (Gott and Gunn 1972; Crone et al. 1994). For $\Omega_o = 0.2, \Lambda = 0$ this corresponds to 785″; we normalise all projected cluster–centric distances (R_{proj}) to this value.

5.3.3 Completeness

To estimate the completeness of our final catalogue, we compare our galaxy sample with the photometric CNOC1 galaxy sample, which is complete to about $r = 23.5$ (Abraham et al. 1996). Galaxies were matched in right ascension and declination coordinates, verified by interactive inspection in ambiguous cases. The number of galaxies in our catalogue matched in this manner is shown in the bottom panel of Figure 5.4, in bins of CNOC1 r magnitude. We then compute the difference between this distribution and that of galaxies in the CNOC1 sample that lie within the same area of sky; this difference is shown in the top panel of Figure 5.4. Note that this procedure does not account for the small number of galaxies in the present sample which have no match in CNOC1; these usually arise from cases where our su-

perior sampling and seeing is able to resolve an object into multiple objects. There are also cases of discrepancy where objects are classified as stellar in one catalogue, but not the other. Figure 5.4 shows that our galaxy sample is $> 90\%$ complete to $r \approx 21$, and falls to 50% completeness at $r = 21.7$. For our adopted cosmology of $\Omega_o = 0.2, \Lambda = 0$, $r = 21.7$ corresponds to an absolute magnitude of $M_r = -17.5 + 5 \log h$, including a K-correction of 0.23 mag[4].

We used this matched sample to correct the zero points of our R-band photometry, on a per-field basis, by computing the mean offset Δr, between the CNOC1 photometry and the present photometry, for the galaxies we have in common brighter than $r = 21.7$. We adjusted our r magnitudes according to this difference, which is, in general, $|\Delta r| < 0.3$ mag. After applying this correction, the difference the two measures for galaxies brighter than $r = 21.7$ has a 3σ-clipped *r.m.s.* of 0.12 mag (to be compared with 0.21 mag, before this correction). This corrected correlation is shown in Figure 5.5. Outlying points are often deblended galaxies, the photometry of which depends on the algorithm used and the seeing conditions, which may not be the same for both measurements. This procedure allows us to apply a reliable magnitude cut to the final sample, by ensuring the r photometry is on a consistent system. However, the same correction cannot be applied to the other filters, as the zero point varies significantly between exposures.

To correct for the incompleteness that sets in around r=21.1, we calculated a statistical weight, $W_{H\alpha}$, which is the ratio of the number of galaxies

[4]Based on model spectral energy distributions of Coleman, Wu and Weedman (1980), independent of SED type to within 0.02 mag.

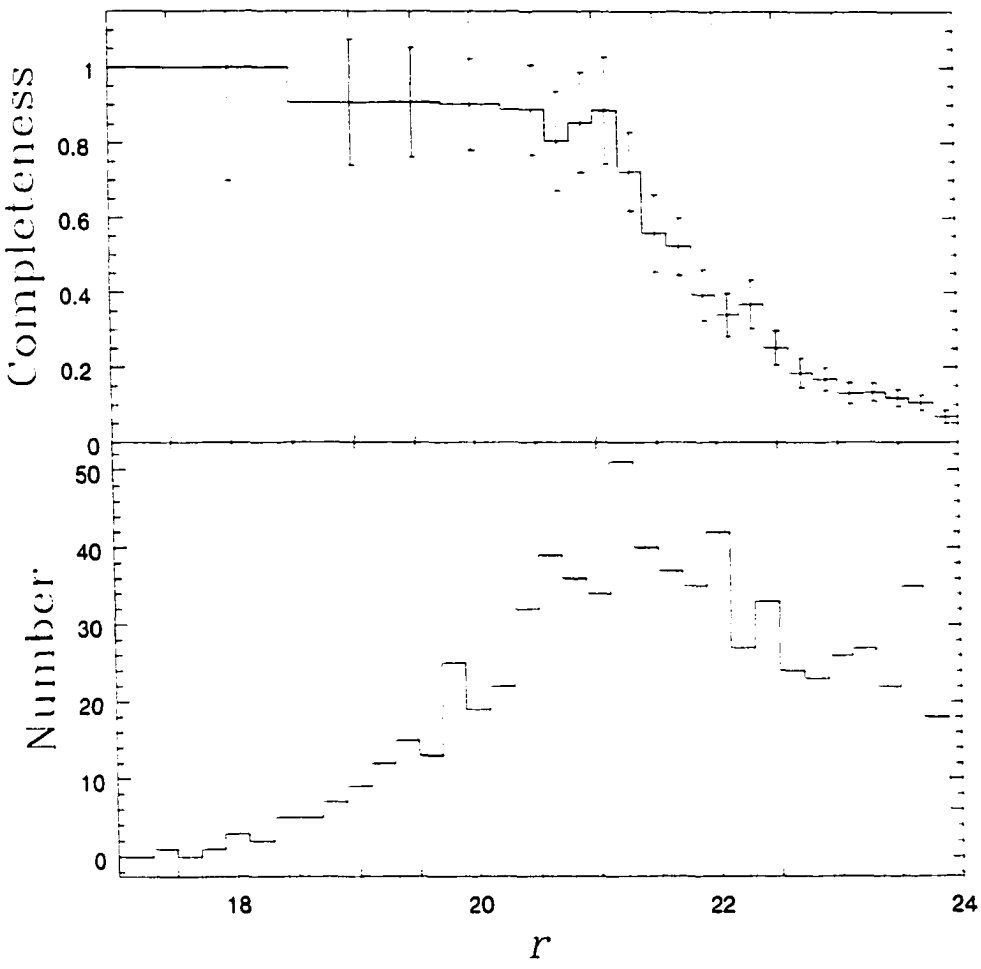

Figure 5.4: The *bottom panel* shows the total number of galaxies in the Hα sample that correspond to a galaxy in the CNOC1 sample, as a function of r (from the CNOC1 photometry). In the *top panel*, we plot the ratio of the number of galaxies in our final CNOC1-matched Hα sample to the number of galaxies in the CNOC1 photometric catalogue, matched to identical areal coverage. Error bars are 1σ, and are determined as the value in each bin divided by $\sqrt{N}$, where N is the number of galaxies from the Hα sample in that bin. The completeness drops to 50% at $r = 21.7$.

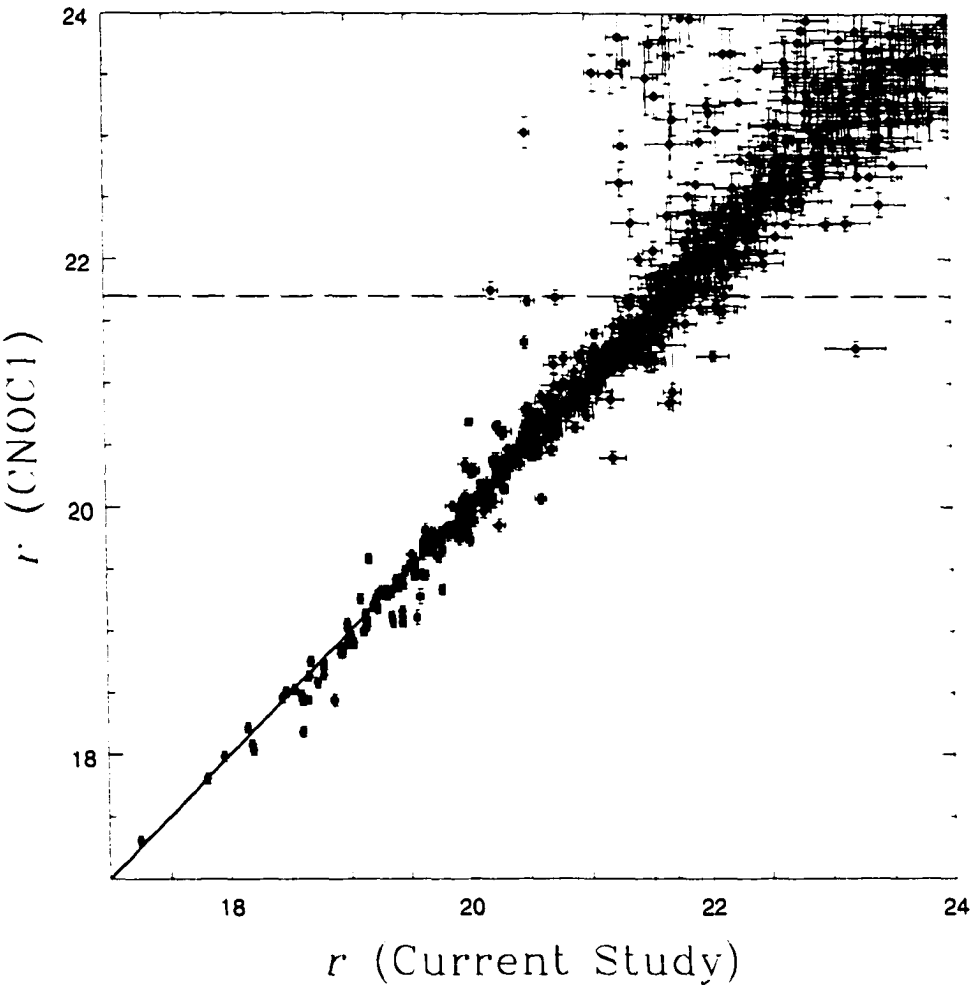

Figure 5.5: r magnitudes from CNOC1, with 1σ error bars, plotted against our measurements, after correction for zero-point offsets in each field as detailed in §5.3.3. The *solid line* is drawn where the two magnitudes are equal, for reference. *Dashed lines* are drawn at $r = 21.7$, our 50% completeness limit. The 3σ clipped *r.m.s.* for galaxies brighter than this limit is 0.12 mag. Outliers on this figure are often blended objects, the magnitudes of which may be sensitive to the deblending algorithm used and the seeing.

in the (area matched) CNOC1 photometric sample to the number in the current sample, binned in magnitude. We approximate $W_{H\alpha} = 1.12$ for $r < 21.1$ and $W_{H\alpha} = 1.78r - 36.4$ for $21.1 < r < 22.1$. When appropriate, this weight is applied to results discussed in §5.4.

5.4 Results

5.4.1 Comparison with CNOC1 [OII] Measurements

There are 166 galaxies in our Hα sample which have spectra available from the CNOC1 sample; for these galaxies we can compare the $W_o(H\alpha)$ measurements with their spectral properties. We will concern ourselves with the rest frame equivalent widths of the Hδ absorption line ($W_o(H\delta)$) and the [OII]λ3727 emission line (W_o(OII)), as defined in Chapter 4. Recall that the former index is positive for absorption features, while the latter is positive in the case of emission. The CNOC1 spectroscopic sample is a subset of a complete photometric sample; statistical weights discussed in Yee et al. (1996) are applied to galaxies in this sample to correct for selection effects due to apparent magnitude (W_m), geometric position (W_c) and colour (W_c), where necessary.

Although we can expect a correlation between the spectral indices and our $W_o(H\alpha)$ measurements, the two are not always directly related. In particular, since the spectra are obtained from a narrow (1.″5) slit centred on the galaxy, they are not necessarily representative of the total integrated light of the galaxy, which we have measured from the Hα images. Furthermore, the W_o(OII) measurements are more sensitive to weak emission, as the index

definition is not as dominated by continuum light.

In Figure 5.6 we compare $W_\circ(H\alpha)$ with $W_\circ$(OII), plotting only galaxies brighter than $r = 21.7$ and with $W_\circ$(OII) uncertainties less than 15Å. In the bottom panel we plot field galaxies, for which the Hα emission line does not fall within our on-line filter wavelength range and, thus, should have $W_\circ(H\alpha)$=0. These measurements are fairly evenly distributed about zero (the median is -1.9Å), with a standard deviation of $\sim$ 37Å. In the top panel we show the $W_\circ$(OII)-$W_\circ(H\alpha)$ relation for cluster members; the solid line represents the mean local relation found by Kennicutt (1992a). Most of the galaxies that have strong $W_\circ$(OII) (i.e. greater than 30Å or so) are also detected in Hα. Low ratios of $W_\circ(H\alpha)/W_\circ$(OII) in some cases are partly due to the fact that the Hα emission often originates from a small (usually central) region of the galaxy (e.g., see Figure 5.12); thus, $W_\circ(H\alpha)$ is low since there is a considerable amount of continuum flux dominating the light, from other regions of the galaxy. The spectroscopic observations, from which $W_\circ$(OII) is measured, only sample the light in a narrow 1.″5 slit placed across the galaxy, so the emission line flux may contribute a larger fraction of the total light in the slit.

Another striking result shown in Figure 5.6 is that there are several galaxies with strong $W_\circ(H\alpha)$ measurements, but weak or absent $W_\circ$(OII). More specifically, there are 51 cluster members that have no detectable [OII] emission ($W_\circ$(OII)$<$ 5Å with 2σ confidence), and 10 of these have Hα detected at the 2σ level. This suggests that $\sim$20% of galaxies for which we do not detect [OII] may in fact have substantial star formation activity.

We can estimate the SFR for galaxies detected in Hα from Equation

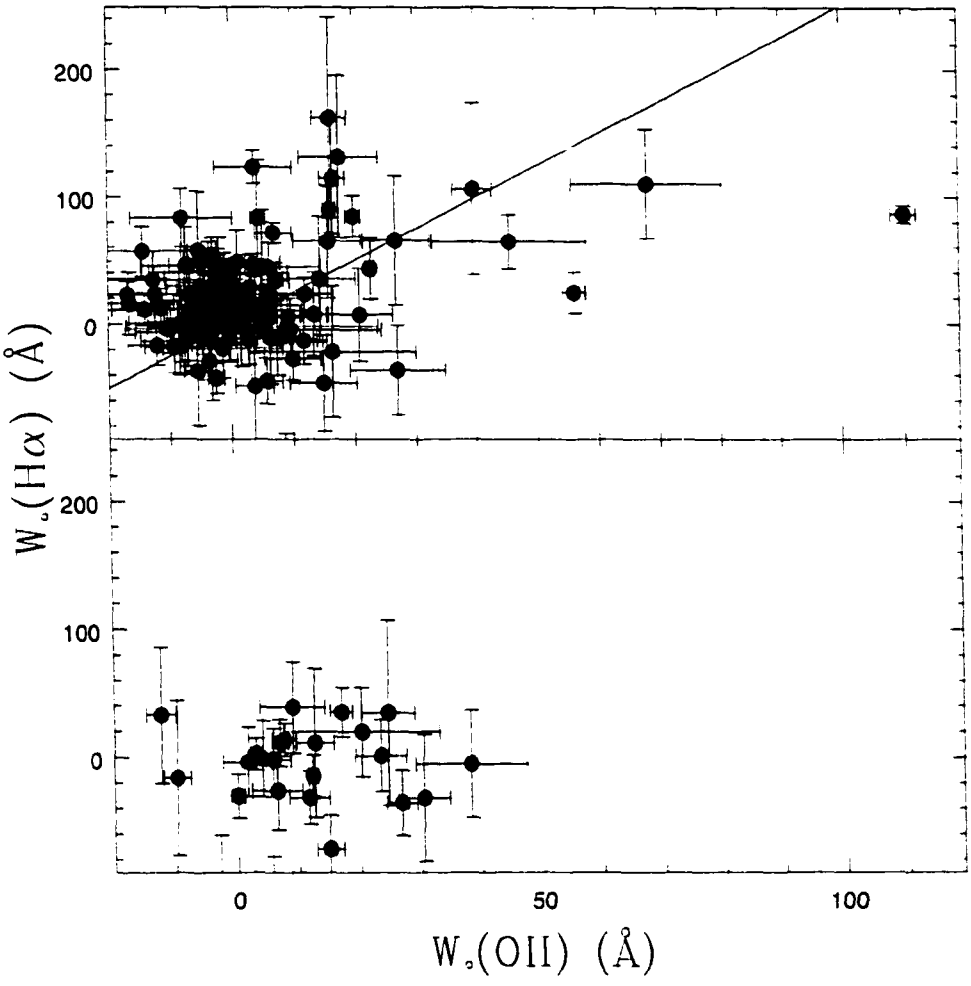

Figure 5.6: For galaxies with redshifts available from the Abraham et al. (1996) catalogue, we show $W_o(H\alpha)$ from our OSIS observations compared with W_o(OII) measured from the CNOC1 spectra. Only galaxies with W_o(OII) uncertainties less than 15Å are shown. In the *bottom panel* we show field galaxies (for which $W_o(H\alpha)$ should equal zero, since their Hα line does not lie within our on-line filter range); the *top panel* shows cluster members. The *solid line* is the mean local relation from Kennicutt (1992a).

5.1, adopting a mean Hα extinction of 1 magnitude and correcting for [NII] contamination assuming [NII]/Hα=0.5 (Kennicutt 1992a). We determine the Hα flux, $f(H\alpha)$, from $W_\circ(H\alpha)$ and the continuum flux f_c, as $f(H\alpha) = f_c W_\circ(H\alpha)/\Delta\lambda$, where $\Delta\lambda = 348$ Å is the FWHM of the on-line filter. The luminosity of the line is then computed assuming a cosmology with $\Omega = 0.2$, $\Lambda = 0$. The relation between SFR and $W_\circ(H\alpha)$ is shown in Figure 5.7; only galaxies brighter than $r = 21.7$ that are detected in Hα at the 2σ level are plotted. The filled symbols are those which have no detectable [OII] emission in their spectra ($W_\circ$(OII)< 5Å with 2σ confidence). These ten galaxies have SFRs between 1 and 4 $h^{-2} M_\odot \mathrm{yr}^{-1}$, comparable to that of the Milky Way (Prantzos and Aubert 1995), despite the absence of [OII].

In Figure 5.8 we show the $W_\circ$(OII)-$W_\circ(H\alpha)$ relation for three subsamples of galaxies. In the bottom panel we plot only galaxies with $g - r > 0.8$ (which lie on the so-called red sequence), and weak ($W_\circ(H\delta)$< 3) absorption lines. In general, these galaxies do not have strong [OII] lines, and few are detected in Hα, either. Galaxies blueward of the red sequence, and with weak $W_\circ(H\delta)$ indices, are shown in the middle panel; most of the galaxies with strong $W_\circ$(OII) are detected in Hα. Finally, in the top panel, we show examples of galaxies with unusually strong Balmer absorption lines. These are objects that have $W_\circ(H\delta)$> 3Å with at least 1σ confidence, and either no detectable $W_\circ$(OII), or positive $W_\circ$(OII), again with 1σ confidence. All of these galaxies have $W_\circ(H\delta)$> 5Å, and would thus be classified either K+A or A+em in the terminology of Chapter 4. The distribution of these points does not appear to be too different from that of the normal, blue galaxies shown in the middle panel, though there is an indication that at least some

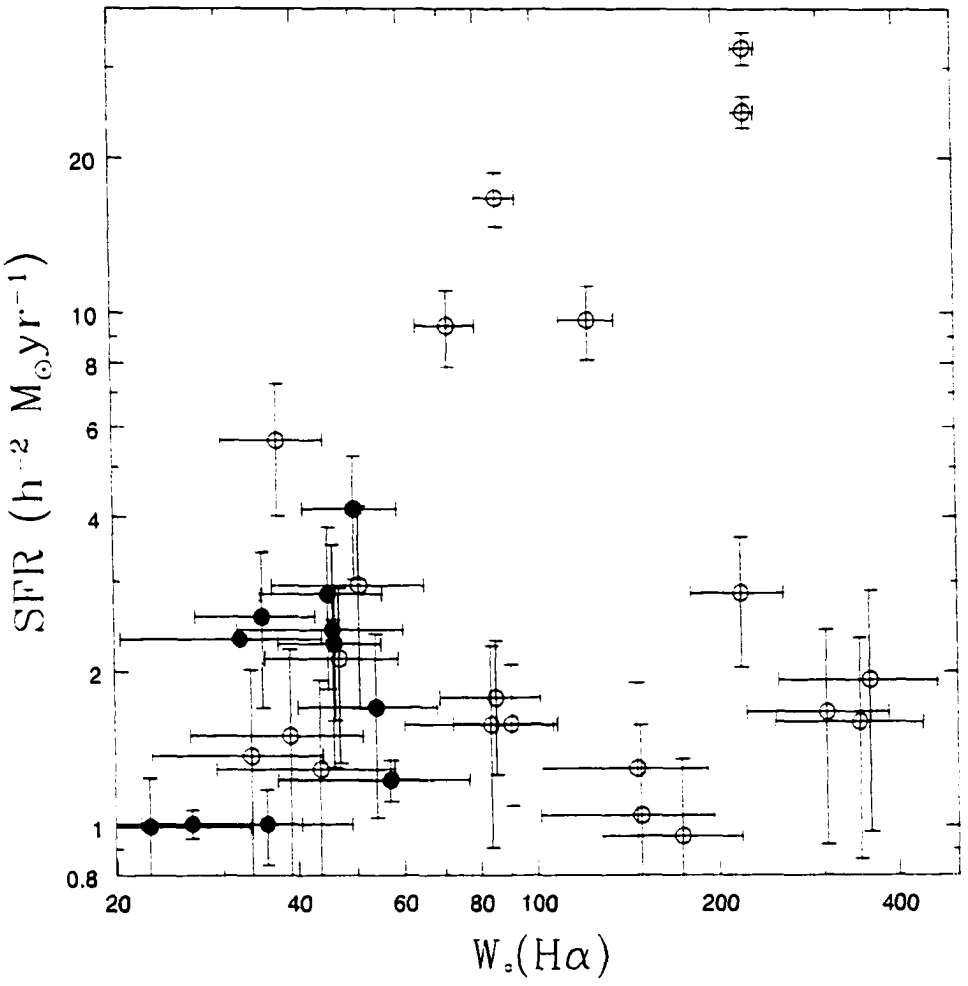

Figure 5.7: We show star formation rates computed from Equation 5.1, as a function of $W_o(H\alpha)$, for galaxies brighter than $r = 21.7$ detected in Hα at the 2σ level. *Filled circles* are galaxies for which a spectrum is available and in which [OII] is undetected at the 2σ level. The SFRs are corrected for [NII] emission and 1 magnitude of extinction, but the plotted values of $W_o(H\alpha)$ are not.

K+A galaxies have strong Hα emission. Recently, Poggianti et al. (1999) have suggested that the A+em galaxies are starburst galaxies in which the [OII] line suffers strong extinction. The few such galaxies in our present sample appear to have fairly normal ratios of $W_o(H\alpha)/W_o(\mathrm{OII})$, however, which suggests that the $W_o(\mathrm{OII})$ line is not preferentially extincted in these galaxies.

5.4.2 Properties of the Full Hα Sample

$W_o(H\alpha)$ measurements for the full catalogue are shown in Figure 5.9. In the bottom panel we show all galaxies, as a function of r; in the top panel, $W_o(H\alpha)$ is plotted against R_{proj}/R_{200}, for only those galaxies brighter than our magnitude limit of $r = 21.7$. Note that both of these figures will include field galaxies, for which $W_o(H\alpha)$ of any strength is not detectable. There is a clear trend for galaxies with strong $W_o(H\alpha)$ to be fainter ($r \gtrsim 20$) and located at large distances from the cluster centre ($\gtrsim 0.1R_{200}$).

To calculate the fraction of galaxies with detected Hα emission, we need to make a statistical correction for the inclusion of field galaxies, which will be relatively more common far from the cluster centre. To do this, we use the CNOC1 spectroscopic sample to calculate the fraction of of cluster members as a function of R_{proj}/R_{200}, including the appropriate statistical weights discussed in 5.4.1. This fraction is shown in Figure 5.10; nearly all of the galaxies within $0.1R_{200}$ are expected to be cluster members, while only ~70% or so near R_{200} are members.

Using this statistical field correction, and the $W_{H\alpha}$ weights discussed in §5.3.3 to correct for incompleteness, we show, in Figure 5.11, the fraction

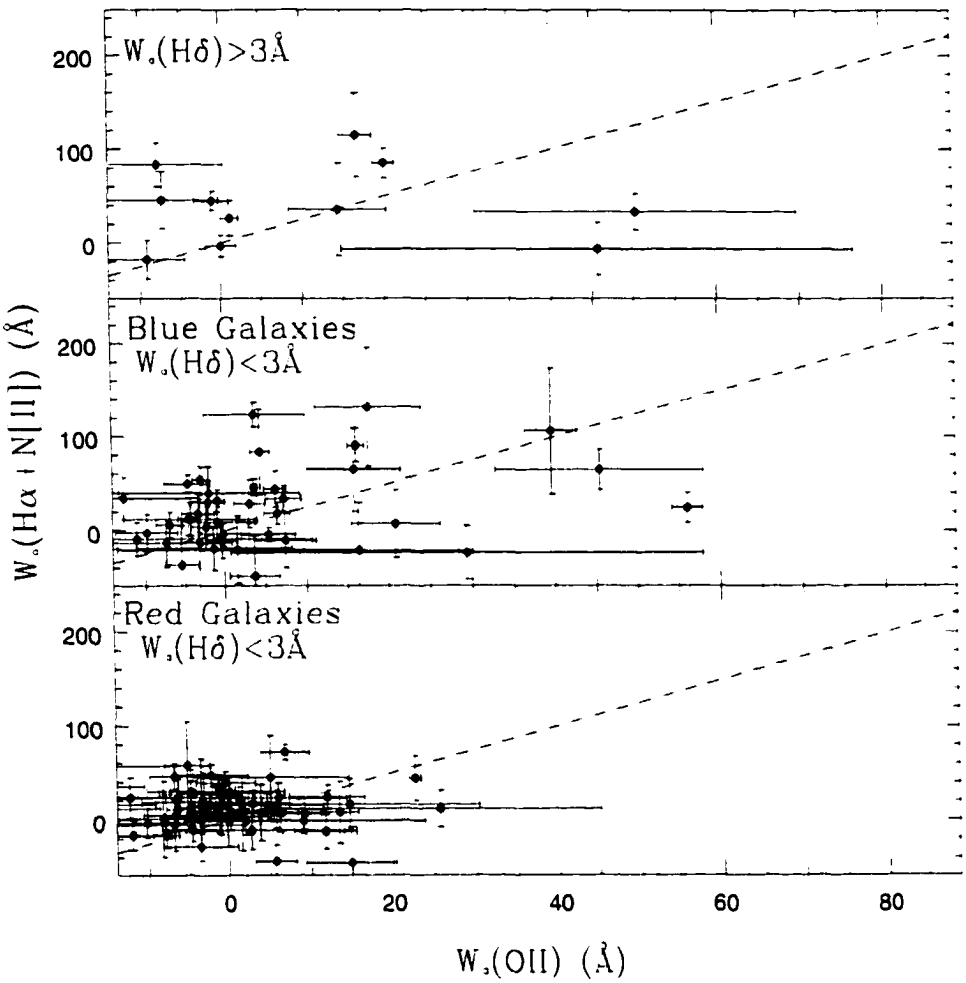

Figure 5.8: We show the $W_o(H\alpha)$-W_o(OII) relation for galaxies matched with the CNOC1 spectroscopic sample, with uncertainties on W_o(OII) less than 40Å. In the *bottom panel*, we show galaxies with $g - r > 0.8$, and $W_o(H\delta) < 3$ Å. In the *middle panel* we show galaxies with $g - r < 0.8$ and $W_o(H\delta) < 3$ Å. These two samples represent the "normal" populations of red and blue galaxies, respectively. In the *top panel* we show those galaxies that have $W_o(H\delta) > 3$ Å, with at least 1σ confidence, and those galaxies which have either no [OII] emission, or positive [OII] emission, with 1σ confidence. The *dashed line* in all three panels represents the local relation of Kennicutt (1992a).

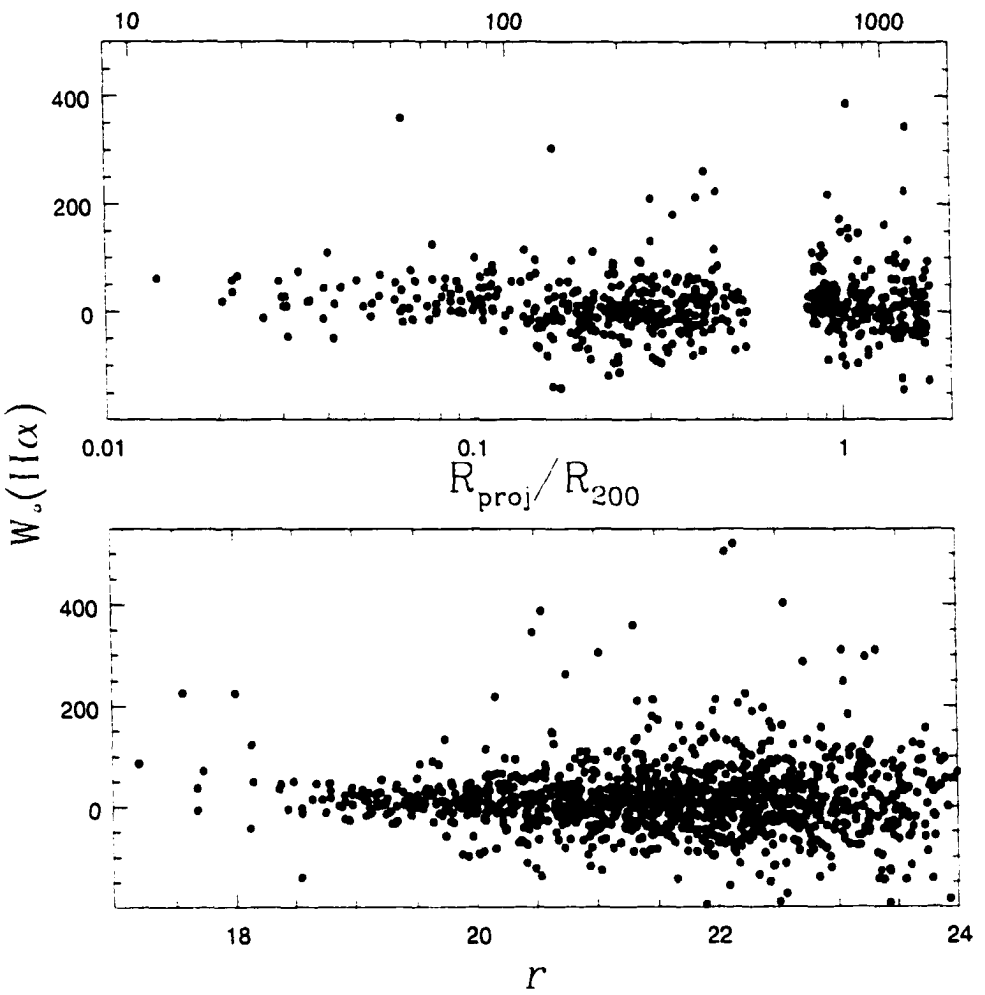

Figure 5.9: In the *bottom panel*, we show $W_o(H\alpha)$ measurements for all galaxies in our sample, as a function of r. The sample is 50% complete at $r \approx 21.7$; galaxies brighter than this limit are shown in the *top panel*, as a function of projected distance from the BCG, normalised to R_{200} on the bottom scale, and in arcseconds on the top scale. Galaxies with Hα emission tend to be fainter than $r = 20$, and to be located at large distances from the cluster centre.

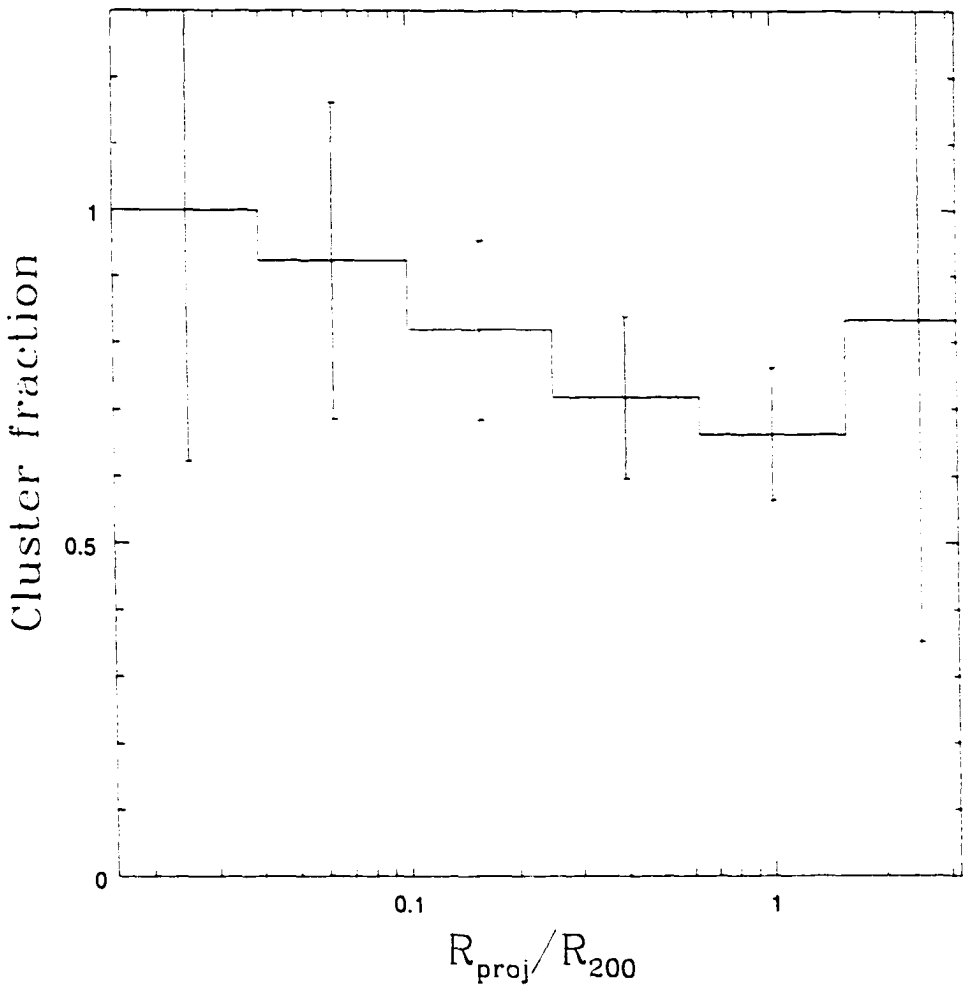

Figure 5.10: The ratio of cluster members to total number of galaxies (brighter than $r = 21.7$) in the CNOC1 spectroscopic catalogue, weighted appropriately as discussed in §5.4.1, as a function of projected distance from the BCG, normalised to R_{200}. Error bars are 1σ, and are computed as the plotted value divided by the square root of the number of cluster galaxies in that bin. This is used to correct the fraction of cluster members with detected Hα for field contamination.

of galaxies that have $W_o(H\alpha)> 0$ Å with 2σ confidence, as a function of R_{proj}/R_{200}. There is a clear increase in the incidence of galaxies with detectable emission with increasing distance from the cluster centre. A total of 13.8±2.3% of all cluster members in the sample have detectable Hα emission.

5.4.3 Morphology

In order to compare the morphology of galaxies in the different filters, we must attempt to match the seeing in each image. The list of stellar objects extracted from each field (see §5.3) is used to compute the PSF for each image; we then use the *psfmatch* routine to convolve the three images with the best seeing to match the PSF of the image with the worst.

The convolved images in the RC, BC and on-line filters were then combined in the following way to produce a continuum subtracted Hα image. First, a continuum image was created by averaging the RC and BC images, after first scaling each one by a factor of $10^{\Delta M_o/2.5}$, where $\Delta M_o = m'_{o,on} - m'_{o,i}$, and $m'_{o,i} = m_{o,i} - A_i\chi_i + 2.5 \log t_i$ for filter i (compare Equation 5.6). This allows for a correct combination of the two fluxes, given their different transmission functions. This continuum image was then multiplied by the scale factor determined to match the on-line flux in stellar objects (which corrects for fluctuations in the zero point, see §5.3.2.6), and subtracted from the PSF-matched on-line image, to produce a final image in Hα+[NII] light.

The good seeing and resolution of our OSIS observations allows us to resolve the emission in many cases. Although a full analysis is beyond the scope of the present work, we show three particular examples in Figure 5.12 which reveal interesting structure in Hα emission. The BCG image (which

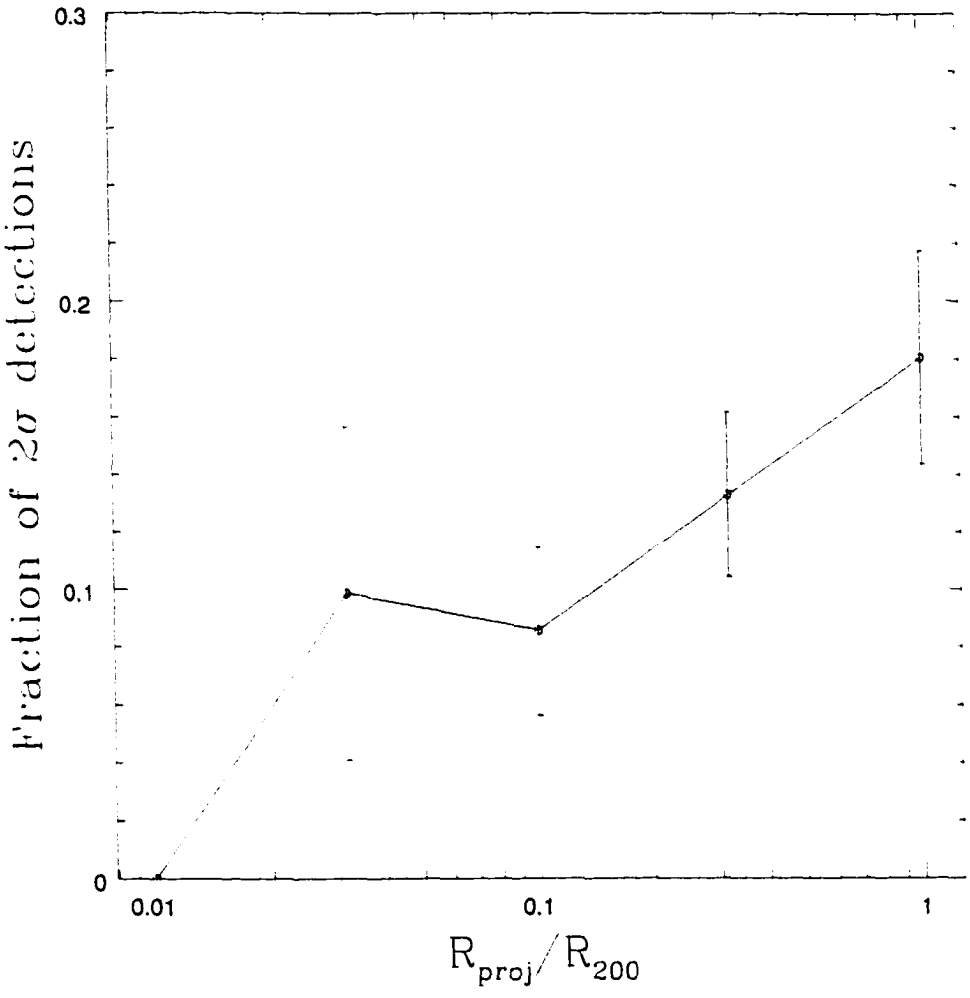

Figure 5.11: The fraction of cluster members with $W_o(H\alpha)>$ 0Å, with at least 2σ confidence. The fractions are corrected for field contamination, and for incompleteness, as discussed in the text.

also has strong [OII] emission in its spectrum) shows that the emission is very localised to an asymmetric band, starting in the centre of the image and extending outwards about 5″(12 h^{-1} kpc). The lowest contour represents an Hα surface brightness of 21.8 mag/arcsec. The total value of $W_o(H\alpha)$ is fairly low (86.6±6.8Å), despite the large flux, because the total light is dominated by the bright continuum, which is present over a much larger area. The equivalent width in the central region (in an aperture with a 16 pixel radius), is considerably larger: 150±7 Å.

Two fainter galaxies are shown in the bottom panel of Figure 5.12; in this case, the lowest contour level is drawn at 22.6 mag/arcsec. Shown in the bottom left panel is a single galaxy in which the Hα emission is resolved into two distinct regions. This may be indicative of a recent accretion event, where the nuclei of the two galaxies have not yet completely merged. Finally, in the bottom right panel, we show a pair of cluster galaxies which have remarkably similar Hα structure. Most notable is the asymmetry of this emission, suggestive of a bow shock (e.g. Devine and Bally 1999; Kenney and Koopmann 1999). The centre of the cluster is almost due east (to the right of this image) from these galaxies; thus, if the shock is due to passage through the intra-cluster medium, the galaxies' orbits are not exactly radial.

5.5 Conclusions

We have measured $W_o(H\alpha)$ for 1189 galaxies over fields covering 270 □′ about the cluster Abell 2390. We confirm the presence of a gradient in star formation activity within this cluster; the fraction of galaxies in which Hα

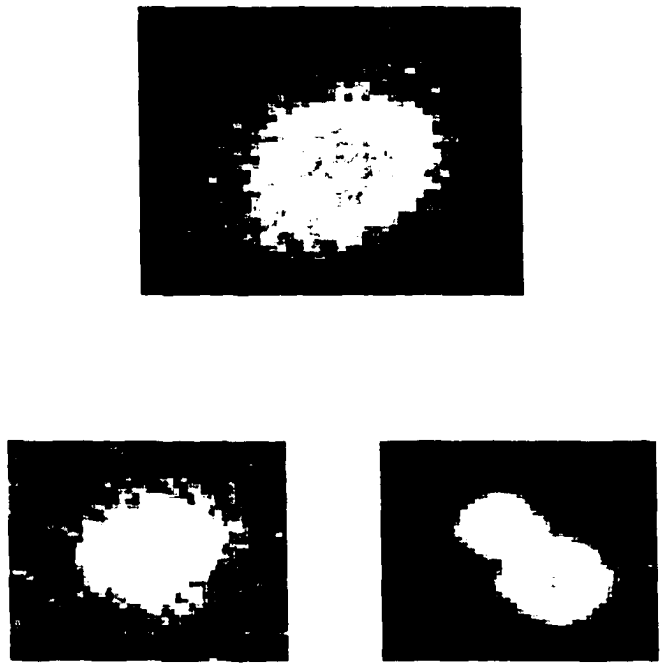

Figure 5.12: Hα contours are plotted on top of the continuum images of three galaxies. The BCG is shown in the *top panel*; the emission is clearly resolved and asymmetrically distributed. In the *bottom left panel* we show a single galaxy with clear evidence for two distinct centres of Hα emission, possibly indicative of a merger remnant. The *bottom right* panel shows a pair of galaxies with similar Hα structures, suggestive of a bow shock. East is to the right, north to the bottom.

emission is detected increases from zero in the central regions ($R_{proj}/R_{200} <$ 0.02, excluding the BCG) to 18±4% at R_{200}. For 166 of these galaxies, we compare $W_\circ(H\alpha)$ with $W_\circ$(OII), the latter measured from CNOC1 spectra. Approximately 20% of CNOC1 galaxies in which the [OII] emission line is not detected with 2σ confidence have detectable Hα emission, indicative of star formation rates up to 4 $h^{-2}M_\odot \mathrm{yr}^{-1}$. This confirms that the total cluster star formation rate will be underestimated if [OII] is used as a star formation indicator. In particular, some K+A galaxies (which have strong Hδ absorption but no detectable [OII]) are detected in Hα, which suggests that dust may be partly responsible for the unusual appearance of these spectra.

Chapter 6

Conclusions

We have analysed the spectra of 1823 galaxies in the fields of 15 X-ray luminous clusters at $0.2 < z < 0.55$, from the CNOC1 redshift survey. Star formation rates were determined from the equivalent width of the [OII] emission line, and systematic differences between cluster and field galaxies, as a function of galaxy morphology, were considered. Star formation rates are also determined from Hα equivalent widths, for cluster galaxies in A2390, to investigate systematic effects that may result from using [OII] as a star formation indicator. We consider the D4000 and $W_\circ(H\delta)$ spectral indices, calibrated on spectrophotometric models, to establish the recent star formation history of galaxies in this sample.

There is a clear correlation of star formation history and galaxy morphology with distance from the cluster centre. Galaxies in the cluster centre are mostly bulge dominated, with weak or absent $W_\circ$(OII) and $W_\circ(H\alpha)$ emission, red colours and large D4000 indices. With increasing distance from the cluster centre, the mean star formation rate also increases, but does not become equal to the mean in the field, even at $2R_{200}$. These correlations

are all consistent with an age gradient, in the sense that the last episode of star formation occurred more recently for galaxies farther from the cluster centre. This is not a mere reflection of the morphology–radius relation: cluster galaxies show less star formation than field galaxies with similar physical sizes, fractional bulge luminosities, and redshifts. If these correlations reflect an evolutionary sequence, this implies that the timescales for morphological transformation are longer than those for changes in the observable star formation rate.

There is no evidence for a population of cluster galaxies undergoing enhanced star formation, relative to field galaxies. The fraction of cluster galaxies with the strongest [OII] emission lines, W_o(OII)> 40Å, is 1.4±0.4%, significantly less than the field fraction of 4.3±1.1%. From the fraction of galaxies with strong $W_o(H\delta)$, but weak or absent W_o(OII), we conclude that less than ∼10% of the galaxies in both the cluster and the field may have undergone short starbursts in the last 2 Gyr. The A+em galaxies, which may be dust obscured starburst galaxies, are two times more common in our field sample than in the cluster. Thus, there is no evidence that these clusters *induce* star formation in any galaxy.

The fraction of K+A galaxies in the CNOC1 sample is less than 5%; there is no evidence that these objects are more common in the cluster sample than in the field sample. We find that the large uncertainties on the spectral line indices lead to an overestimate of this fraction; when we account for this effect, only 1.2±0.8% of the field galaxies more luminous than $M_r = -18.8 + 5\log h$ are classified K+A, consistent with the LCRS $z = 0.1$ fraction of 0.30% (Zabludoff et al. 1996) at the $\sim 1\sigma$ level. It is still unclear what

physical mechanism is responsible for generating these unusual spectral types. There appears to be a large excess of PSF galaxies, relative to PSB galaxies, which may be taken as evidence that truncated star formation *without* a short starburst phase may play a significant role in galaxy evolution. However, $\sim$ 20% of galaxies in A2390 which do not have detectable [OII] emission *are* detected in Hα; this demonstrates that dust obscuration (particularly in K+A galaxies) may be responsible for suppressing evidence for star formation at these redshifts.

These observations show that X-ray luminous clusters at $z \approx 0.3$ do not enhance star formation in galaxies, regardless of morphology, relative to the field population. The simplest model of cluster formation consistent with the data is that star formation ceases shortly after a galaxy is accreted into a cluster. Since there are very few galaxies with strong $W_\circ(H\delta)$ indices, which would indicate recent, abrupt truncation of star formation, we postulate that this activity may cease over a relatively long time, $\gtrsim$ 2 Gyr, which is consistent with the gas consumption time scale of normal, isolated galaxies. Therefore, a model in which cluster galaxies lack a mechanism for refuelling star formation (i.e., via infall from a gaseous halo) may be able to explain the radial correlation of SFR within these clusters.

Bibliography

Abell, G. O.: 1958, *Astrophys. J. Supp.* **3**, 211

Abell, G. O.: 1965, *Annual Review of Astronomy and Astrophysics* **3**, 1

Abraham, R. G., Ellis, R. S., Fabian, A. C., Tanvir, N. R., and Glazebrook, K.: 1998, *M.N.R.A.S.* **303**, 6411

Abraham, R. G., Smecker-Hane, T. A., Hutchings, J. B., Carlberg, R. G., Yee, H. K. C., Ellingson, E., Morris, S., Oke, J. B., and Rigler, M.: 1996, *Astrophys. J.* **471**, 694

Abramopoulos, F. and Ku, W. H.-M.: 1983, *Astrophys. J.* **271**, 446

Allington-Smith, J. R., Ellis, R. S., Zirbel, E. L., and Oemler, A.: 1993, *Astrophys. J.* **404**, 521

Andreon, S. and Ettori, S.: 1999, *Astrophys. J.* **516**, 647

Antonuccio-Delogu, V. and Colafrancesco, S.: 1994, *Astrophys. J.* **421**, 1

Arnaud, M., Rothenflug, R., Bloulade, O., Vigroux, L., and Vangioni-Flam, E.: 1992, *Astron. & Astrophys.* **254**, 49

Bahcall, J. and Sarazin, C.: 1977, *Astrophys. J.* **213**, 137

Bahcall, N. A.: 1977, *Astrophys. J. Lett.* **218**, 93

Balogh, M. L., Babul, A., and Patton, D. R.: 1999a, *astro-ph/* 9809159

Balogh, M. L., Morris, S. L., Yee, H. K. C., Carlberg, R. G., and Ellingson,

E.: 1997, *Astrophys. J. Lett.* **488**, 75

Balogh, M. L., Morris, S. L., Yee, H. K. C., Carlberg, R. G., and Ellingson, E.: 1999b, *Astrophys. J.* accepted

Balogh, M. L., Schade, D., Morris, S. L., Yee, H. K. C., Carlberg, R. G., and Ellingson, E.: 1998, *Astrophys. J. Lett.* **504**, 75

Balsara, D., Livio, M., and O'Dea, C. P.: 1994, *Astrophys. J.* **437**, 83

Barbaro, G. and Poggianti, B. M.: 1997, *Astron. & Astrophys.* **324**, 490

Barger, A. J., Aragón-Salamanca, A., Ellis, R. S., Couch, W. J., Smail, I., and Sharples, R. M.: 1996, *M.N.R.A.S.* **279**, 1

Barger, A. J., Aragón-Salamanca, A., Smail, I., Ellis, R. S., Couch, W. J., Dressler, A., Oemler, A., Poggianti, B. M., and Sharples, R. M.: 1998, *Astrophys. J.* **501**, 522

Barnes, J. E. and Hernquist, L. E.: 1991, *Astrophys. J. Lett.* **370**, 65

Barrientos, F., Schade, D., and López-Cruz, O.: 1996, *Astrophys. J. Lett.* **460**, 89

Baugh, C. M., Cole, S., and Frenk, C. S.: 1996, *M.N.R.A.S.* **283**, 1361

Böhm-Vitense, E.: 1992, *Introduction to Stellar Astrophysics Vol. 3: Stellar Structure and Evolution*, Cambridge University Press: Cambridge

Bertin, E. and Arnouts, S.: 1996, *Astron. & Astrophys. Supp.* **117**, 393

Bhavsar, S. P.: 1981, *Astrophys. J. Lett.* **246**, 5

Biviano, A., Katgert, P., Mazure, A., Moles, M., den Hartog, R., Perea, J., and Focardi, P.: 1997, *Astron. & Astrophys.* **321**, 84

Blitz, L., Spergel, D. N., Teuben, P. J., Hartmann, D., and Burton, W. B.: 1999, *Astrophys. J.* **514**, 818

Bohlin, R. C., Hill, J. K., Jenkins, E. B., Savage, B. D., Snow, T. P., Spitzer,

L., and York, D. G.: 1983, *Astrophys. J. Supp.* **51**, 277

Bothun, G. D. and Dressler, A.: 1986, *Astrophys. J.* **301**, 57

Bothun, G. D. and Gregg, M. D.: 1990, *Astrophys. J.* **350**, 73

Bower, R. G., Ellis, R. S., Rose, J. A., and Sharples, R. M.: 1990, *Astron. J.* **99**, 2

Bower, R. G., Kodama, T., and Terlevich, A.: 1998, *M.N.R.A.S.* **299**, 1193

Broadhurst, T. J., Ellis, R. S., and Shanks, T.: 1988, *M.N.R.A.S.* **235**, 827

Bruzual, G.: 1981, *Ph.D. thesis*, University of California, Berkeley

Bruzual, G. and Charlot, S.: 1993, *Astrophys. J.* **405**, 538

Butcher, H. and Oemler, A.: 1978a, *Astrophys. J.* **219**, 18

Butcher, H. and Oemler, A.: 1978b, *Astrophys. J.* **226**, 559

Butcher, H. and Oemler, A.: 1984, *Astrophys. J.* **285**, 426

Byrd, G. and Valtonen, M.: 1990, *Astrophys. J.* **350**, 89

Caldwell, N., Rose, J. A., and Dendy, K.: 1998, *Astron. J.* **117**, 140

Caldwell, N., Rose, J. A., Franx, M., and Leonardi, A. J.: 1996, *Astron. J.* **111**, 78

Caldwell, N., Rose, J. A., Sharples, R. M., Ellis, R. S., and Bower, R. G.: 1993, *Astron. J.* **106**, 473

Caplan, J. and Deharveng, L.: 1986, *Astron. & Astrophys.* **155**, 297

Caplan, J., Ye, T., Deharveng, L., Turtle, A. J., and Kennicutt, R. C.: 1996, *Astron. & Astrophys.* **307**, 403

Carlberg, R. G., Morris, S. L., Yee, H. K. C., and Ellingson, E.: 1997a, *Astrophys. J.* **479**, 19

Carlberg, R. G., Yee, H. K. C., and Ellingson, E.: 1997b, *Astrophys. J.* **478**, 462

Carlberg, R. G., Yee, H. K. C., Ellingson, E., Abraham, R., Gravel, P., Morris, S., and Pritchet, C. J.: 1996, *Astrophys. J.* **462**, 32

Carlberg, R. G., Yee, H. K. C., Ellingson, E., Morris, S. L., Abraham, R., Gravel, P., Pritchet, C. J., Smecker-Hane, T., Hartwick, F. D. A., Hesser, J. E., Hutchings, J. B., and Oke, J. B.: 1997c, *Astrophys. J. Lett.* **485**, 13

Carlberg, R. G., Yee, H. K. C., Ellingson, E., Pritchet, C. J., Abraham, R., Smecker-Hane, T., Bond, J. R., Couchman, H. M. P., Crabtree, D., Crampton, D., Davidge, T., Durand, D., Eales, S., Hartwick, F. D. A., Hesser, J. E., Hutchings, J. B., Kaiser, N., Mendes De Oliveira, C., Myers, S. T., Oke, J. B., Rigler, M. S., Schade, D., and West, M.: 1994, *J. Royal Astron. Society of Canada* **88**, 39

Cavaliere, A. and Fusco-Femiano, R.: 1976, *Astron. & Astrophys.* **49**, 137

Coleman, G. D., Wu, C. C., and Weedman, D. W.: 1980, *Astrophys. J. Supp.* **43**, 393

Collins, C., Burke, D., Romer, A., Sharples, R., and Nicol, R.: 1997, *Astrophys. J. Lett.* **479**, 117

Couch, W. J., Barger, A. J., Smail, I., Ellis, R. S., and Sharples, R. M.: 1998, *Astrophys. J.* **497**, 188

Couch, W. J., Ellis, R. S., Sharples, R. M., and Smail, I.: 1994, *Astrophys. J.* **430**, 121

Couch, W. J. and Sharples, R. M.: 1987, *M.N.R.A.S.* **229**, 423

Cowie, L. L., Songaila, A., and Barger, A. J.: 1999, *astro-ph/* 9904345

Cowie, L. L., Songaila, A., Hu, E. M., and Cohen, J. G.: 1996, *Astron. J.* **112**, 839

Crone, M. M., Evrard, A. E., and Richstone, D. O.: 1994, *Astrophys. J.* **434**, 402

Curtis, H. D.: 1918, *Pub. Lick. O.* **13**, 9

David, L., Forman, W., and Jones, C.: 1991, *Astrophys. J.* **380**, 39

Devine, D. and Bally, J.: 1999, *Astrophys. J.* **510**, 197

Dressler, A.: 1980, *Astrophys. J.* **236**, 351

Dressler, A. and Gunn, J. E.: 1982, *Astrophys. J.* **263**, 533

Dressler, A. and Gunn, J. E.: 1983, *Astrophys. J.* **270**, 7

Dressler, A., Oemler, A., Butcher, H. R., and Gunn, J. E.: 1994, *Astrophys. J.* **430**, 107

Dressler, A., Oemler, A., Couch, W. J., Smail, I., Ellis, R. S., Barger, A., Butcher, H. R., Poggianti, B. M., and Sharples, R. M.: 1997, *Astrophys. J.* **490**, 577

Dressler, A., Smail, I., Poggianti, B. M., Butcher, H., Couch, W. J., Ellis, R. S., and Oemler, A.: 1999, *astro-ph/* 9901263

Dressler, A., Thompson, I. B., and Shectman, S.: 1985a, *Astrophys. J.* **288**, 481

Dressler, A., Thompson, I. B., and Shectman, S. A.: 1985b, *Astrophys. J.* **288**, 481

Ebeling, H., Edge, A. C., Fabian, A. C., Allen, S. W., Crawford, C. S., and Böhringer, H.: 1997, *Astrophys. J. Lett.* **479**, 101

Efron, B.: 1981, *Biometrika* **68**, 589

Efron, B. and Tibshirani, R.: 1986, *Statistical Science* **1**, 54

Eke, V. R., Cole, S., and Frenk, C. S.: 1996, *M.N.R.A.S.* **263**, 280

Eke, V. R., Cole, S., Frenk, C. S., and Henry, J. P.: 1998, *M.N.R.A.S.* **298**,

1145

Ellis, R. S., Smail, I., Dressler, A., Couch, W. J., Oemler, A., Butcher, H., and Sharples, R. M.: 1997, *Astrophys. J.* **483**, 582

Evrard, A. E.: 1991, *M.N.R.A.S.* **248**, 8p

Fabricant, D. G., McClintock, J. E., and Bautz, M. W.: 1991, *Astrophys. J.* **381**, 33

Fioc, M. and Rocca-Volmerange, B.: 1997, *Astron. & Astrophys.* **326**, 950

Fisher, D., Fabricant, D., Franx, M., and van Dokkum, P.: 1998, *Astrophys. J.* **498**, 195

Fujita, Y.: 1998, *Astrophys. J.* **509**, 587

Fujita, Y. and Nagashima, M.: 1999, *astro-ph/* 9812378

Fujita, Y. and Takahara, F.: 1999, *astro-ph/* 9905083

Fujita, Y., Takizawa, M., Nagashima, M., and Enoki, M.: 1999, *astro-ph/* 9904386

Fukugita, M., Shimasaku, K., and Ichikawa, T.: 1995, *P.A.S.P.* **107**, 945

Gallagher, J. S., Bushouse, H., and Hunter, D. A.: 1989, *Astron. J.* **97**, 700

Gavazzi, G. and Jaffe, W.: 1987, *Astrophys. J.* **310**, 53

Ghigna, S., Moore, B., Governato, G., Lake, G., Quinn, T., and Stadel, J.: 1998, *M.N.R.A.S.* **300**, 146

Giavalisco, M., Steidel, C. C., and Macchetto, F. D.: 1996, *Astrophys. J.* **470**, 189

Gioia, I. M. and Luppino, G. A.: 1994, *Astrophys. J. Supp.* **94**, 583

Gioia, I. M., Maccacaro, T., Schild, R. E., Wolter, A., Stocke, J. T., Morris, S. L., and Henry, J. P.: 1990, *Astrophys. J. Supp.* **72**, 567

Giovanelli, R. and Haynes, M.: 1985, *Astrophys. J.* **292**, 404

Gisler, G. R.: 1978, *M.N.R.A.S.* **183**, 633

Gott, J. R. and Gunn, J.: 1972, *Astrophys. J.* **176**, 1

Gunn, J. E., Hoessel, J. G., and Oke, J. B.: 1986, *Astrophys. J.* **306**, 30

Guzman, R., Gallego, J., Koo, D. C., Phillips, A. C., Lowenthal, J. D., Faber, S. M., Illingworth, G. D., and Vogt, N. P.: 1997, *Astrophys. J.* **489**, 559

Hamilton, D.: 1985, *Astrophys. J.* **297**, 371

Hammer, F., Flores, H., Lilly, S. J., Crampton, D., LeFèvre, O., Rola, C., Mallen-Ornelas, G., Schade, D., and Tresse, L.: 1997, *Astrophys. J.* **481**, 49

Hashimoto, Y., Oemler, A., Lin, H., and Tucker, D. L.: 1998, *Astrophys. J.* **499**, 589

Henriksen, M. J. and Byrd, G.: 1996, *Astrophys. J.* **459**, 82

Henriksen, M. J. and Jones, C.: 1996, *Astrophys. J.* **465**, 666

Henry, J. P. and Arnaud, K. A.: 1991, *Astrophys. J.* **372**, 410

Henry, J. P., Gioia, I., Maccacaro, T., Morris, S. L., Stocke, J. T., and Wolter, A.: 1992, *Astrophys. J.* **386**, 408

Hill, J. M. and Oegerle, W. R.: 1993, *Astron. J.* **106**, 3

Hogg, D. W., Cohen, J. G., Blandford, R., and Pahre, M. A.: 1998, *Astrophys. J.* **504**, 622

Hubble, E.: 1936, *The Realm of the Nebula*, Yale University Press: New Haven

Hubble, E. and Humason, M. L.: 1931, *Astrophys. J.* **74**, 43

Hudson, M. J., Smith, R. J., Lucey, J. R., Schlegel, D. J., and Davies, R. L.: 1999, *Astrophys. J. Lett.* **512**, 79

Humason, A. J.: 1956, *Astron. J.* **61**, 97

Kaiser, N.: 1991, *Astrophys. J.* **383**, 104

Kauffmann, G.: 1995, *M.N.R.A.S.* **274**, 153

Kaufman, M., Bash, F. N., Kennicutt, R. C., and Hodge, P. W.: 1987, *Astrophys. J.* **319**, 61

Kelson, D. D., van Dokkum, P. G., Franx, M., Illingworth, G. D., and Fabricant, D.: 1997, *Astrophys. J. Lett.* **478**, 13

Kenney, J. D. P. and Koopmann, R. A.: 1999, *Astron. J.* **117**, 181

Kennicutt, R. C.: 1983, *Astrophys. J.* **272**, 54

Kennicutt, R. C.: 1992a, *Astrophys. J.* **388**, 310

Kennicutt, R. C.: 1992b, *Astrophys. J. Supp.* **79**, 255

Kennicutt, R. C.: 1999, *astro-ph/* 9807187

Kennicutt, R. C., Tamblyn, P., and Congdon, C. W.: 1994, *Astrophys. J.* **435**, 22

King, C. and Ellis, R. S.: 1985, *Astrophys. J.* **288**, 456

Kinney, A. L., Calzetti, D., Bohlin, R. C., McQuade, K., Storchi-Bergmann, T., and Schmitt, H. R.: 1996, *Astrophys. J.* **467**, 38

Kodama, T., Bower, R. G., and Bell, E. F.: 1998, *M.N.R.A.S.* **302**, 152

Koo, D. C.: 1981, *Astrophys. J. Lett.* **251**, 75

Koo, D. C., Guzmán, R., Gallego, J., and Wirth, G. D.: 1997, *Astrophys. J.* **478**, 49

Koopmann, R. A. and Kenney, J. D. P.: 1998, *Astrophys. J.* **497**, 75

Kormendy, J.: 1985, *Astrophys. J.* **295**, 73

Kron, R. G.: 1980, *Astrophys. J. Supp.* **43**, 305

Larson, R. B., Tinsley, B. M., and Caldwell, C. N.: 1980, *Astrophys. J.* **237**, 692

Lauer, T. R. and Postman, M.: 1994, *Astrophys. J.* **425**, 418

Lavery, R. J. and Henry, J. P.: 1986, *Astrophys. J. Lett.* **304**, 5

Lewis, A. D., Ellingson, E., Morris, S. L., and Carlberg, R. G.: 1999, *Astrophys. J.* **517**, 587

Lilly, S. J., Ellis, R. S., Fevre, O. L., Brinchmann, J., Tresse, L., Abraham, R., Hammer, F., Crampton, D., Colless, M., Glazebrook, K., Mallen-Ornelas, G., and Broadhurst, T.: 1998, *Astrophys. J.* **500**, 75

Lilly, S. J., Tresse, L., Hammer, F., Crampton, D., and LeFèvre, O.: 1995, *Astrophys. J.* **455**, 108

Lin, H., Kirshner, R. P., Shectman, S. A., Landy, S. D., Oemler, A., Tucker, D. L., and Schechter, P. L.: 1996, *Astrophys. J.* **464**, 60

Lin, H., Yee, H. K. C., Carlberg, R. G., and Ellingson, E.: 1997, *Astrophys. J.* **475**, 494

Lin, H., Yee, H. K. C., Carlberg, R. G., Morris, S. L., Sawicki, M., Patton, D. R., Wirth, G., and Shepherd, C. W.: 1999, *Astrophys. J.* **518**, 533

Lutz, R. K.: 1979, *The Comp. J.* **23**, 262

MacLaren, I., Ellis, R. S., and Couch, W. J.: 1988, *M.N.R.A.S.* **230**, 249

Markevitch, M., Forman, W. R., Sarazin, C. L., and Vikhlinin, A.: 1998, *Astrophys. J.* **503**, 77

Mathieu, R. D. and Spinrad, H.: 1981, *Astrophys. J.* **251**, 485

Melnick, J. and Sargent, W. L. W.: 1977, *Astrophys. J.* **215**, 401

Mitchell, R. J., Culhane, J. L., Davison, P. J. N., and Ives, J. C.: 1976, *M.N.R.A.S.* **176**, 29P

Moore, B., Katz, N., Lake, G., Dressler, A., and Oemler, A.: 1996, *Nature* **379**, 613

Moore, B., Lake, G., and Katz, N.: 1998, *Astrophys. J.* **495**, 139

Morgan, W. W.: 1961, *Proc. Nat. Acad. Sci.* **47**, 905

Morris, S. L., Hutchings, J. B., Carlberg, R. G., Yee, H. K. C., Ellingson, E., Balogh, M. L., Abraham, R. G., and Smecker-Hane, T.: 1998, *Astrophys. J.* **507**, 84

Moss, C. and Whittle, M.: 1993, *Astrophys. J. Lett.* **407**, 17

Mushotzky, R. F., Loewenstein, M., Arnaud, K. A., Tamura, T., Fukazawa, Y., Matsushita, K., Kikuchi, K., and Hatsukade, I.: 1996, *Astrophys. J.* **466**, 686

Newberry, M. V., Boroson, T. A., and Kirshner, R. P.: 1990, *Astrophys. J.* **350**, 585

Nichol, R. C., Holden, B. P., Romer, A. K., Ulmer, M. P., Burke, D. J., and Collins, C. A.: 1997, *Astrophys. J.* **481**, 644

Niklas, S. and Wielebinski, R.: 1997, *Astron. & Astrophys.* **322**, 19

Nulsen, P. E. J.: 1982, *M.N.R.A.S.* **198**, 1007

Oemler, A.: 1974, *Astrophys. J.* **194**, 1

Oke, J. B.: 1974, *Astrophys. J. Supp.* **27**, 21

Oke, J. B.: 1990, *Astron. J.* **99**, 1621

Osterbrock, D. E.: 1960, *Astrophys. J.* **132**, 325

Osterbrock, D. E.: 1989, *Astrophysics of Gaseous Nebulae and Active Galactic Nuclei*, University Science Books : Mill Valley, California

Patton, D. R., Pritchet, C. J., Yee, H. K. C., Ellingson, E., and Carlberg, R. G.: 1997, *Astrophys. J.* **475**, 29

Phillipps, S., Driver, S. P., Couch, W. J., and Smith, R. M.: 1998, *Astrophys. J.* **498**, 119

Poggianti, B. M. and Barbaro, G.: 1996, *Astron. & Astrophys.* **317**, 379

Poggianti, B. M., Smail, I., Dressler, A., Couch, W. J., Barger, A. J., Butcher, H., Ellis, R. S., and Oemler, A.: 1999, *Astrophys. J.* **518**, 576

Ponman, T. J., Cannon, D. B., and Navarro, J. F.: 1999, *Nature* **397**, 135

Postman, M. and Geller, M. J.: 1984, *Astrophys. J.* **281**, 95

Prantzos, N. and Aubert, O.: 1995, *Astron. & Astrophys.* **302**, 69P

Rakos, K. D., Odell, A. P., and Schombert, J. M.: 1997, *Astrophys. J.* **490**, 194

Rakos, K. D. and Schombert, J. M.: 1995, *Astrophys. J.* **439**, 47

Ramírez, A. C. and de Souza, R. E.: 1998, *Astrophys. J.* **496**, 693

Rieke, G. H., Loken, K., Rieke, M. J., and Tamblyn, P.: 1993, *Astrophys. J.* **412**, 99

Rosati, P., Ceca, R. D., Norman, C., and Giacconi, R.: 1998, *Astrophys. J. Lett.* **492**, 21

Rose, J. A., Bower, R. G., Caldwell, N., Ellis, R. S., Sharples, R. M., and Teague, P.: 1994, *Astron. J.* **108**, 6

Rowan-Robinson, M., Mann, R. G., Oliver, S. J., Efstathiou, A., Eaton, N., Goldschmidt, P., Mobasher, B., Serjeant, S. B. G., Sumner, T. J., Danese, L., Elbaz, D., Franceschini, A., Egami, E., Kontizas, M., Lawrence, A., MCMahon, R., Norgaard-Nielsen, H. U., Perez-Fournon, I., and Gonzalez-Serrano, J. I.: 1997, *M.N.R.A.S.* **289**, 490

Salpeter, E. E.: 1955, *Astrophys. J.* **121**, 161

Salvador-Soleé, E., Sanromà, M., and Jordana, J. J.: 1989, *Astrophys. J.* **474**, 561

Sanromà, M. and Salvador-Soleé, E.: 1990, *Astrophys. J.* **360**, 16

Schade, D., Carlberg, R. G., Yee, H. K. C., López-Cruz, O., and Ellingson, E.: 1996a, *Astrophys. J. Lett.* **464**, 63

Schade, D., Lilly, S. J., LeFèvre, O., Hammer, F., and Crampton, D.: 1996b, *Astrophys. J.* **464**, 79

Scheepmaker, A., Ricker, G. R., Brecher, K., Ryckman, S. G., Ballintine, J. E., Doty, J. P., Downey, P. M., and Lewin, W. H. G.: 1976, *Astrophys. J. Lett.* **205**, 65

Sharples, R. M., Ellis, R. S., Couch, W. J., and Gray, P. M.: 1985, *M.N.R.A.S.* **212**, 687

Smail, I., Dressler, A., Couch, W. J., Ellis, R. S., Oemler, A., Butcher, H., and Sharples, R. M.: 1997, *Astrophys. J. Supp.* **110**, 213

Smail, I., Edge, A. C., Ellis, R. S., and Blandford, R. D.: 1998, *M.N.R.A.S.* **293**, 123

Smith, R. M., Driver, S. P., and Phillipps, S.: 1997, *M.N.R.A.S.* **287**, 415

Spitzer, L. and Baade, W.: 1951, *Astrophys. J.* **113**, 413

Steidel, C. C., Giavalisco, M., Dickinson, M., and Adelberger, K. L.: 1996a, *Astron. J.* **112**, 352

Steidel, C. C., Giavalisco, M., Pettini, M., Dickinson, M., and Adelberger, K. L.: 1996b, *Astrophys. J. Lett.* **462**, 17

Torman, G.: 1998, *M.N.R.A.S.* **297**, 648

Trentham, N.: 1997, *M.N.R.A.S.* **286**, 133

Tresse, L. and Maddox, S. J.: 1998, *Astrophys. J.* **495**, 691

Valluri, M.: 1993, *Astrophys. J.* **408**, 57

van den Bergh, S.: 1960, *Astrophys. J.* **131**, 558

van den Bergh, S.: 1991, *P.A.S.P.* **103**, 390

van den Bergh, S.: 1994, *Astron. J.* **107**, 1328

van der Hulst, J. M., Kennicutt, R. C., Crane, P. C., and Rots, A. H.: 1988, *Astron. & Astrophys.* **195**, 38

van Haarlem, M. and van de Weygaert, R.: 1993, *Astrophys. J.* **418**, 544

Veilleux, S., Bland-Hawthorn, J., Cecil, G., Tully, R. B., and Miller, S. T.: 1999, *astro-ph/* 9902366

Vikhlinin, A., McNamara, B., Forman, W., Jones, C., and Quintana, H.: 1998, *Astrophys. J. Lett.* **498**, 21

White, R. E. and Sarazin, C. L.: 1991, *Astrophys. J.* **367**, 476

White, S. D. M. and Rees, M. J.: 1978, *M.N.R.A.S.* **183**, 341

Whitmore, B. C. and Gilmore, D. M.: 1991, *Astrophys. J.* **367**, 64

Whitmore, B. C., Gilmore, D. M., and Jones, C.: 1993, *Astrophys. J.* **407**, 489

Yee, H. K. C., Ellingson, E., and Carlberg, R. G.: 1996, *Astrophys. J. Supp.* **102**, 269

Yee, H. K. C., Sawicki, M. J., Ellingson, E., and Carlberg, R. G.: 1995, in A. Buzzoni, A. Renzini, and A. Serrano (eds.), *ASP Conference Series*, 86, p. 301, ASP: San Francisco

Zabludoff, A. I. and Franx, M.: 1993, *Astron. J.* **106**, 4

Zabludoff, A. I., Zaritsky, D., Lin, H., Tucker, D., Hashimoto, Y., Shectman, S. A., Oemler, A., and Kirshner, R. P.: 1996, *Astrophys. J.* **466**, 104

Zwicky, F.: 1933, *Helv. phys. Acta* **6**, 110

Zwicky, F.: 1938, *P.A.S.P.* **50**, 218

A. A Description of the PEGASE Models

In this Appendix we will discuss in more detail the PEGASE models shown in Figure 4.11, on which our galaxy classification system (§4.3.3) is partly based.

The large, open star in Figure 4.11 represents the model result for a galaxy with a constant star formation rate, of any intensity. It represents the maximum Hδ absorption one can expect in a normal galaxy; emission filling will reduce its value by between roughly 1 and 3.5Å (Barbaro and Poggianti 1997). This point lies blueward of our D4000 cut, within the SF region. All of the galaxies in the SF region are either spirals, irregulars, or "starburst" galaxies, and do not have $W_o(H\delta)$ stronger than the model constant star-formation point (with the exception of NGC 3034, discussed in §4.3.2). Only if the star formation activity has begun recently (within the last 200 Myr, Barbaro & Poggianti, 1997) will Hδ emission overwhelm the absorption and the galaxies will then occupy the short starburst (SSB) region of this figure.

The long-dashed line in Figure 4.11 traces the evolutionary path of a galaxy with an exponentially decaying star formation rate; it evolves from "birth" at D4000$\approx$ 1, redward. In this case, a decay time of τ = 2 Gyr is adopted, and the galaxy is evolved to 11 Gyr, which we expect to be the maximum age of CNOC1 galaxies, in reasonable cosmological models[1]. Most of the local spirals in the Kennicutt 1992b and Kinney et al. 1996 samples

[1]Beyond an age of 11 Gyr, the models only increase in D4000 at a rate of about 0.05/Gyr.

lie close to this curve. Galaxies of this type with ages greater than about 5 Gyr will lie in the Passive region; clearly this includes not only E and S0 type galaxies, but also early type spirals. Note that the oldest models have $W_o(H\delta) < 0$; this reflects the nature of our specific index definition, which in this case is telling more about features in the continuum, rather than the intrinsic Hδ absorption (see §4.2.2).

The evolution of a galaxy produced by an initial burst of star formation lasting 200 Myr is shown as the short-dashed line in Figure 4.11. After the burst ends, this spectrum always has stronger $W_o(H\delta)$ than the exponentially decaying star-formation model, until D4000$>$ 1.7. It spends roughly 300 Myr in the bHDS region and another 300 Myr in the rHDS region.

The dotted line represents the evolution of a galaxy which underwent constant star formation for 4 Gyr, followed by a 200 Myr starburst involving 30% of its mass, after which all star formation was terminated. This model track only follows the evolution after the end of the starburst. The model closely traces the initial burst model, but does not reach as strong values of $W_o(H\delta)$. The duration and strength of the burst are quite arbitrary; longer bursts and bursts involving smaller amounts of stellar mass result in weaker maximum $W_o(H\delta)$ indices; this parameter space has been explored extensively by Poggianti & Barbaro 1996, though we warn that our $W_o(H\delta)$ indices are defined differently and are not directly comparable with theirs.

The rHDS galaxies can originate not only from a terminated SSB phase, but also from a galaxy in which long-term star formation has recently ended (e.g., Couch and Sharples 1987; Newberry et al. 1990). We model this latter case by terminating star formation in a galaxy which has undergone constant

star formation for 4 Gyr; this is shown in Figure 4.11 as the solid line. Once the star formation is terminated, the galaxy quickly reddens, passing into the rHDS region within 100 Myr. It then spends about 300 Myr in the rHDS region before $W_o(H\delta)$ further weakens and the spectrum becomes a Passive type.